# ABSTRACT

## JOINT SOURCE CHANNEL CODING FOR PROGRESSIVE IMAGE TRANSMISSION

by
**Minyi Zhao**

Recent wavelet-based image compression algorithms achieve best ever performances with fully embedded bit streams. However, those embedded bit streams are very sensitive to channel noise and protections from channel coding are necessary. Typical error correcting capability of channel codes varies according to different channel conditions. Thus, separate design leads to performance degradation relative to what could be achieved through joint design. In joint source-channel coding schemes, the choice of source coding parameters may vary over time and channel conditions. In this research, we proposed a general approach for the evaluation of such joint source-channel coding scheme. Instead of using the average peak signal to noise ratio (PSNR) or distortion as the performance metric, we represent the system performance by its average error-free source coding rate, which is further shown to be an equivalent metric in the optimization problems.

The transmissions of embedded image bit streams over memory channels and binary symmetric channels (BSCs) are investigated in this dissertation. Mathematical models were obtained in closed-form by error sequence analysis (ESA). Not surprisingly, models for BSCs are just special cases for those of memory channels. It is also discovered that existing techniques for performance evaluation on memory channels are special cases of this new approach. We further extend the idea to the unequal error protection (UEP) of embedded images sources in BSCs. The optimization problems are completely defined and solved. Compared to the equal error protection (EEP) schemes, about 0.3 dB performance gain is achieved by UEP for typical BSCs. For some memory channel conditions, the performance

improvements can be up to 3 dB. Transmission of embedded image bit streams in channels with feedback are also investigated based on the model for memory channels. Compared to the best possible performance achieved on feed forward transmission, feedback leads to about 1.7 dB performance improvement.

# JOINT SOURCE CHANNEL CODING FOR PROGRESSIVE IMAGE TRANSMISSION

by
Minyi Zhao

A Dissertation
Submitted to the Faculty of
New Jersey Institute of Technology
in Partial Fulfillment of the Requirements for the Degree of
Doctor of Philosophy of Electrical Engineering

Department of Electrical and Computer Engineering

May 2001

## APPROVAL PAGE

## JOINT SOURCE CHANNEL CODING FOR PROGRESSIVE IMAGE TRANSMISSION

**Minyi Zhao**

| | |
|---|---|
| Dr. Ali N. Akansu, Dissertation Advisor<br>Professor of Electrical and Computer Engineering, NJIT | Date |
| Dr. Richard Haddad, Committee Member<br>Professor of Electrical and Computer Engineering, NJIT | Date |
| Dr. Hongya Ge, Committee Member<br>Assistant Professor of Electrical and Computer Engineering, NJIT | Date |
| Dr. Raashid A. Malik, Committee Member<br>Visiting Professor of Electrical and Computer Engineering, NJIT | Date |
| Dr. William A. Pearlman, Committee Member<br>Professor of Electrical, Computer and Systems Engineering, RPI | Date |

## BIOGRAPHICAL SKETCH

**Author:** Minyi Zhao

**Degree:** Doctor of Philosophy

**Date:** May 2001

### Undergraduate and Graduate Education:

- Doctor of Philosophy in Electrical Engineering,
  New Jersey Institute of Technology, Newark, NJ, 2001
- Master of Engineering in Electrical Engineering,
  Tianjin University, Tianjin, P. R. China, 1989.
- Bachelor of Science in Electrical Engineering,
  Tianjin University, Tianjin, P. R. China, 1986.

**Major:** Electrical Engineering

### Publications and Presentations:

A. A. Alatan, Minyi Zhao, and A. N. Akansu,
"UEP of SPIHT encoded image bit-streams", *IEEE Journal on Selected Areas in Comm.*, vol.18(6), pp. 814–818, June, 2000.

Minyi Zhao and A. N. Akansu,
"Performance evaluation and optimization of embedded image sources in BSCs", to appear in *IEEE Signal Proc. Letters*, 2001.

Minyi Zhao and A. N. Akansu,
"Optimal UEP of embedded images bit streams in BSCs", to be submitted to *IEEE Trans. Multimedia*, in preparation.

Minyi Zhao and A. N. Akansu,
"Robust transmission of progressive images in wireless channels", to be submitted to *IEEE Trans. Circuit Sys. Video Tech.*, in preparation.

Minyi Zhao and A. N. Akansu,
"Progressive image transmission in channels with feedback", to be submitted to *IEEE Trans. Image Processing*, in preparation.

Minyi Zhao, A. A. Alatan, A. N. Akansu,
"A new method for optimal rate allocation for progressive image transmission over noisy channels", Proceedings of *DCC*2000, pp. 213–222, Snowbird, Utah.

Minyi Zhao, A. A. Alatan, A. N. Akansu,
"Dynamic UEP of progressive image bit streams over noisy channels", Proceedings of *ICASSP*2000, vol. IV, pp. 2095-2098, Turkey.

Minyi Zhao and A. N. Akansu,
"Optimization of dynamic UEP schemes for embedded image sources in BSCs", Proceedings of *ICIP*2000, Vancouver, CA.

Minyi Zhao and A. N. Akansu,
"Robust transmission of progressive images over G-E channels", Proceedings of *CISS*2000, vol.I, TA5-25-30, Princeton, NJ.

Minyi Zhao and A. N. Akansu,
"JSCC for progressive images in channels with memory", Proceedings of the *34th Asilomar Conf. on Signals, Systems, and Computers,* November, 2000, Asilomar, CA.

Minyi Zhao, William A. Pearlman, and A. N. Akansu,
"JSCC of Hybrid ARQ schemes for progressive image transmissions", submitted to the *CISS'01*, Baltimore, MD.

Minyi Zhao and A. N. Akansu,
"Progressive image transmission by ARQ with code combining", submitted to the *ICASSP'01*, Salt Lake City, UT.

Minyi Zhao and A. N. Akansu,
"Optimal protection of embedded image sources: a general approach", accepted by the *DCC'01*, Snowbird, Utah.

Minyi Zhao and C. Chang,
"An analysis of an FLIR sensor model", MNJRDS Proceedings, pp. 166-170, Jan., 1996, Singapore.

J. Lu, J. Wang, and Minyi Zhao,
"Computerized DIPLOG field surveying system", Journal of Tianjin University, vol. 2, pp. 98-102, 1992.

To my wife
Wang Yu

## ACKNOWLEDGMENT

I would like to express my sincere gratitude to my dissertation advisor, Prof. Ali N. Akansu, for his support, academic guidance and all the encouragement throughout my graduate study at NJIT. It is him who guided me to the challenging research topic which turns out to be a exciting and fruitful one. I also want to thank Prof. Haddad, Prof. Ge, Prof. Malik, and Prof. Shi for providing excellent courses, reading the dissertation and serving on my dissertation committee.

My special thanks go to Prof. William A. Pearlman (Rensselaer Polytechnic Institute), who provided invaluable comments and suggestions on my research. I benefit so much from the source codes of SPIHT and the algorithm itself, which leads me to the spirit of compression. I am also grateful to Dr. William Turin (AT&T Research) who helped a lot on fading channel modeling and the related Markov chain theory.

I want to thank Dr. Aydin A. Alatan for the extensive discussions we had on the research topic and his assistance with computer simulations. I also thank my friends in NJCMR for their friendship, discussions and help during my years in NJIT, especially Xiaodong, Feihong and Surong. Lastly, I want to thank my wife Wang Yu, without whom the completion of my dissertation would not have been possible.

## TABLE OF CONTENTS


| Chapter | | Page |
|---|---|---|
| 1 | INTRODUCTION | 1 |
| | 1.1 Background and Motivation | 3 |
| | 1.2 Overview of the Dissertation | 7 |
| 2 | SCALABLE SOURCE AND CHANNEL CODING AND THEIR COMBINATIONS | 9 |
| | 2.1 Introduction | 9 |
| | 2.2 Scalable Image Coding Algorithms | 10 |
| | 2.2.1 Wavelet Zerotrees | 11 |
| | 2.2.2 Embedded Bit Streams | 15 |
| | 2.3 Multi-resolution Channel Coding | 18 |
| | 2.4 Joint Source-Channel Coding | 19 |
| 3 | PROGRESSIVE IMAGE TRANSMISSION IN BINARY SYMMETRIC CHANNELS | 23 |
| | 3.1 Rate-based Performance Evaluation | 24 |
| | 3.2 Embedded Image Source Modeling | 28 |
| | 3.3 EEP Optimization | 30 |
| | 3.3.1 EEP Optimization Algorithm | 30 |
| | 3.3.2 Simulation Results and Discussions | 34 |
| | 3.4 Progressive UEP Schemes | 38 |
| | 3.4.1 After-channel Source Models | 42 |
| | 3.4.2 UEP Optimization | 43 |
| | 3.4.3 Necessary Condition for UEP Gain | 45 |
| | 3.4.4 Upper Bounds for UEP Gain | 46 |
| | 3.4.5 Side-information and Overhead | 47 |

## TABLE OF CONTENTS
## (Continued)

**Chapter** **Page**


3.4.6 Simulation Results and Discussions . . . . . 48

3.5 UEP with Bit Class Demultiplexing . . . . . 51

3.5.1 Error Resilience of Bit Classes . . . . . 56

3.5.2 Bit-stream Syntax and Overheads . . . . . 59

3.5.3 Error Protection . . . . . 59

3.5.4 Simulation Results and Discussions . . . . . 60

3.6 Concluding Remarks . . . . . 65

4 PROGRESSIVE IMAGE TRANSMISSION IN FADING CHANNELS . . . 67

4.1 Fading Channel Modeling . . . . . 69

4.2 Single-BSC-Based Techniques . . . . . 71

4.3 Statistical Averaging Approach . . . . . 72

4.4 Error Sequence Analysis (ESA) . . . . . 73

4.5 Relationship with Existing Techniques . . . . . 75

4.6 Performance Upper Bound . . . . . 76

4.7 Simulation Results and Discussions . . . . . 77

4.8 Concluding Remarks . . . . . 79

5 PROGRESSIVE IMAGE TRANSMISSION IN CHANNELS WITH FEEDBACK INFORMATION . . . . . 83

5.1 Type-I Hybrid ARQ . . . . . 83

5.1.1 Optimization Algorithm for Hybrid ARQ . . . . . 84

5.1.2 Delay Analysis . . . . . 86

5.1.3 Simulation Results . . . . . 87

5.1.4 Concluding Remarks . . . . . 89

5.2 Type-II Hybrid ARQ . . . . . 89

5.2.1 Code Combining of Hybrid ARQ . . . . . 93

5.2.2 Simulation Results and Discussions . . . . . 96

## TABLE OF CONTENTS

## (Continued)


**Chapter** **Page**

5.2.3 Concluding Remarks . . . . . 99

5.3 Conclusions . . . . . 99

6 CONCLUSIONS AND PERSPECTIVES . . . . . 104

6.1 Conclusions and Major Contributions . . . . . 105

6.2 Future Work . . . . . 106

REFERENCES . . . . . 107

## LIST OF TABLES


| Table | | Page |
|---|---|---|
| 2.1 | Channel classification | 20 |
| 3.1 | Optimal code rate comparison | 35 |
| 3.2 | Optimal 2-rate UEP code pairs for BSCs $10^{-1}, 10^{-2}$ (denominators only, numerators = 8) | 49 |
| 3.3 | Optimal 3-rate UEP RCPC code rate tri-tuples for BSCs $\epsilon = 10^{\{-1,-2\}}$ (denominators only, numerators = 8) | 50 |
| 4.1 | G-E Channel parameters | 77 |
| 5.1 | G-E Channel parameters | 88 |
| 5.2 | G-E Channel parameters | 96 |

## LIST OF FIGURES


| Figure | | Page |
|---|---|---|
| 1.1 | Progressive image transmission system | 3 |
| 2.1 | DWT and zerotree structure | 13 |
| 2.2 | Error propagation of SPIHT bit streams | 17 |
| 3.1 | Rate- vs. distortion-based performance evaluations | 25 |
| 3.2 | Rate-Distortion analysis of embedded image sources | 27 |
| 3.3 | After-channel embedded source statistics | 31 |
| 3.4 | Bit rate allocation | 32 |
| 3.5 | Results of RCPC code rate optimization | 36 |
| 3.6 | PSNR comparisons of the two methods | 37 |
| 3.7 | Optimal protections for EEP and dEEP | 39 |
| 3.8 | PSNR improvements of the dynamic EEP scheme over the EEP scheme on SPIHT | 40 |
| 3.9 | Deterministic time-varying channel model for $M$-rate progressive UEP schemes | 41 |
| 3.10 | Bit stream partition for 2-rate UEP schemes | 43 |
| 3.11 | Optimization processes for the BSC of $\epsilon = 10^{-1}$ | 52 |
| 3.12 | 2-rate UEP optimal partition results | 53 |
| 3.13 | 3-rate UEP optimization results, BSC $\epsilon = 10^{-1}$ | 54 |
| 3.14 | Comparison between EEP and UEP | 55 |
| 3.15 | SPIHT bit stream delmultiplexing and re-multiplexing | 58 |
| 3.16 | PSNR comparisons with LENA | 63 |
| 3.17 | PSNR comparisons with GOLDHILL | 64 |
| 4.1 | Finite state Markov chain channel models | 69 |

## LIST OF FIGURES

## (Continued)


| Figure | | Page |
|---|---|---|
| 4.2 | Optimization of protection levels, ESA | 79 |
| 4.3 | PSNR comparisons of the methods with LENA image | 80 |
| 4.4 | Performance evaluation method comparison with LENA image | 81 |
| 4.5 | Doppler effect on system performance, G-E channel 2, LENA image | 81 |
| 5.1 | Water-filling for type-I SW-HARQ | 85 |
| 5.2 | Protection level optimization for type-I HARQ | 90 |
| 5.3 | Comparison of FEC and type-I HARQ schemes | 91 |
| 5.4 | Comparison of FEC and type-I HARQ schemes by PSNR performances with LENA image | 92 |
| 5.5 | Water-filling for SW-HARQ with code combining | 94 |
| 5.6 | Protection level optimization for type-II SW-HARQ | 101 |
| 5.7 | Comparison of FEC, type-I and -II SW-HARQ schemes | 102 |
| 5.8 | Comparison of FEC, type-I and -II SW-HARQ schemes by PSNR performances with LENA image | 103 |

# ABBREVIATIONS

| | |
|---|---|
| ACK | Acknowledgement |
| ARQ | Automatic Repeat ReQuest |
| BER | Bit Error Rate |
| BSC | Binary Symmetric Channel |
| CFB | Channels with Feedback |
| CRC | Cyclic Redundancy Check |
| DCT | Discrete Cosine Transform |
| DWT | Discrete Wavelet Transform |
| dEEP | dynamic Equal Error Protection |
| EBCOT | Embbedded Blocking Coding with Optimal Truncation |
| EEP | Equal Error Protection |
| ESA | Error Sequence Analysis |
| EZW | Embedded Wavelet Zerotree |
| FEC | Forward Error Correction |
| FEFRL | First Error-Free Run Length |
| FLC | Fixed Length Coding |
| FSMC | Finite State Markov Chain |
| G-E | Gilbert-Elliott |
| HARQ | Hybrid Automatic Repeat ReQuest |
| JPEG | Joint Photographic Experts Group |
| JSCC | Joint Source-Channel Coding |
| MC | Monte Carlo |
| NAK | Negative Acknowledgement |
| PSNR | Peak Signal to Noise Ratio |
| RCPC | Rate Compatible Punctured Convolutional |
| SA | Statistical Averaging |
| SPIHT | Set Partitioning In Hierachical Trees |
| SW | Stop-and-Wait |
| UEP | Unequal Error Protection |
| VLC | Variable Length Coding |

# CHAPTER 1
# INTRODUCTION

Recent advances in image compression techniques result in very efficient and resourceful representations of images in noiseless environment. When transmitted in noisy channels unprotected, those bit streams are easily corrupted and both the objective and subjective reconstructed image qualities are unacceptable in most cases. In fact, detailed analysis of the simulations shows that a single bit of error may destroy the whole bit stream due to error propagation. Generally speaking, this is because compactly compressed data is very sensitive to errors and those algorithms are no exceptions either. Thus, some form of channel protections are necessary for robust image communications. Of the various protection schemes, the concatenated cyclic redundancy check code and rate-compatible punctured convolutional code (CRC-RCPC) channel protection proposed by Sherwood [57] *et al* is very promising (Figure 1.1). However, both the source and channel codes in the scheme are developed under Shannon's "separation principle" which assumes impractical conditions such as known channel conditions, equal importance of source codes, and perfect channel codes etc. Those assumptions are more and more violated in modern communication systems. Considering other limitations such as bandwidth, delay, power constraints, and time-varying channel conditions etc., joint design of source and channel coding schemes provides the possibility of achieving the best possible system performances.

Conventionally, the performance of image transmission system in Figure 1.1 is represented by average PSNR at point A [57, 58, 36]. Given a channel code set, the best overall system performance is obtained by trying each rate of the channel code set with Monte Carlo (MC) simulations and picking out the one that generates the highest average peak signal to noise ratio(PSNR). Obviously, the method is a PSNR- or distortion-based approach. While such a method is straightforward and simple

for channel types such as binary symmetric channels (BSCs), its complexity quickly goes up for more practical channel types such as memory channels and channels with feedback information. Other limitations of the method include its dependence on images and source codec used for optimization.

In this dissertation, the joint source-channel coding (JSCC) problem for progressive image transmissions in different channel types and conditions are investigated with a new rate-based approach. The key idea is that the performance of embedded image sources transmitted over a general noisy channel (without any type limitations) can also be represented by the average first error-free run length (FEFRL) of the bit streams. Moreover, maximization of the average FEFRL is shown to be equivalent to the maximization of the average PSNR. Along this direction, the expressions for the average FEFRL for both memoryless and memory channels are obtained, all in closed-form. The optimization problem is greatly simplified with the source model. The approach is then further extended to the channels with feedback information by adding a rate control algorithm. With this proposed approach, we also investigate the topics such as performance upper bounds for unequal error protection (UEP) and memory channel transmissions, motion effects on the quality of progressively received images. It is also shown that some of the existing approaches for performance evaluation on memory channels are simply special cases of the proposed method. Significant performance can be achieved with this new approach on some memory channel conditions. It is also of interest to note that the performance optimization algorithms for embedded image transmission over memoryless, memory, and feedback channels are similar with the proposed source model.

## 1.1 Background and Motivation

With the exploitation of discrete wavelet transform (DWT), new quantization techniques, and improving entropy coding algorithms, significant performance improvements have been achieved by recent image compression algorithms [56, 54, 65, 73, 34, 64, 32, 8]. The bit streams produced by those algorithms share some common features such as embeddedness, reducing bit significance and error sensitivity to channel noise. The embeddedness property can be used for progressive image transmissions and provides the possibility of exact rate control which is highly desirable in multimedia communications. However, the error sensitivity generates serious problems when the bit streams are transmitted in noisy channels. Generally speaking, the error sensitivity comes from the variable length coding (VLC) techniques which are inevitably used in all kinds of high performance compression algorithms. The error sensitivity can be so serious that the first bit error can propagate to the end of the bit stream and destroy the received image quality thoroughly. Thus, some form of channel protection is needed when such bit streams are transmitted in a noisy environment. A protected progressive image transmission system is depicted in Figure 1.1 in which the concatenated CRC-RCPC scheme proposed in [57] is selected as the protection method. Of course other channel coding schemes may also be used for the channel coding block.

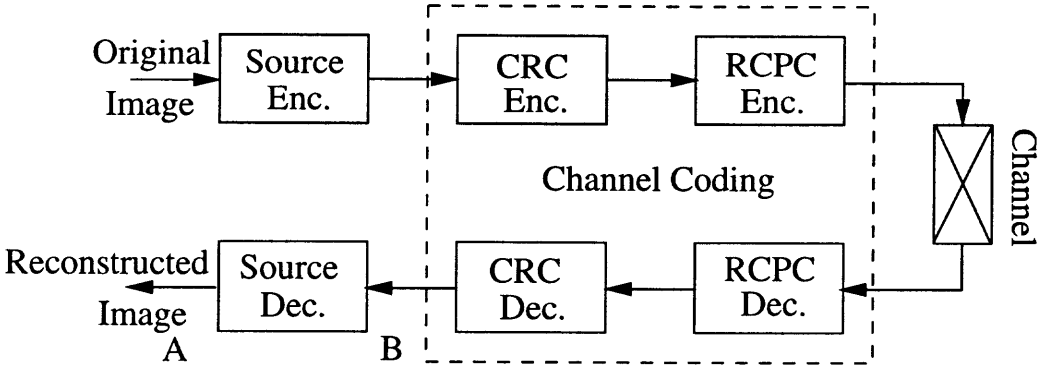


**Figure 1.1** Progressive image transmission system

Of many forward error correction (FEC) schemes, the concatenated CRC-RCPC is preferable because of its simplicity of implementation, flexibility of adjusting protection levels in and between noisy channels, and good performance compared to other schemes. If an embedded source coder is used, then both the source and channel coding in Figure 1.1 are realized with one codec. The scheme is capable of dealing with different channel conditions by using different bit rate allocations. Moreover, progression is inherent in such a scheme, which is highly desirable in numerous applications. A main reason for the good performance of the system is that the embedded source and channel codec allows flexible bit rate allocation between source and channel coding which is necessary to achieve optimal system performance.

As the assumptions for the "separate" design are more and more violated in modern communications, it is of interest to investigate the problem of optimizing the overall system performance by considering the source and channel coding schemes jointly. Simply speaking, the general joint source-channel coding problem that is dealt with in the research is:

Given a bit rate constraint and RCPC code set on a channel, how to *evaluate* and *optimize* the system performance?

Consider the situation in which some bit streams with equal lengths are transmitted over a noisy channel, as depicted in Figure 1.1. Conventionally, the system performance in Figure 1.1 is represented at point A by the average PSNR. The performance optimization problem can then be solved by trying each RCPC code rate in the code set with Monte Carlo simulations on a selected image set and selecting the rate that gives out the highest average PSNR. While such a method is straightforward and simple for channel types such as BSCs, its complexity quickly goes up for UEP schemes and memory channels. Furthermore, the optimization results are dependent on the images and source codec used in the optimization. A new and general approach for this problem is proposed in the dissertation. A re-

check of Figure 1.1 immediately shows that by using average PSNR as the system performance metric, the subsystems are lumped together in the approach so that any performance variations can only be observed after numerous times of source and channel decoding. If the system performance is evaluated at point B instead of A using the average first error-free run length (FEFRL), a PSNR can also be obtained from average FEFRL accordingly with only one source decoding. By doing so, the subsystems right to point B can be treated as an "effective" channel which is general enough to accommodate common channel types such as memoryless and memory channels. Obviously, performance evaluation at point B is independent of both the images and specific embedded image codec involved. Furthermore, the average FEFRL for the aforementioned channel types can all be expressed in closed-form which greatly simplifies the optimization problem.

It may seem strange that a "*joint*" source-channel coding problem is solved by "separating" the subsystems. In fact, it can also be thought of a "*joint*" source-channel coding approach with one subsystem (the source decoder here) treated differently while the rest of the whole source-channel coding system is still optimized jointly. This point becomes more clear in later chapters when the relationship between the conventional and proposed approach is revealed.

The first task in the joint source channel-coding problem is modeling the source. By analyzing the behavior of embedded image bit streams transmitted in noisy channels, a rate-based approach is proposed to evaluate the overall system performance. Such an approach is applied to the BSC cases first and some interesting results were obtained. After that, the idea is extended to the performance optimization of the UEP schemes, which is a more challenging problem. The joint source channel coding problems associated with UEP are clearly defined and complete solutions on BSCs presented.

The memoryless channels or BSCs are quite useful in comparing different optimization techniques. However, they might be too simple to accommodate practical communication scenarios. Historically, two state finite state Markov chain (FSMC) or Gilbert-Elliott (G-E) channels are extensively used to approximate slow fading channels [35, 1, 36] encountered in wireless communications. Performance evaluations for such kinds of channels can be put into either single- or double-state category. For the single-state method, either the "worst" state or the average bit error rate (BER) is used to further simplify the memory channel model [35, 58]. Two-state approaches include using the error-free or error-burst run lengths of the G-E model, or obtaining the average FEFRL by statistical averaging method [78, 61, 10]. However, those two-state approaches also imply some unrealistic assumptions. For example, the states transit only after a whole image bit stream has been transmitted and the bit stream lengths are infinite. Obviously, those assumptions are not reasonable in practical systems. To solve the problems we proposed a new techniques called error sequence analysis (ESA) in this dissertation. With error sequence analysis, the average FEFRL model is obtained in closed-form for FSMC channels. Interestingly, previous results on BSCs and existing techniques can be easily shown to be special cases of it. An added advantage of the source models derived from ESA is that they do not impose any limitations on the structure of the memory channels used. Thus, the memory channel approximation for the fading channels can be more accurate, with new models available.

The basic CRC-RCPC system is also well suited for the automatic repeat request (ARQ) schemes on channels with feedback information. According to the information theory, the overall communication system performance can be further improved with feedback information at the price of time delay. In wireless communications, such kind of feedback channels usually exist and can be used to obtain better performance through ARQ schemes at the price of delay or throughput reduction. In

this dissertation, the results of ESA are applied to the channels with feedback cases with the aid of water-filling rate control technique. The optimization algorithms for type-I and -II stop-and-wait hybrid FEC/ARQ schemes are presented. For typical wireless communication scenarios, the additional delay incurred by the stop-and-wait strategy is shown to be close to that of the FEC scheme. Furthermore, no additional system overhead is incurred in the form of packet number within the proposed scheme.

## 1.2 Overview of the Dissertation

The dissertation proposes to tackle the problem of optimizing the overall system performance of progressive image bit streams transmitted over noisy channels, or source-optimized channel coding. Unlike the conventional distortion-based method which treats the source coding system as a whole, a rate-based approach is proposed to evaluate the system performance with its error-free source coding rate. This rate-based approach is exploited to investigate the joint source-channel coding problem for several types of channels, i.e. memoryless or BSCs, deterministic time varying channels for UEP schemes, FSMC channels and channels with feedback information.

Chapter 2 briefly reviews the embedded zerotree based image coding algorithms and the multi-resolution channel codes. The joint source-channel coding problem for progressive image transmission is then introduced after modeling the embedded image sources transmitted over a general noisy channel.

Chapters 3 explains the relationship between the proposed rate-based approach and the conventional distortion-based approach. The rest of the chapter deals with the joint source-channel coding problem on BSCs. The mathematical source model is presented in closed-form. Performance optimization algorithms are developed based on the model. The idea is then extended to the UEP cases. Topics covered

include problem definition and complete solution for UEP schemes on BSCs, system performance upper bounds and PSNR improvements.

Chapter 4 formulates the joint source-channel coding problem on memory channels which are used to approximate fading channels in wireless communications. Both the ESA and the source model obtained are presented. The result is then shown to include models on BSCs and existing techniques as special cases.

Chapter 5 investigates the joint source-channel coding problem on channels with feedback information. Optimization algorithms for type-I and -II hybrid ARQ schemes with stop-and-wait strategy are developed. Delay analysis and performance improvements are also reported.

In Chapter 6, previous research is summarized together with a contribution list. Ongoing and future work are also reported in Chapter 6.

# CHAPTER 2

# SCALABLE SOURCE AND CHANNEL CODING AND THEIR COMBINATIONS

## 2.1 Introduction

The fast progress in the technologies such as coding techniques, VLSI and communication theory enables more and more information and services be provided by modern communication systems. Contents that can be transferred among end users are encircling speech, data, and multimedia contents such as images, video, audio etc. Usually huge amounts of data with different delay and error sensitivity are generated from those sources and transmitted over a heterogeneous communication network. The heterogeneity of networks refers to the facts that the same network can be used for singlecasting for transmitter to user receiver and multicasting for transmitter to users with different receiver capability at the same time, and the transmission media such as wireless and wireline linkage coexist. Channel capacities for wireless link and some wirelines such as copper lines are very limited. Thus, information needs to be compressed before transmitted over such communication channels. Different receiver requirements on the quality of service and computational capabilities also put additional scalability constraints on the compression algorithms such as data scalability and algorithm simplicity. Highly scalable data ensures that no performance penalty will be incurred when truncated, and low complexity reduces the decoding load and the power consumption for the receivers. Thus, general requirements on content processing or efficient source representation are at least threefold, i.e., high compression, high scalability and low complexity. In the dissertation, the discussion is limited to image representations. However, the results are applicable to any multimedia streams possessing the same embedded nature.

Recent DWT-based image coding algorithms such as embedded zerotree for wavelet (EZW) and its derivative set partitioning in hierarchical trees (SPIHT) etc.

satisfy all three requirements. Loosely speaking, the reason for such impressive coding performance lies in the fact that DWT is a multi-resolution decomposition in nature. Appropriate exploitation of such a feature produces high scalability together with good compression. The algorithm simplicity originates from the tree-structured data defined in the transform domain and the efficient set partitioning rule for the zerotrees. Such zerotree-based wavelet image coders can be viewed as two-class (zero and non-zero) classification strategy on statistical modeling in the frequency domain.

However, the variable length coding (VLC) techniques used in such kind of compression algorithms also make the data streams very sensitive to channel noise. When those bit streams are transmitted in noisy environments, some channel protections are necessary in order to get acceptable image quality. Now the problem is how to achieve the best reconstructed image quality under some bit rate constraint for different channel conditions by corresponding bit rate allocations between source and channel coding schemes? Solution to such a problem depends on several factors such as bit rate constraint, channel conditions, source and channel coding performances and even optimization algorithms. It is apparent that such a jointly optimized system also requires channel code scalability so that no performance penalty is incurred due to different allocation strategies.

## 2.2 Scalable Image Coding Algorithms

A typical transform coding algorithm for image compression is composed of three parts. Namely a transformation which aims to remove the correlations among image pixels, a quantizer which compresses the data to be transmitted and a lossless entropy coding engine. One implementation of such a scheme is the well known JPEG image compression standard. It uses discrete cosine transform (DCT) to decorrelate the image pixels. Run-length coding based quantization procedure further compresses the data. The performance of JPEG is greatly surpassed recently

by the new generation DWT-based algorithms. Common features of those new algorithms include high compression, rate or performance scalability of bit streams, multi-resolution representation, and algorithm simplicity. The reasons for the excellent performance and flexibilities over DCT-based coding techniques lie in the fact that each component of the basic transform coding scheme has been improved. More specifically, the DWT provides better energy compaction and space-frequency resolution than DCT. The multi-resolution property of DWT also makes the scheme suitable for integrating human vision system. In the quantization process, the residual correlations between subbands are efficiently utilized by those algorithms with new data structure such as zerotree. One common feature of the bit streams generated by those algorithms is the embeddedness which enables precise rate control for both encoding and decoding without any sacrifice in the reconstructed image quality. In this section, the new algorithms based on zerotrees [56, 54] will be briefly reviewed and the structure of the embedded bit streams and their behavior in noisy channels analyzed. An after-channel source model is then set up based on the analysis.

### 2.2.1 Wavelet Zerotrees

A typical image is composed of large area of textured background with high statistical spatial correlation and a small portion of object edges or boundaries. While those low frequency backgrounds contribute most of the signal energy of the image, the high frequency edges take on more perceptual significance. DCT based coders decompose images into equal bandwidth subbands, thus pixel correlations at high frequency can not be removed effectively. This inefficiency gets punished at low bit rates and results in blockiness.

Wavelet transform provides a multi-resolution representation for the images in which all frequency components can be decorrelated efficiently. A typical octave-

band decomposition or DWT is illustrated in Figure 2.1(a). The image is first critically sampled and divided into four subbands. Coarser "scale" coefficients are then obtained by identical operations on the low-low bands. Thus, there are three subbands for each scale and the remaining lowest frequency represents the information at all coarser scales. Within such a multi-resolution representation, information for edges is contained in the position of a large number of small valued coefficients at fine scales. The remaining challenge is how to make effective usage of the multi-resolution representation to code the information corresponding to edges. A direct visual inspection of the transform coefficients indicates that the residual correlations among the coefficients manifest as self-similarities across subbands. This self-similarity can be well exploited by defining a tree-structured data in the transform domain (Figure 2.1(b)). If all the elements of the tree are smaller than a pre-defined threshold $T$, it is called a *zerotree*. By using such a data structure on dyadicly decomposed image data, lots of coefficient can be coded together or 'jointly', thus greatly increasing the efficiency of coding.

The first implementation of the zerotree concept was reported in [33]. Its incompleteness was later on corrected in EZW [56] and obtained better performance than that of DCT-based JPEG. SPIHT [54] further improves the coding efficiency of EZW by adding a set partitioning rule on the tree-structured data and achieves state-of-the-art rate-distortion performance, with an astonishing simple algorithm.

After the transform, compression and embedding can be achieved at the same time by using zerotrees with bit plane encoding. By representing the absolute values of the 2-D matrix of DWT coefficients in binary form, 2-D bit planes are formed from the highest, i.e. the one includes the most significant bit of the largest coefficient, to lower ones. Residual correlations among the coefficients still exist and exhibit as self-similarities across scales in significance maps. This self-similarity can be well

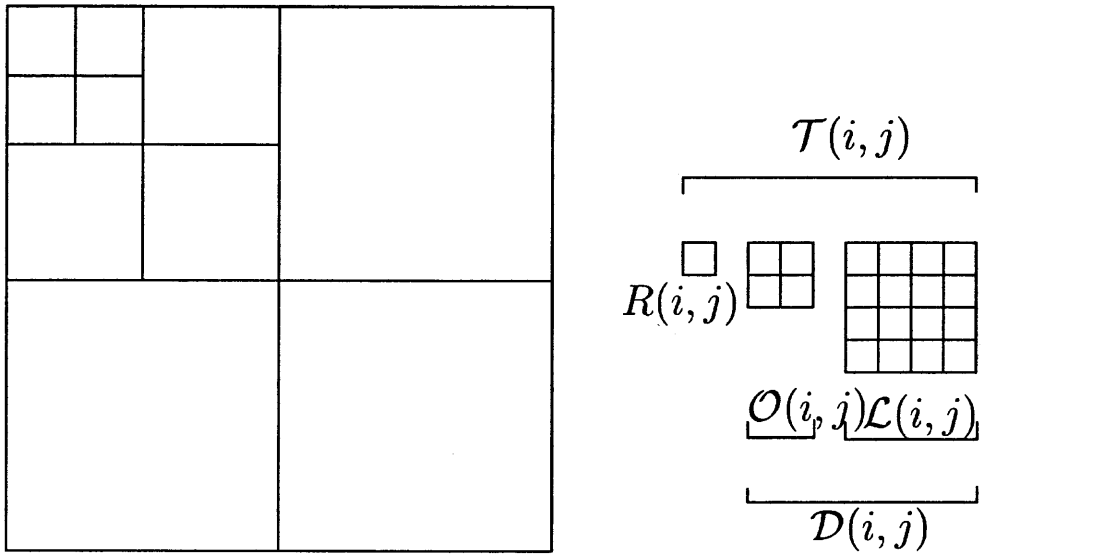


(a) 3-scale DWT

(b) Set partitioning on Zerotree

**Figure 2.1** DWT and zerotree structure

exploited by using the tree-shaped data structure depicted in Figure 2.1(b). In a dyadic subband system, with the exception of the highest frequency subbands, every coefficient at a given scale can be related to a set of coefficients at the next finer scale of similar orientation. If the magnitudes of *all* the elements in such a tree are smaller than a predefined threshold value, it is called a *zerotree.* The zerotree is based on the hypothesis that if a wavelet coefficient at a coarse scale is insignificant with respect to a given threshold $T$, then *all* the wavelet coefficients of the same orientation in the same spacial location at finer scales are likely to be insignificant with respect to $T$. Such a hypothesis is *almost* always true for each bit plane. In other words, the self-similarities in the bit plane are well predicted by the zerotrees. The zerotrees in higher bit planes might be very large since the total number of elements increases quickly with finer scales. Due to the good energy compaction of DWT, the percentage of zerotrees is high, especially at higher bit planes. Furthermore, zerotrees at all scales are self-terminating at the transform coefficient matrix boundaries so there is no need to send additional symbols to describe their extent.

The zerotree concept is used in the EZW algorithm to obtain fully embedded image bit streams with better performance than that of DCT-based JPEG. The basic idea of EZW is to code each zerotree on a bit plane with only one symbol. Since the probability $p$ of a zerotree on a bit plane is close to 1, and its information content $-\log p$ is very small. This corresponds to the spirit of entropy coding in which a random variable with high probability should be encoded with the shortest possible symbol string. In EZW, quantization is done by scanning each bit plane in two passes. In the first or dominant passes, the zerotrees and non-zerotrees are differentiated and coded separately. In fact there are four possibilities for each significance test, a zerotree (ZT), a significant element (POS or NEG), or an isolated zerotree (ISZ) with one or more significant elements somewhere down the tree. By using two symbols to represent a significant element, the sign information and the significance are coded together to generate embedded symbol stream. The position information of the significant elements are implied through execution path which can be duplicated at the decoder. For isolated zerotrees, they are coded with the ISZ symbol which signals more search is needed in finer scales, for both the encoder and decoder. On the second or subordinate passes, the magnitude of all the significant elements are coded and refined. There are further technical details regarding the priority of the wavelet coefficients and adaptive arithmetic coding which will not be further discussed here. The interested reader is referred to [56] for more details.

The encoding strategy of zerotrees in the EZW is very efficient but its treatment of significant elements and isolated zerotrees can be further improved. This is implemented in its derivative SPIHT [54] and achieves additional 0.3-0.6 $dB$ gain. The SPIHT algorithm improves the coding efficiency on non-zerotrees by using set partitioning rules on the tree-structured data and coding each non-zerotree immediately after it is discovered. In the set partitioning rule, a tree $\mathcal{T}(i,j)$ stemming from a coefficient at position $(i,j)$ is divided into root element $R(i,j)$ and its descendant

set $\mathcal{D}(i,j)$, i.e.

$$\mathcal{T}(i,j) = R(i,j) + \mathcal{D}(i,j) \tag{2.1}$$

The descendant set $\mathcal{D}(i,j)$ is further divided into offspring set $\mathcal{O}(i,j)$ of $R(i,j)$ and leaf set $\mathcal{L}(i,j)$, i.e.

$$\mathcal{D}(i,j) = \mathcal{O}(i,j) + \mathcal{L}(i,j) \tag{2.2}$$

By using such a set partitioning rule in the sorting passes on a bit plane, a whole non-zerotree is coded without multiplexing with binary codes from any other trees. As in EZW, a zerotree is always coded with a "0" and all the significant elements are coded together with its sign and refined in the refinement passes. Surprisingly, performance gains from this simple idea is about 0.6 $dB$ over EZW.

Both EZW and SPIHT use adaptive arithmetic coding to further compress the output data streams from the zerotree encoder. But it is a must for EZW to surpass the performance of JPEG and generate binary bit streams. The encoding engine of SPIHT is binary and the bit stream is so efficient that its performance is better than EZW without using any entropy coding. Thus, SPIHT obtains even better performance than EZW with simple and symmetric algorithms for encoder and decoder while the bit stream is also fully embedded.

### 2.2.2 Embedded Bit Streams

Bit streams generated by EZW and SPIHT are fully embedded or progressive, i.e. for two given rates $R_1 > R_2$, the rate $R_2$ code is a prefix to the rate $R_1$ code. Such property is of great practical interests for the following reasons

- the encoder can achieve a precise bit rate;
- the decoder can cease decoding at any point and generate the best possible image quality. This is of practical interest in a heterogeneous communication environment;

- it is very useful for indexing and browsing.

The embeddedness property varies slightly from algorithm to algorithm. While EZW and SPIHT generates fully embedded bit streams, JPEG2000 bit streams are partially embedded with a controllable number of scalable points. The SPIHT algorithm is used as the source codec throughout the dissertation. For the bit streams produced by SPIHT, sub-streams from sorting and refinement passes are multiplexed together from bit plane to bit plane. Sign bits are multiplexed in the sorting pass bits. Besides the rate scalability for any point of the bit stream, there are additional self-terminating points corresponding to the end of each bit plane.

Such efficient bit streams are built to be transmitted in noiseless channels and are quite sensitive to channel noise. In fact, computer simulations show that bit errors propagate in the bit streams and all the information received after the first bit in error can not be used in image reconstruction (Figure 2.2). Thus, the quality of the reconstructed image can be either represented by the PSNR reached before the first bit error happens (Figure 2.2(c)), or equivalently by the first error free run length (FEFRL) of the bit stream.

The behavior of embedded bit streams in noisy channels can be explained as follows. Since VLC bits are used to encode the significance maps in sorting passes, bit errors will cause the decoder lose synchronization and propagate to the end of the bit stream. For the SPIHT algorithm, VLC bits are extensively used in its sorting passes and multiplexed with fixed length coded (FLC) bits to generate very efficient embedded bit streams. In fact, the whole fully embedded bit stream of SPIHT can be treated as a prefix codeword, i.e., it is self-puncturing. Moreover, each added bit is also self-puncturing. Consequently, for an error-free bit stream, correct decoding of the current bit does not depend on its future bits but previous ones. When a bit error happens in the VLC bits of such an embedded bit stream, the decoder will lose synchronization because correct backward references will be impossible.

(a) No error, 0.25 *bpp*

(b) 1 bit error, 0.25 *bpp*

(c) Error-free decoding

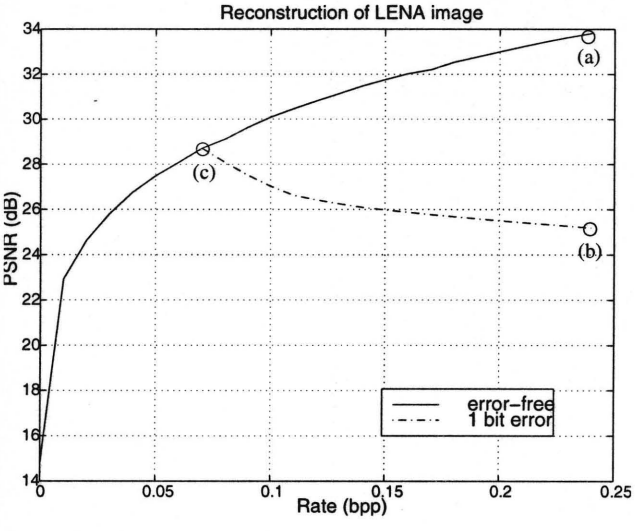


(d) PSNR performances

**Figure 2.2** Error propagation of SPIHT bit streams

The error will then propagate to the end of the received bit stream and make the decoded images unacceptable in most cases. In other words, all the bits received after the first error bit are unusable. Bit errors after the first one will make the reconstructed images even worse. Thus, further decoding will be destructive rather than constructive and the PSNR of the reconstructed images will begin to decrease at that point. On the other hand, the sign bits multiplexed in sorting passes and all the refinement bits are FLC bits. Errors on those bits are localized to a single elements in transform domain and do not propagate. But due to the good energy compaction property of the DWT, the percentage of FLC bits are low, especially at low bit rates. It is reasonable to assume that the first bit error in the bit streams always hits a VLC bit and the decoding should stop just before it. Thus, the performance of the embedded image sources transmitted over noisy channels can be represented by either the PSNR obtained from the FEFRL or simply by the FEFRL model itself.

## 2.3 Multi-resolution Channel Coding

From the discussion in previous section, it is known that the significance or the amount of information of each bit decreases along the embedded bit stream. Thus, bit errors at different locations of the bit stream cause different amount of additional distortion. With such knowledge of the embedded image bit streams, it is desirable for the channel code to provide different levels of error protection for different parts of the bit stream. This can be done by using a multi-resolution channel code, which might be in the form of block codes, trellis codes, or convolutional codes. The rate-compatible punctured convolutional (RCPC) codes [28] are used as the channel codes in the research since it provides the additional rate-compatible property which means that all the code bits of a higher rate code are usable by the lower rate codes, or in other words, the higher rate codes are embedded into the lower rate codes of the family. If the higher rate codes are not sufficiently powerful to decode

channel errors, only supplemental bits which were previously punctured have to be sent in order to upgrade the code. This makes the RCPC code well suited for hybrid forward error correction/automatic repeat request (FEC/ARQ) channel protection and jointly designed source channel coding schemes. Furthermore, since codes are compatible, rate variation within a data partition or unequal error protection (UEP) is possible to achieve with one encoder and one decoder for all the code rates. Thus, a multiple-resolution channel code such as an RCPC code provides additional system simplicity.

The simplicity and flexibility of the RCPC code make it an appropriate channel code in the concatenated CRC-RCPC scheme [57] in which RCPC codes serve as error correction codes and CRC as error detection code. The outer CRC code detects any uncorrected errors after Viterbi decoding for the RCPC codes, so that the image will not be corrupted by the disastrous error propagation. Such a combination is necessary for optimal protection of embedded image sources since decoding needs to stop just before the first error detected. The best possible performance is achieved if the bit rate allocation between the source and channel coding is appropriate or optimal which in turn requires multiple-rate channel codes.

## 2.4 Joint Source-Channel Coding

Under the separation principle, the new generation of wavelet-based source coders assume noiseless channel conditions and produce very efficient but extremely fragile bit streams. In fact a single bit error will propagate to the end of the bit stream and yield catastrophic source decoding failure. On the other hand, uncorrected channel errors are inevitable in modern communication systems, even with channel protection. The variety of channel conditions pose the challenging problem of how to achieve the best possible performance with the rate scalable source and channel

codes under some bit rate constraints and in different channel types. Furthermore, the decreasing importance of the source bit asks for unequal protection levels.

Historically, channel codes are also developed under the separation principle which assumes equal importance of source bits. This assumption is violated for those embedded image bit streams. Another violated assumption implied in separately designed source-channel coding system is the imperfectness of the channel codes which means residual errors will be present after channel decoding.

A communication system in which the source and channel codes are designed or optimized in a dependent fashion is called "joint source-channel code (JSCC)". It allows for strategies where the choice of source code parameters varies over channel conditions, and the choice of channel code parameters varies with source features and statistics. Joint source-channel coding applies to any system in which the conditions of the separation theorem are violated and dependence between source and channel code arises. In summary, reliance on separation principle may result in performance degradation relative to what could be achieved through joint design.

The noisy channel models in Figure 1.1 can be put into several categories such as memoryless channels, predictable time-varying channels for UEP, memory or finite state Markov chain (FSMCs) models for slow fading channels, and channels with feedback (Table 2.1). To obtain the best end-to-end system performance with

| **Channel Types** | Feedforward (FEC) | Feedback (Hybrid-ARQ) | |
|---|---|---|---|
| | | Type-I | Type-II |
| Memoryless | EEP, UEP | Optimization | Code combining |
| Memory | ESA | Delay analysis | Best performance |

**Table 2.1** Channel classification

equal error protection (EEP) schemes in BSCs, conventional method such as that of [57] allocates the bit budget between source and channel coding by conducting Monte Carlo simulations. However, such average distortion-based method depends on the operational rate-distortion function of the source codec and training images. It is

almost impossible to obtain source models in closed-form. Those shortcomings make the performance optimization very difficult for more complicated schemes such as UEP and channel types like FSMC channels. In this dissertation, a new rate-based approach is developed for the joint source-channel coding problem for progressive image transmissions in various kinds of noisy channels. The basic idea is to obtain the average FEFRL in closed-form for BSCs and maximize it with the available RCPC code set. This idea is also applied to the challenging problem of designing optimal UEP schemes for the embedded image bit streams in BSCs and some interesting results are obtained.

Two-state FSMC or Gilbert-Elliott (G-E) channels are often used to approximate flat slow fading channels encountered in wireless communication. The evaluation of the performance of embedded image bit streams transmitted over such kinds of channel models remains an unsolved problem. By conducting error sequence analysis (ESA) on the received bit stream, we obtain source models in closed-form. Such models are general enough to include previous results for BSCs and the existing methods are shown to be special cases for ESA. Significant PSNR improvements are expected and achieved for the time-varying channels since assumptions for the separation principles are more severely violated here. In the research, multipath and motion incurred Doppler effects on the system performance are all investigated. PSNR improvements are over 3 dB better than previous results under some channel conditions.

Feedback channels usually exist in practical communication systems. The overall system performance for progressive image transmission can be further improved by an ARQ scheme with feedback information at the price of additional time delay. The basic CRC-RCPC system is also well suited for the ARQ schemes on channels with feedback information and some efforts have been made to optimize the performance for different ARQ schemes. In [36], the performance of type-I hybrid-

ARQ schemes with stop-and-wait strategy on both memoryless and memory channels are evaluated and optimized. In [12], hybrid ARQ scheme using code combining is investigated on typical BSCs with a rate-based method. In this dissertation, the approach developed for feed-forward channels is further extended to the feedback channel cases by adding a water-filling rate control algorithm. System performance for type-I and -II hybrid ARQ schemes are optimized to achieve about 1.7 dB gain than those obtained on feed-forward channels with optimal EEP schemes.

# CHAPTER 3

# PROGRESSIVE IMAGE TRANSMISSION IN BINARY SYMMETRIC CHANNELS

It is well known that variable length coding (VLC) in a source encoder makes the output data stream very sensitive to channel noise since the receiver may lose synchronization on decoding such errors. When transmitted in noisy channels, proper channel protections are necessary in order to make the received image quality acceptable. Recently, a concatenated cyclic redundancy check code and rate-compatible punctured convolutional code (CRC-RCPC) channel coding scheme [57] is proposed to protect the fragile embedded image and video [9, 47] bit streams in noisy channels. The channel protection scheme is widely accepted due to its good system performance, flexibility and simplicity. The initial attempts to optimize such a scheme started from a simple progressive image transmission scenario in which an embedded image compression algorithm such as SPIHT is used as the source codec and the channels are a class of binary symmetric channels (BSCs). It is already shown in Chapter 2 that when an embedded image coder is used, the source decoding should stop before the first error encountered. Intuitively, the system performance can be evaluated by the average of peak signal to noise ratio (PSNR) obtained from the first error-free run lengths (FEFRL) of the embedded bit streams at point A (Figure 1.1). The disadvantages of such a distortion-based evaluation and optimization is quite obvious. The optimization results are dependent on the images and individual source codec used and the computational complexity is high. In this chapter, the average FEFRL is proposed to represent the system performance and its expression in BSCs is obtained in closed form. It is shown that maximization of average FEFRL and averagge PSNR are equivalent. Such a method is justified to be simpler and more powerful when dealing with more complicated schemes such as

unequal error protection (UEP) and channel types such as memory channels in later chapters.

### 3.1 Rate-based Performance Evaluation

Consider the case in which embedded image bit streams with length $L_s$ are transmitted over a general noisy channel. The position where the first bit error happens is denoted as $k+1$. Obviously, the FEFRL $L_{sef} = k$ is a random variable and the performance of the received bit stream can be evaluated in two ways. Since all the information of the reconstructed image comes from the FEFRL of the bit stream (point A in Figure 1.1), its PSNR can be expressed as

$$\rho_{_P}(R_{sef}) \triangleq 10 \log \left[ \frac{\sigma_{_P}^2}{\mathcal{D}(R_{sef})} \right] \tag{3.1}$$

where $\rho_{_P}$ is used to denote the PSNR for simplicity purpose in the dissertation, $R_{sef} = L_{sef}/N$ is the error-free source coding rate for an $N$ pixel image, $\sigma_{_P} \triangleq 255$ according to the PSNR definition, and $\mathcal{D}(R_s)$ is the operational distortion rate function of the source codec. $L_{sef}$, $k$, and $R_{sef}$ will be used interchangeably hereinafter without further specifications. Conventionally the expectation of (3.1) is used to represent the overall system performance

$$\overline{\rho}_{_P} \triangleq E\left[\rho_{_P}\right] = \sum_{k=0}^{L_s} \rho_{_P}\left(R_{sef}\right) p\left(R_{sef}\right) \tag{3.2}$$

where $p\left(R_{sef}\right)$ is the probability distribution function of the error-free source rate (or normalized FEFRL). Due to the lack of closed-form $\mathcal{D}(R_s)$, (3.2) can not be expressed in closed-form and the average PSNR (Figure 3.1) obtained from Monte Carlo simulations is often used to represented the overall system performance on a specific channel as

$$\overline{\rho}_{_P} = \frac{1}{J} \sum_{j=1}^{J} \rho_{_P}\left[R_{sef}(j)\right] \tag{3.3}$$

where $j = 1, 2, ..., J$, $J$ is the total number of simulations, and $\rho_P [R_{sef}(j)]$ is the PSNR of the $j$th trial obtained from (3.1).

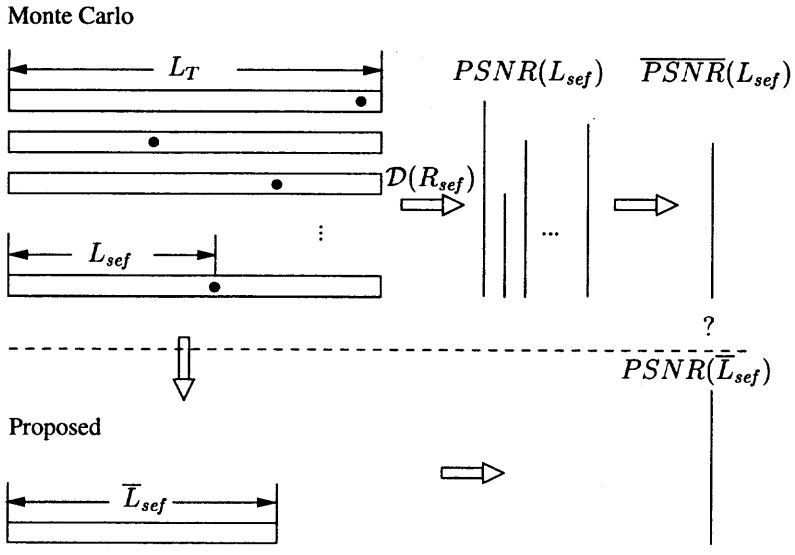


**Figure 3.1** Rate- vs. distortion-based performance evaluations

Such a system evaluation approach is widely accepted and used [57, 59, 58, 35, 36]. It is clear from (3.1), (3.2) and (3.3) that such an approach is dependent on both the images and the source codec used. Alternatively, the overall system performance may also be evaluated at point B in Figure 1.1 by using the average FEFRL

$$\overline{L}_{sef} \triangleq E[L_{sef}] = \sum_{k=0}^{L_s} L_{sef}\, p(L_{sef}) \tag{3.4}$$

where $L_{sef}$ is the FEFRL of the bit stream (Figure 3.1). The corresponding PSNR can be obtained using (3.1) as

$$\rho_P(\overline{R}_{sef}) = 10 \log \left[ \frac{\sigma_P^2}{\mathcal{D}(\overline{R}_{sef})} \right] \tag{3.5}$$

with only one source decoding!

It is clear from Figure 3.1 that PSNR values obtained from (3.5) and (3.3) might be different. Thus, it is of further interests to investigate the relationship between the conventional method (3.3) and the proposed one (3.5), or equivalently,

the relationship between the average distortion

$$\overline{D} = \frac{1}{J}\sum_{j=1}^{J} \mathcal{D}\left[R_{sef}(j)\right] \tag{3.6}$$

and the distortion incurred from the average error-free source coding rate $\mathcal{D}\left(\overline{R}_{sef}\right)$.

A divide-and-conquer approach is used here to solve the problem. First, the simplest case of the problem is considered in which the transmission is noiseless. For noise-free transmissions, all the bit streams will be received error-free, i.e.

$$L_{sef}(j) = \overline{L}_{sef} = L_s \quad \forall \quad 1 \leq j \leq J \tag{3.7}$$

Substitutions of (3.7) into (3.3), (3.5), and (3.6), we immediately have

$$\overline{\rho}_P = \rho_P(\overline{R}_{sef}) \tag{3.8}$$

and

$$\overline{D} = \mathcal{D}\left(\overline{R}_{sef}\right) \tag{3.9}$$

Next, for each of the $J$ simulations, the complement of $R_{sef}$ is defined as (Figure 3.2)

$$R^c_{sef}(j) \triangleq R_s - R_{sef}(j) \tag{3.10}$$

where $R_s = L_s/N$ and $N$ is the number of pixels in an image.

It is known that for most of the current embedded image coders, the bit significance reduces along the source bit stream. In fact, due to the convexity of the source codec rate-distortion function $\mathcal{D}(R)$, the additional distortion incurred by the stop-before-error strategy in a single trial can be expressed as (see Figure 3.2)

$$\Delta D(j) = \beta R^c_{sef}(j) + \delta D(j) \tag{3.11}$$

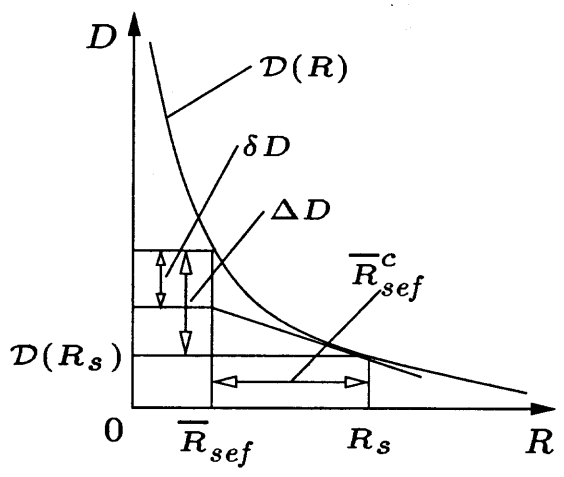


**Figure 3.2** Rate-Distortion analysis of embedded image sources

where

$$\beta = \left.\frac{d\mathcal{D}(R)}{dR}\right|_{R=R_s} \tag{3.12}$$

and $\delta D \geq 0$ reflects the fact that each subsequent bit lowers $\Delta D$ less (Figure 3.2). For a single experiment, the total distortion is $D(j) = \mathcal{D}(R_s) + \Delta D(j)$ and the average PSNR can now be expressed as

$$\overline{\rho}_P = \frac{10}{J}\sum_{j=1}^{J} \log \frac{\sigma_P^2}{\mathcal{D}(R_s) + \beta R^c_{sef}(j) + \delta D(j)} \tag{3.13}$$

Similarly, the PSNR obtained from $\overline{R}_{sef}$ can be expressed as

$$\rho_P\left(\overline{R}_{sef}\right) = 10 \log \frac{\sigma_P^2}{\mathcal{D}(R_s) + \beta \overline{R}^c_{sef} + \overline{\delta D}} \tag{3.14}$$

where $\overline{R}^c_{sef} = R_s - \overline{R}_{sef}$. Now consider the cases in which the channels are very clean. It will be seen later in this chapter that for very clean channels, the average error-free source coding rate $\overline{R}_{sef}$ is close to $R_s$. Thus, it is reasonable to assume that $\overline{\delta D} \to 0$ (Figure 3.2) and (3.11) can now be written as

$$\Delta D(j) = \beta \overline{R}^c_{sef}(j) \tag{3.15}$$

(3.15) means that in a small range near $R_s$, the convex function $\mathcal{D}(R)$ is approximately linear in its argument. Then $\log \frac{1}{\mathcal{D}(R)}$ or $\rho(R)$ is convex in $R$. Using Jensen's

inequality $E[f(X)] \geq f(E[X])$ [18], we have

$$\overline{\rho}_P \geq \rho_P\left(\overline{R}_{sef}\right) \tag{3.16}$$

with equality holds when the channel is noiseless. (3.16) means that for the embedded image bit streams transmitted over a specific channel, the PSNR obtained from average FEFRL is upper bounded by the average PSNR of FEFRLs.

Finally, for the general cases the assumption of (3.15) is not necessary. However, the relationship between (3.3) and (3.5) is not clear in those cases. It should also be noted that a direct comparison between (3.6) and $\mathcal{D}\left(\overline{R}_{sef}\right)$ would be more persuasive. Those are left as open problems.

## 3.2 Embedded Image Source Modeling

The rate-based system evaluation approach (3.4) provides a new and simple approach to solve the system performance optimization problem linked with progressive image transmission in noisy channels. The development of mathematical models for such an approach starts from the simplest case by setting up a scenario in which embedded source bit streams are transmitted over a BSC. The position of the first bit error is denoted as $k+1$. Obviously the first error-free run length (FEFRL) $L_{sef} \triangleq k$ of the bit stream is a random variable and its probability density can be described by the following bi-modal geometric distribution

$$p(k) = \begin{cases} (1-\epsilon)^k \epsilon & 0 \leqslant k < L_s \\ (1-\epsilon)^{L_s} & k = L_s \end{cases} \tag{3.17}$$

where $\epsilon$ is the bit error probability (or bit error rate (BER)) of the BSC, $L_s$ is the length of the source bit stream. With the probability distribution function (3.17), the mean $\mu$ and the variance $\sigma^2$ of the random variable FEFRL $L_{sef}$ can be easily

obtained as

$$\begin{cases} \mu &= E\left[L_{sef}\right] \\ &= \sum_{k=0}^{L_s} k\, p(k) \\ &= \frac{q}{(1-q)}\left(1-q^{L_s}\right) \\ &\triangleq \psi(q, L_s) \\ \sigma^2 &= E\left[L_{sef}^2\right] - \mu^2 \\ &= \sum_{k=0}^{L_s} k^2\, p(k) - \mu^2 \\ &= \frac{q}{(1-q)^2}\left\{1 - q^{L_s}\left[q^{L_s+1} + (1-q)(2L_s+1)\right]\right\} \end{cases} \tag{3.18}$$

where $q = 1 - \epsilon$. Compared to (3.2) and (3.3), the advantages of using $\overline{R}_{sef}$ to evaluate the system performance in Figure 1.1 is now obvious: it is independent of images and the performance of source codec, and in closed-form.

It is clear from (3.18) that both the average FEFRL $\overline{L}_{sef}$ (or $\mu$) and its standard deviation $\sigma$ are functions of the source bit stream length $L_s$ and the bit error rate $\epsilon$ of the BSC. Using (3.18), the statistics of the embedded image source transmitted over BSCs (with BER $\epsilon = \{10^{-1}, 10^{-2}, 10^{-3}\}$ and $\epsilon = \{10^{-5}, 10^{-6}\}$) without any protections are depicted in Figure 3.3(a) and (b), respectively. The source coding rate $R_s$ is selected to be in the range of 0.1 to 1 *bpp* for the two figures. As you can see from Figure 3.3(a), the percentages of error-free reception are higher for better channel conditions, which means better reconstructed image quality. It is also discovered from this figure that for a specific channel, the percentage of average FEFRL becomes higher at low bit rates. In other words, shorter source bit streams require less channel protection. This discovery can be exploited to further improve the system performance. In Figure 3.3(b), both the average FEFRLs and their standard deviations versus the total bit rate constraint $R_T$ are plotted. Obviously, for better channel conditions, not only the average FEFRLs becomes longer, their spreads also get tighter. Thus, maximization of the average FEFRL does secure best

system performance. It is also of interest to note that for BSCs with $\epsilon = 10^{-6}$, the whole bit stream is received almost error-free even without any channel protection.

From (3.18), it is easy to obtain

$$\begin{cases} \lim\limits_{\epsilon \to 0} \mu = L_s \\ \lim\limits_{\epsilon \to 0} \sigma = 0 \end{cases} \tag{3.19}$$

which correspond to our intuition that when a channel is noise-free, the whole bit stream transmitted over it will be received error-free.

## 3.3 EEP Optimization

It is clear from Figure 3.3(a) that channel protection is necessary for the embedded image bit streams transmitted in very noisy channels. A natural problem is how much protection should be provided under some bit rate constraint so that the overall system performance on a channel is the best possible? Within the scheme of Sherwood *et al.* [57], the source packet length and CRC code rate are fixed. So the only adjustable variable of the scheme is the RCPC code rate. Given some bit rate constraint on a channel, different RCPC code rate applied to the EEP scheme corresponds to different bit rate allocation strategy (Figure 3.4) which produces different source bit stream length. Thus, the best system performance is achieved with the RCPC code rate that gives out the highest average PSNR or the longest average FEFRL.

### 3.3.1 EEP Optimization Algorithm

The mathematical model of (3.18) can be used as the target function for the joint source-channel coding optimization problems linked with the EEP scheme. In such a scheme the RCPC code rate is an adjustable variable and the best PSNR performance of the whole system is achieved on a specific BSC when the optimal protection rate

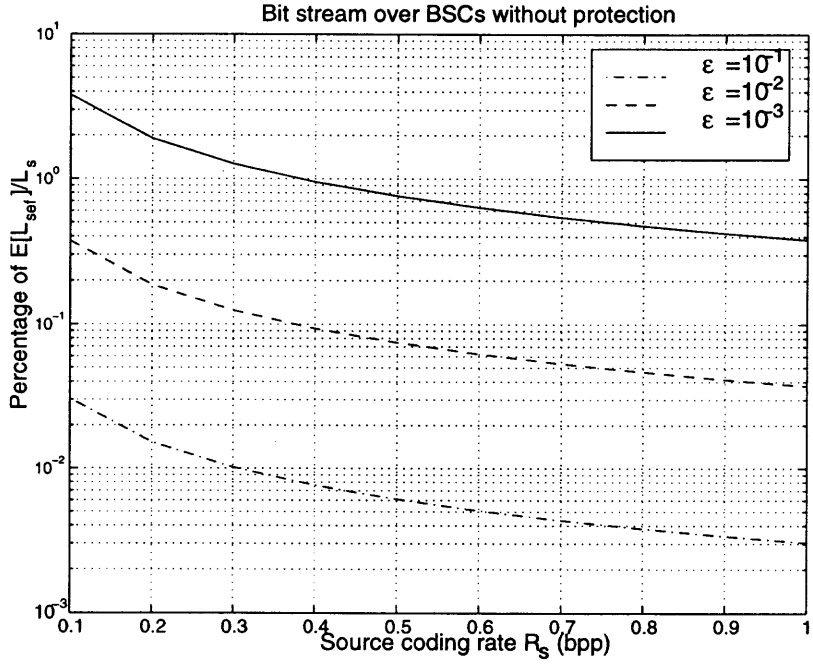


(a) $\frac{\overline{L}_{sef}}{L_s}\%$ for BSCs of $\epsilon = 10^{-1}, 10^{-2}, 10^{-3}$

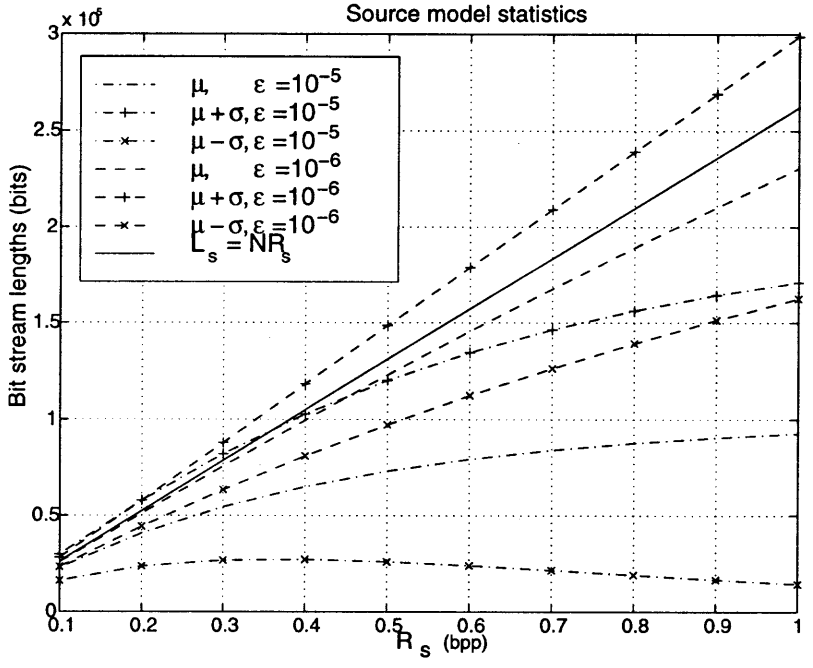


(b) $\overline{L}_{sef}$ and $\sigma$ for BSCs of $\epsilon = 10^{-5}, 10^{-6}$

**Figure 3.3** After-channel embedded source statistics

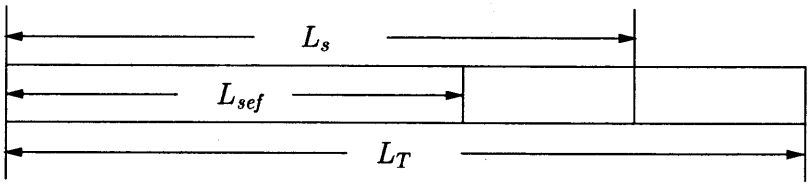


**Figure 3.4** Bit rate allocation

is used. Let $R_T$ be the total bit rate constraint in bit per pixel (*bpp*), $R_s$ and $R_c$ be the source and channel coding rates in *bit per pixel*, respectively. The rate $R_c$ is the number of redundant bits needed for CRC, RCPC, and the Viterbi algorithm flush. With the given RCPC code set on a specific BSC, the problem is to maximize the average PSNR (or minimize the average distortion) of the received image under the constraint of the total bit-rate with the given RCPC code rates $r_{RCPC_i} \in \mathcal{R}_{RCPC}$, i.e.

$$\hat{\rho}_P = \max_{R_s+R_c \leq R_T} \overline{\rho}_P \quad i = 1, 2, ..., |\mathcal{R}_{RCPC}| \tag{3.20}$$

where $\mathcal{R}_{RCPC}$ is the RCPC code rate set with size $|\mathcal{R}_{RCPC}|$. Note that $r_{RCPC_i}$ is unitless. On BSCs, (3.20) can be solved by Monte Carlo simulations using (3.3), as in [57, 35, 37, 5] due to the reason mentioned above.

On the other hand, (3.1) can be rewritten in the form of $\rho_P \triangleq g(R_{sef})$. Since $\mathcal{R}(D)$ is a non-increasing function of distortion $D$ [18], $\mathcal{D}(R_{sef})$ is also a non-increasing function of $R_{sef}$. Note that $\mathcal{D}(R_{sef}) > 0 \; \forall \, R_{sef}$, $\frac{1}{\mathcal{D}(R_{sef})}$ is a non-decreasing function of $R_{sef}$, and $\log(\cdot)$ is also a non-decreasing function, it can be concluded that $g(R_{sef})$ is a non-decreasing function of $R_{sef}$. Thus, (3.20) is equivalent to the following optimization problem

$$\hat{R}_{sef} = \max_{R_s+R_c \leq R_T} \overline{R}_{sef} \quad i = 1, 2, ..., |\mathcal{R}_{RCPC}| \tag{3.21}$$

Remember that the $\overline{R}_{sef}$ is now available in closed-form, and the source coding rate is constrainted by

$$R_s = r'_{CRC} \cdot r_{RCPCi} \cdot R_T \tag{3.22}$$

where

$$r'_{CRC} = \frac{b}{b+c+f} \tag{3.23}$$

is the equavalent CRC code rate and $r_{RCPCi} \in \mathcal{R}_{RCPC}$ are the RCPC code rates. Note that $b$, $c$, and $f$ are the source packet length, CRC code length for each packet, and the length of flush bits, respectively, all in bits. It is clear from (3.23) that any increase in block length $b$ will result in a higher equivalent CRC code rate, i.e.

$$\lim_{b\to\infty} r'_{CRC} = 1 \tag{3.24}$$

This higher equivalent CRC code rate will turn into longer source bit stream length. Under the assumption that the CRC code will detect all the residual errors, the increase in $b$ eventually turns into better system performance. Thus, a fair comparison between different optimization techniques requires identical channel conditions, bit rate constraint, and block length $b$.

Substitution of (3.22) into (3.18) yields

$$\overline{R}_{sef} = \frac{q}{(1-q)}\left(1 - q^{r'_{CRC} r_{RCPCi} L_T}\right) \tag{3.25}$$

where $q = 1 - \epsilon$, $\epsilon$ is the effective BER provided by the RCPC code rate $r_{RCPCi}$ and $R_T$ is the bit rate constraint. With (3.25), the average FEFRL becomes a function of the RCPC code rate and the the total bit rate constraint $R_T$. Thus, (3.21) can be easily solved by the following numerical method,

$$\hat{r}_{RCPC} = \arg\min_{R_T}\left\{\max_{R_s+R_c\leq R_T} \overline{R}_{sef}\right\} \tag{3.26}$$

The results obtained from (3.26) is the strongest code on that channel so that the longest bit streams can be received optimally. It is already known from a previous section that the optimal protection levels might be different for bit streams with different lengths. Thus, it might not be optimal for shorter bit streams transmitted over that channel. If the performance is optimized for each individual bit

rate constraint $R_T$, i.e.,

$$\hat{r}_{RCPC}(R_T) = \arg \max_{R_s+R_c \leq R_T} \overline{R}_{sef} \tag{3.27}$$

thus, the optimal protection levels might differ on a channel and it is called a dynamic EEP (dEEP) scheme.

### 3.3.2 Simulation Results and Discussions

It is now clear that for the progressive image transmission system depicted in Figure 1.1, its performance can be either the conventional average PSNR or the PSNR obtained directly from the average FEFRL. Both of the methods were tested with SPIHT on three BSCs $\epsilon = 10^{-\{1,2,3\}}$. The RCPC code set used in the simulation is selected from [24] with rates $\mathcal{R}_{RCPC} = \{\frac{8}{32}, \frac{8}{31}, ..., \frac{8}{9}\}$. The total bit rate constraint $R_T$ is in the range of $[0.1, 1.0](bpp)$. The source bit packet length $b$, number of CRC bits $c$ and flush bits $f$ are 200, 16, and 6, respectively. In the analysis and simulations, it was assumed that the probability of an undetected error after RCPC and CRC decoding is zero.

For the three BSCs, the source coding rates $R_s$ and $\overline{R}_{sef}$ versus the RCPC code rate indexes are plotted in Figure 3.5 using (3.22) and (3.25), respectively. In Figure 3.5(a) and (b), it can be seen that the average FEFRLs increase with stronger protection levels (here represented by higher code rate indexes). At some point, the average FEFRLs begin to decrease. This is because the bit stream is already overprotected, or in other words, too much bit rate has been allocated for channel protection. Obviously, when the source bit stream is optimally or over protected, we have $\overline{R}^c_{sef}(j) \rightarrow 0$ which justifies our expectation. It is also apparent that the optimal RCPC code rates are higher for smaller bit rate constraint or shorter bit streams. Thus, the performance can be further improved by assigning higher code rate at low bit rates. For the BSC with BER equals $10^{-3}$, the weakest RCPC code

rate will provide the optimal protection (Figure 3.5(c)). Stronger codes will result in overprotection and performance degradation.

For the EEP scheme, the optimal code rates obtained by both of these two methods for the 3 BSCs are listed in Table 3.1 and plotted in Figure 3.7(a). The equivalence of the maximization of $\overline{R}_{sef}$ and average PSNR for such optimization problems is justified by the identical optimal code rate obtained for each channel. The curve in Figure 3.7(a) is a general guideline for selecting optimal protection levels on a class of BSCs satisfying $10^{-3} \leq \epsilon \leq 10^{-1}$.

| Channels | $10^{-1}$ | $10^{-2}$ | $10^{-3}$ |
|---|---|---|---|
| Sherwood et al. [57] | 8/27 | 8/12 | 8/9 |
| Proposed method | 8/27 | 8/12 | 8/9 |

**Table 3.1** Optimal code rate comparison

The experiments of [57] were then repeated with 1000 Monte Carlo simulations on the three BSCs using *LENA* and *GOLDHILL* images and SPIHT without arithmetic coding. The PSNR results are depicted in Figure 3.6 together with those by the proposed method. It is seen from Figure 3.6 that in BSCs $\epsilon = 10^{-\{1,2\}}$, PSNR performances by the proposed method are almost identical with, or even slightly better than those from Monte Carlo simulations. The experiment results can be explained as follows. In the Monte Carlo simulations of [57] and this dissertation, the decoding stopped before the block with the first bit error. Usually, some error-free bits in that block have to be discarded. Obviously, the new method takes some advantages over the conventional one in this aspect. For the BSC of $\epsilon = 10^{-3}$, the bit stream is almost error-free after RCPC decoding. The two identical curves in Figure 3.6 correspond to the equalities of (3.8) and (3.9).

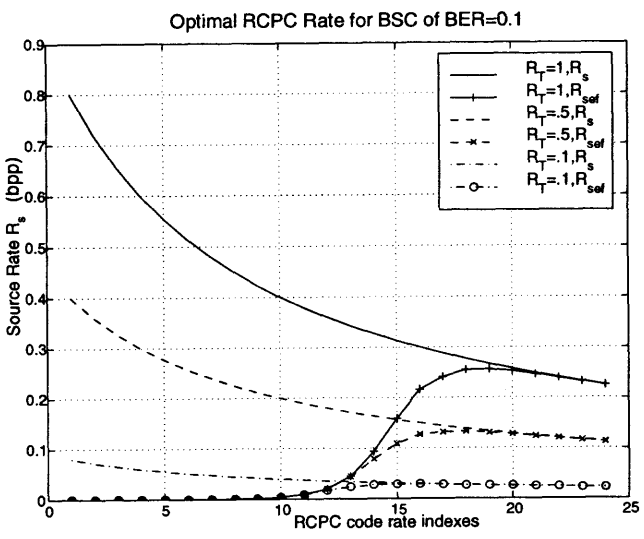


(a) BSC of $\epsilon = 10^{-1}$

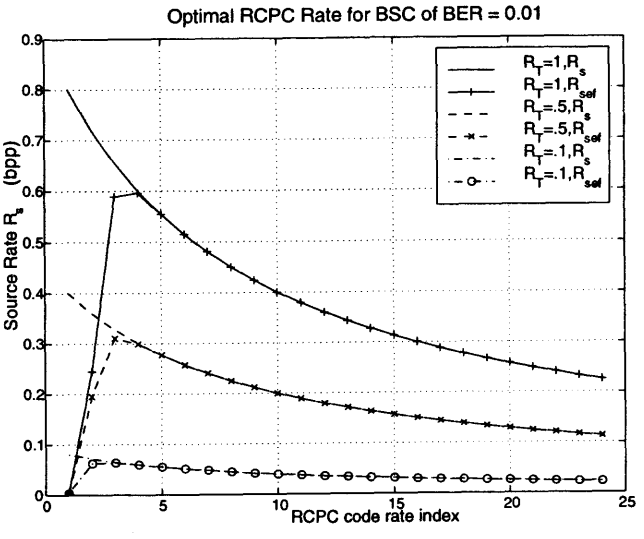


(b) BSC of $\epsilon = 10^{-2}$

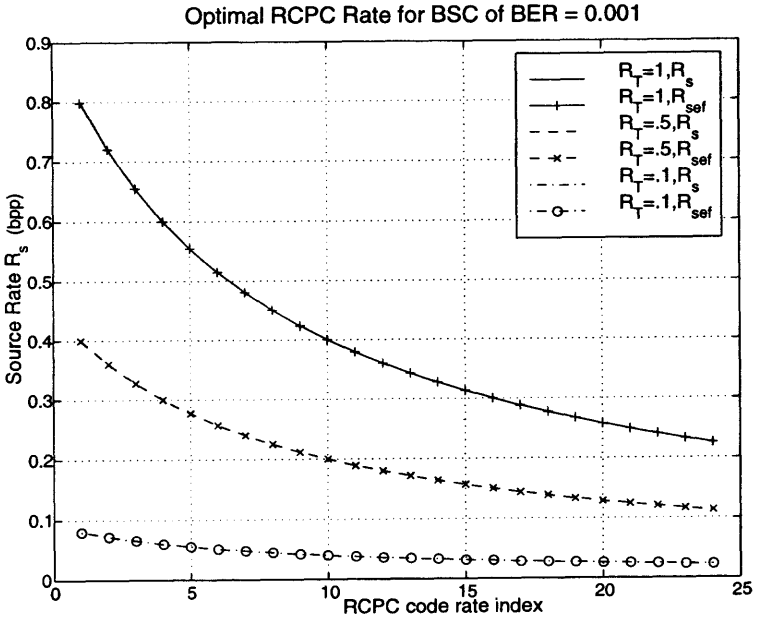


(c) BSC of $\epsilon = 10^{-3}$

**Figure 3.5** Results of RCPC code rate optimization

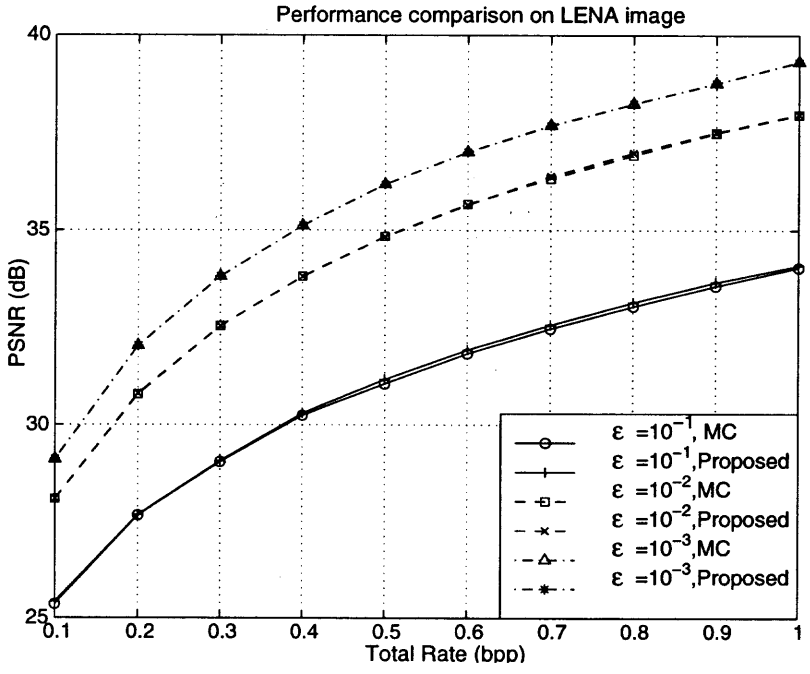


(a) LENA

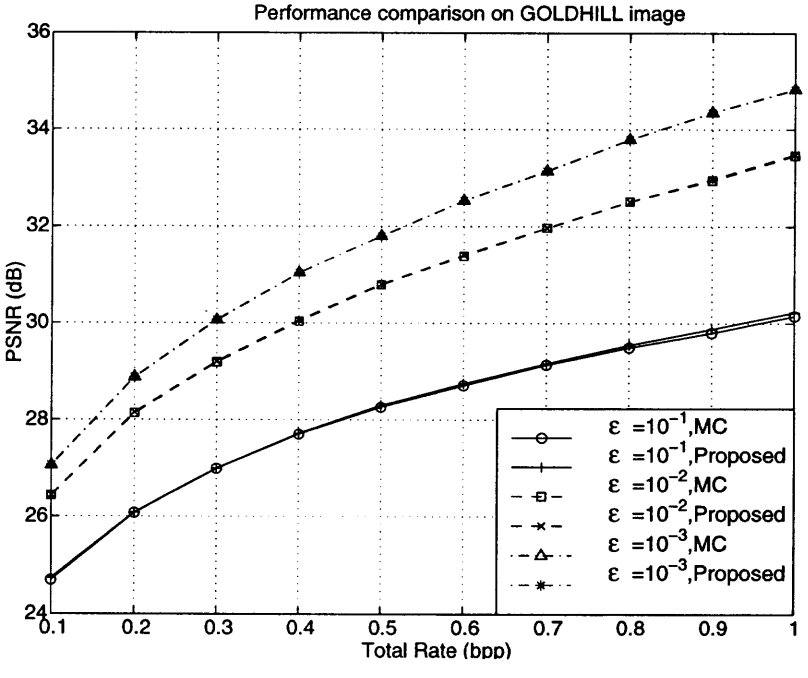


(b) GOLDHILL

**Figure 3.6** PSNR comparisons of the two methods

Dynamic EEP schemes were also implemented by assigning higher optimal code rates for lower bit constraints and tested them in the BSCs $\epsilon = 10^{-\{1,2\}}$. The optimal protection rate profiles for the two BSCs are plotted in Figure 3.7(b). For each BSC, the different optimal RCPC code rate for the corresponding bit rate constraint $R_T$ are obtained using (3.27). It is clear that for lower bit rate constraint or shorter bit streams, the optimal protections are indeed weaker. All the PSNR results for this simulation are obtained using (3.5) and depicted in Figure 3.8. It can be seen that the PSNR improvement of the dynamic EEP scheme over the EEP scheme [57] is up to 0.3 $dB$. Moreover, such a dEEP scheme can be overhead-free compared to the EEP scheme since the protection profiles can be easily stored in both the transmitters and receivers.

## 3.4 Progressive UEP Schemes

One important feature of the fully embedded image sources is that the bit importance decreases along the bit streams. Thus, by reducing the protection levels for the later part of the bit stream properly, the performance of the optimal EEP scheme might be further improved since more source bits can be transmitted and received correctly. It is apparent that such a UEP scheme is still progressive in nature and the different protection levels turn the effective channel (as seen to the left of point B in Figure 1.1) into a deterministic time-varying one (Figure 3.9). Without lost of generality, consider an $M$ level progressive UEP scheme where $M \leq |\mathcal{R}_{RCPC}|$. The total bit stream length is first divided into $M$ partitions, then each partition is assigned a different protection rate. In order to achieve the best possible system performance under UEP in the sense that the average FEFRL is maximized, both the partition points and the protection rates for each of the bit streams partitions should be optimized. Furthermore, the optimal partition points and protection levels need

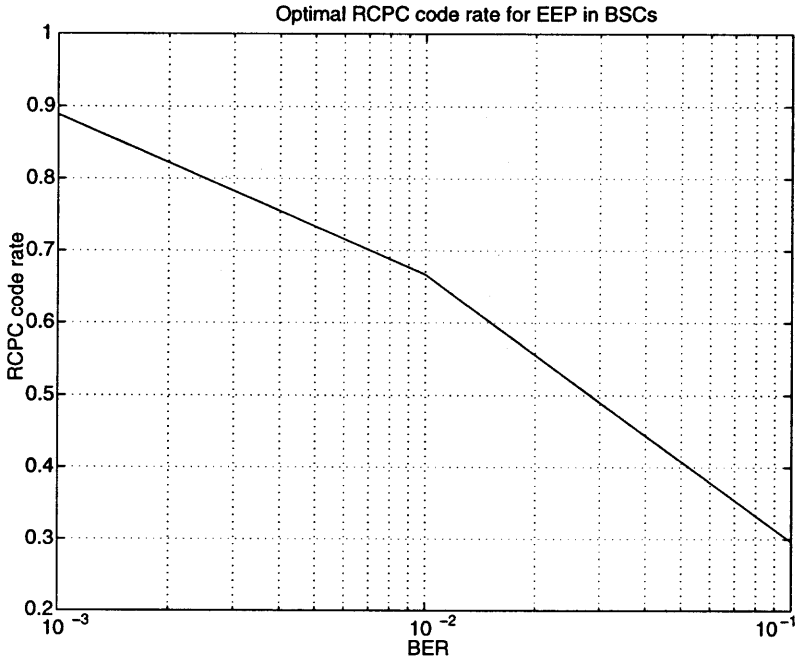


(a) Optimal EEP protections

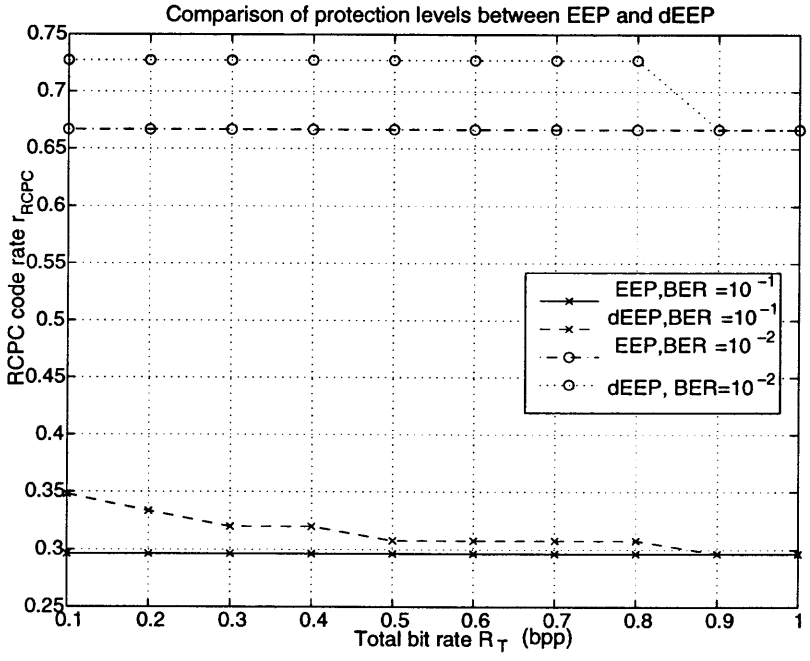


(b) EEP and dEEP comparisons

**Figure 3.7** Optimal protections for EEP and dEEP

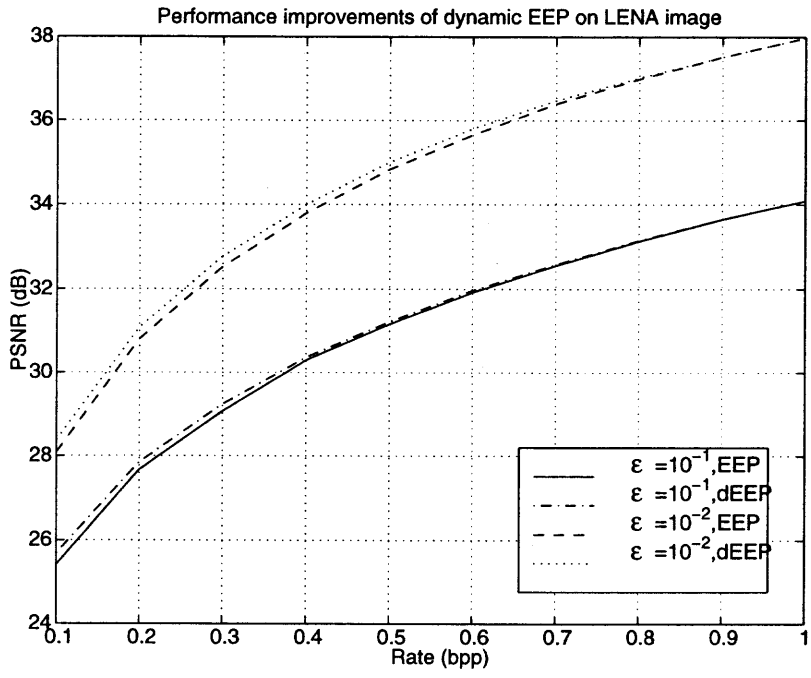


(a) LENA

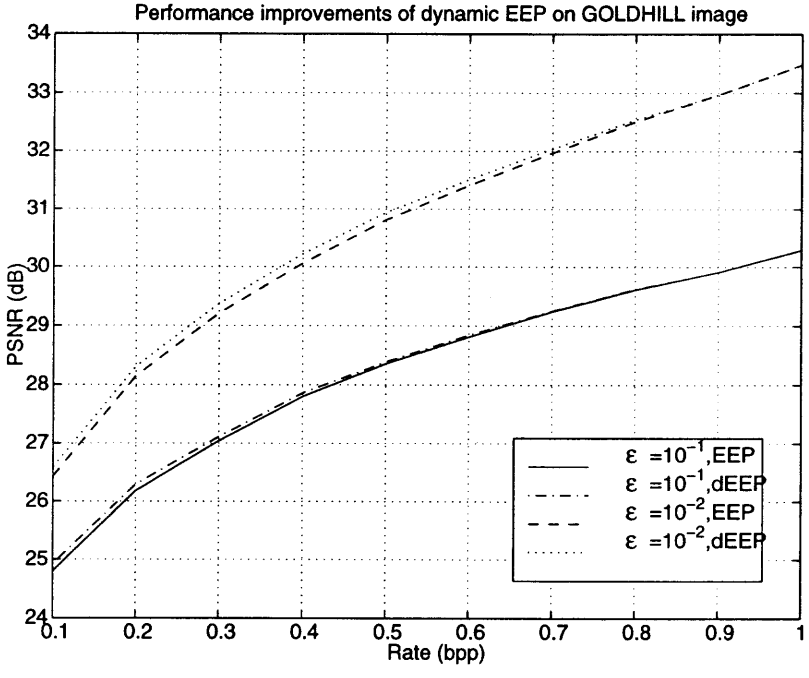


(b) GOLDHILL

**Figure 3.8** PSNR improvements of the dynamic EEP scheme over the EEP scheme on SPIHT

to be transmitted to the receivers in the headers so that the decoders know where and how to switch among the available channel coding rates. Obviously, the increase in the number of protection levels will result in the increase in the amount of side information to be carried in the bit stream header, which may eventually consume all the UEP gains from the optimization of the partition points and protection levels. Thus, the optimization problem of progressive UEP under some bit rate constraint on a specific channel is threefold,

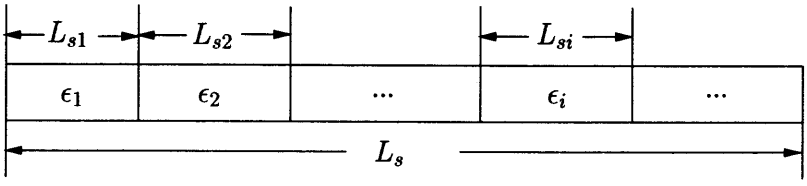


**Figure 3.9** Deterministic time-varying channel model for $M$-rate progressive UEP schemes

1. How many protection levels are optimal?

2. For an $M$-rate UEP, how to partition the bit stream optimally with $M-1$ partition points?

3. For a specific partition, what is the optimal code rate set for that UEP?

Obviously, the complete solutions should provide optimal results for all three problems simultaneously.

The performance optimization for UEP schemes on BSCs has been tackled with both distortion-based [36] and rate-based [12] approaches, on problem 3 only. Solution on problem 2 is usually *ad hoc* and problem 1 is never defined explicitly before. In this section, with the rate-based performance evaluation approach proposed in previous sections, a closed-form embedded image source model for UEP is developed, and complete solutions are obtained for all three UEP optimization problems on BSCs.

### 3.4.1 After-channel Source Models

For such a challenging problem, the analysis starts from the simplest UEP scheme, i.e., the 2-rate case. First consider a BSC with bit error probability $\epsilon$ and source bit streams with length $L_s$ to be transmitted over it. Under equal error protection, the average FEFRL $\overline{L}_{sef}$ can be expressed as in Section 3.2:

$$\begin{aligned} \overline{L}_{sef} &= \frac{q}{1-q}\left(1-q^{L_s}\right) \\ &\triangleq \psi(q, L_s) \end{aligned} \tag{3.28}$$

where $q \triangleq 1-\epsilon$.

For the 2-rate UEP schemes, the two distinctive RCPC code rates generate two 'effective' BSCs as seen by the source bit streams (see Figure 3.10). With the FEFRL model in mind the probability distribution for the position of the first bit error in the bit stream can be expressed as

$$p(k) = \begin{cases} (1-\epsilon_1)^k \epsilon_1 & 0 \leqslant k < L_{s1} \\ (1-\epsilon_1)^{L_{s1}}(1-\epsilon_2)^{k-L_{s1}}\epsilon_2 & L_{s1} \leqslant k < L_s \\ (1-\epsilon_1)^{L_{s1}}(1-\epsilon_2)^{L_{s2}} & k = L_s \end{cases} \tag{3.29}$$

where $\epsilon_1$ and $\epsilon_2$ are the 'effective' BERs provided by the corresponding RCPC code rate $r_{RCPC1}$ and $r_{RCPC2}$, respectively, and

$$\begin{cases} L_{s1} &= r'_{CRC} \cdot r_{RCPC1} \cdot L_1 \\ L_{s2} &= r'_{CRC} \cdot r_{RCPC2} \cdot (L_T - L_1) \end{cases}$$

The average FEFRL can then be obtained from its probability density function (3.29) as

$$\begin{aligned} \overline{L}_{sef} &= \sum_{k=0}^{L_s} k p(k) \\ &= \psi(q_1, L_{s1}) + q_1^{L_{s1}} \psi(q_2, L_{s2}) \end{aligned} \tag{3.30}$$

where $L_{s1} + L_{s2} = L_s$.

For $M$-rate UEP schemes under some total bit rate constraint $R_T$, the corresponding bit stream length $L_T = NR_T$ is partitioned into $M$ sections with $L_T =$

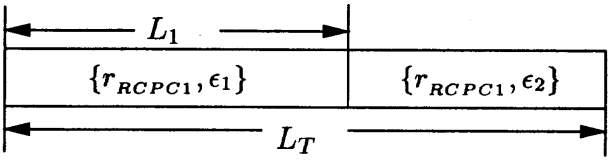


**Figure 3.10** Bit stream partition for 2-rate UEP schemes

$\sum_{i=1}^{M} L_i$, where $N$ is the number of pixels in an image. Each of the partitions $L_i$ is then protected by a distinctive RCPC code with rate $r_{RCPCi} \in \mathcal{R}_{RCPC}$. The source bit partition lengths are constrained by

$$\sum_{i=1}^{M} L_{si} = L_s$$

where

$$L_{si} = r'_{CRC} \cdot r_{RCPCi} \cdot L_i$$

The expression of $\overline{L}_{sef}$ for 2-rate UEP can be easily generalized to the $M$-rate cases as

$$\overline{L}_{sef} = \sum_{i=1}^{M} q_{i-1}^{L_{si-1}} \cdots q_{M-1}^{L_{sM-1}} \psi(q_i, L_{si}) \tag{3.31}$$

where $q_i = 1 - \epsilon_i$, $L_{s0} \triangleq 0$, and

$$\sum_{i=1}^{M} L_{si}/(r'_{CRC} \cdot r_{RCPCi}) = L_T \tag{3.32}$$

It can be verified from (3.31) that

$$\lim_{\{\epsilon_i\} \to 0} \overline{L}_{sef} = \sum_{i=1}^{M} L_{si} = L_s \tag{3.33}$$

which justifies our intuition that the whole bit stream is error-free when the channel is noiseless.

### 3.4.2 UEP Optimization

As in the previous subsection, optimization attempts start from the simplest 2-rate UEP case. Let $R_T$ be the total bit rate, $R_s$ and $R_c$ be the source and channel

coding rates, respectively. The optimal partition point $\hat{L}_1$ and the optimal code rate pair $\{\hat{r}_{c1}, \hat{r}_{c2}\}$ are to be found such that the $\overline{L}_{sef}$ is maximized, i.e.

$$\hat{L}_{sef} = \max_{R_s+R_c \leq R_T} \overline{L}_{sef} \tag{3.34}$$

For 2-rate cases. The optimal tri-tuple for 2-rate UEP in the bit rate range is

$$\left\{\hat{L}_1, \hat{r}_{c1}, \hat{r}_{c2}\right\}_{R_T}^{ch} = \arg\max_{L_1} \left\{ \max_{R_s+R_c \leq R_T} \overline{L}_{sef} \right\} \tag{3.35}$$

Such tri-tuples can be obtained by the following optimization algorithm:

1. search for $\{\hat{r}_{c1}, \hat{r}_{c2}\}_{L_1}$ on $\{\mathcal{R}_{RCPC} \times \mathcal{R}_{RCPC}\}$ for all possible partitions satisfying $0 \leq L_1 \leq L_T$,
2. repeat 1 for designated $R_T$ for $\left(\hat{L}_1, \hat{r}_{c1}, \hat{r}_{c2}\right)_{R_T}^{ch}$.

For 3-rate UEP, the optimal partition pair $\{\widehat{L}_1, \widehat{L}_2\}$ and the optimal RCPC code rate tri-tuple $\{\widehat{r}_{ci}, i = 1, 2, 3\}$ are needed to be found such that the $\overline{L}_{sef}$ is maximized, i.e.

$$\widehat{L}_{sef} = \max_{R_s+R_c \leq R_T} \overline{L}_{sef} \tag{3.36}$$

under the constraints $L_1 < L_2$ and $r_{c1} < r_{c2} < r_{c3}$. It can be solved by by the following optimization algorithm:

1. Code rate tri-tuple $\{\tilde{r}_{ci}\}_{\{L_1,L_2\}}$ optimization: under the constraints of $R_s+R_c \leq R_T$, $r_{c1} < r_{c2} < r_{c3}$, and $0 \leq L_1 \leq L_2 \leq L_T$,

$$\{\tilde{r}_{ci}\}_{\{L_1,L_2\}} = \arg\left\{ \max_{R_s+R_c \leq R_T} \overline{L}_{sef} \right\} \tag{3.37}$$

for a specific partition set $\{L_1, L_2\}$,

2. Partition pair optimization: under the constraint of $0 \leq L_1 < L_2 \leq L_T$,

$$\left\{\widehat{L}_1, \widehat{L}_2, \widehat{r}_{ci}\right\} = \arg\left\{ \max_{R_s+R_c \leq R_T} \overline{L}_{sef} \left( \{\tilde{r}_{ci}\}_{\{L_1,L_2\}} \right) \right\} \tag{3.38}$$

3. repeat 1, 2 for designated $R_T$.

### 3.4.3 Necessary Condition for UEP Gain

It is desirable to use UEP schemes only when some gains in the form of

$$\Delta\hat{L}_{sef} = \hat{L}_{sef}^{UEP} - \hat{L}_{sef}^{EEP} > 0 \tag{3.39}$$

exists, i.e. better than the optimal EEP scheme. This is because the design and implementation of UEP schemes will eventually consume additional system resources in the form of overhead and complexity. Suppose bit rate constraint $R_T$, an RCPC code rate set $\mathcal{R}_{RCPC}$, and a specific channel are given, with $r_{RCPC_K}$ as the highest rate code in the code rate set and optimal protection rate $\hat{r}_{RCPC}$ for EEP scheme on that channel, a necessary condition for such UEP gain on a specific channel is given in the following proposition:

**Theorem 1** *For a given $\mathcal{R}_{RCPC}$, the necessary condition for the existence of UEP gain over optimal EEP scheme $\Delta\hat{L}_{sef} > 0$ is $\exists R_T \in [R_{\min}, R_{\max}]$ under which $\hat{r}_c < r_{c_K}$ on that binary symmetric channel.*

**Proof** : Consider an optimal EEP scheme with $\hat{r}_c = r_{c_K}\ \forall R_T \in [R_{\min}, R_{\max}]$ on a channel, we have

$$\hat{L}_{sef}^{EEP} = \psi\left(q_K, L_s\right) \tag{3.40}$$

and obviously

$$\psi\left(q_K, L_s\right) > \psi\left(q_i, L_s'\right) \tag{3.41}$$

where $L_s$ and $L_s'$ are obtained under the same rate constraint $R_T$. It is also easy to verify the following fact for the channel which will be used in later proof

$$q_K^{L_s} \cong 1 \tag{3.42}$$

For the same $R_T$, assume we have a 2-rate optimal UEP scheme by partitioning $L_T$ into

$$L_T = L_1 + L_2 \tag{3.43}$$

and the maximum error-free bit stream length is

$$\hat{L}_{sef}^{UEP} = \psi(q_i, L'_{s1}) + q_i^{L'_{s1}} \psi(q_j, L'_{s2}) \tag{3.44}$$

where $L'_{s1} = r'_{CRC} r_{c_i} L_1$ and $L'_{s2} = r'_{CRC} r_{c_j} L_2$. Now for the partition in (3.43),(3.40) can be rewritten in the following form

$$\hat{L}_{sef}^{EEP} = \psi(q_K, L_{s1}) + q_K^{L_{s1}} \psi(q_K, L_{s2}) \tag{3.45}$$

where $L_{s1} = r'_{CRC} r_{c_K} L_1$ and $L_{s2} = r'_{CRC} r_{c_K} L_2$. Since $q_K < q_i < 1$ and $L'_{s1} < L_{s1}$, it is apparent that

$$q_K^{L_{s1}} < q_i^{L'_{s1}} < 1 \tag{3.46}$$

Combining (3.40), (3.41), (3.44), (3.45), and (3.46), $\hat{L}_{sef}^{UEP} - \hat{L}_{sef}^{EEP} < 0$ is apparent. Furthermore, such derivation can be easily generalized to the $M$-rate UEP cases. □

### 3.4.4 Upper Bounds for UEP Gain

When the necessary condition for UEP gain is satisfied, there might be some gain to be achieved through the use of multiple rate UEP schemes. Obviously such UEP gains are not unlimited because the protection levels can not be relaxed without restriction and the number of available code rates are constrained by the code set. Theoretical performance upper bound is desirable and helpful in the UEP scheme design. Under some bit rate constraint $R_T$, consider an optimal $M \geq 2$ rate UEP scheme with optimal code rate set $\{\widehat{r}_{c1}, ..., \widehat{r}_{cM}\} \in \mathcal{R}_{RCPC}$, where $\widehat{r}_{c1} < ... < \widehat{r}_{cM}$, the average FEFRL can be expressed as

$$\widehat{L}_{sef}^{UEP} = \sum_{i=1}^{M} q_{i-1}^{L_{si-1}} \cdots q_{M-1}^{L_{sM-1}} \psi(q_i, L_{si}) \tag{3.47}$$

where $q_i = 1 - \epsilon_i$, $L_{s0} \triangleq 0$. Define $r_{\min} \triangleq \widehat{r}_{c1}$ and $r_{\max} \triangleq \widehat{r}_{cM}$. The average FEFRL for EEP scheme under the same bit rate constraint $R_T$ is

$$\overline{L}_{sef}^{EEP} = \psi\left(q_{\max}, L_{s\max}\right) \tag{3.48}$$

(3.48) can be rewritten in the following form according to the optimal partition $\{\widehat{L}_i\}$ for (3.47) as

$$\overline{L}_{sef}^{EEP} = \sum_{i=1}^{M} q_{\max}^{L_{si-1}\max} \cdots q_{\max}^{L_{sM-1}\max} \psi(q_{\max}, L_{si\max}) \tag{3.49}$$

where $q_{\max} = 1 - \epsilon_{\min}$, $L_{s0\max} \triangleq 0$, and $L_{si\max} = r'_{CRC} L_i r_{\max}$. It is apparent that

$$\begin{cases} q_{\max} & \geq & q_i \\ L_{si\max} & \geq & L_{si} \end{cases} \tag{3.50}$$

From (3.18), it is easy to obtain

$$\begin{cases} \dfrac{\partial \psi(q, L_s)}{\partial q} & > & 0 \\ \dfrac{\partial \psi(q, L_s)}{\partial L_s} & > & 0 \end{cases} \tag{3.51}$$

Thus,

$$\psi\left(q_{\max}, L_{si\max}\right) > \psi\left(q_i, L_{si}\right) \tag{3.52}$$

The following fact can be verified by simulations

$$q_{\max}^{L_{si\max}} \geq q_i^{L_{si}} \tag{3.53}$$

Combining (3.47), (3.49), (3.52), and (3.53), we have the following upper bound for UEP gains

$$\widehat{L}_{sef}^{UEP}\left(\{q_i\}, \{L_{si}\}\right) < \overline{L}_{sef}^{EEP}(q_{\max}, L_{s\max}) \tag{3.54}$$

on a specific BSC under the bit rate constraint $R_T$.

### 3.4.5 Side-information and Overhead

For an M-rate UEP scheme to work properly, some additional side information such as the partition points and the protection levels need to be transmitted in the source header so that the receiver knows where and how to switch among RCPC code rates along the bit stream. To reduce the amount of overhead, the length of the first and

the second partitions for two- and three-rate UEP schemes are transmitted. Since the source bits are divided into packets, those lengths may be represented in terms of number of packets, thus at most 10 and 5 bits are enough for the first and the second partitions, respectively. In order to send the the RCPC code rate information to the decoder, it is assumed that all the optimal RCPC code rate pairs and tri-tuples are known to both the encoder and the decoder. Such an assumption is reasonable because the optimization results are independent of training images. Thus, only the sequential numbers of the possible optimal pairs and tri-tuples are coded for a specific channel.

### 3.4.6 Simulation Results and Discussions

First, the performance of the the proposed 2-rate dynamic UEP scheme was tested over 3 BSCs with $\epsilon = 10^{-1}$, $10^{-2}$, and $10^{-3}$, respectively. To illustrate the process of optimal tri-tuple searching, the $\overline{L}_{sef}$ at $R_T = 0.2$ *bpp* for the BSC of BER=0.1 is plotted in Figure 3.11(a). Note that the code pair for each point on that curve is optimized. It can be seen that $\overline{L}_{sef}$ does not increase with $L_1$ monotonically. For a specific bit rate constraint, the optimal partition point $\hat{L}_1$ is the peak of the curve. The optimal RCPC code rate pair is the one linked with the peak point. The optimal code pairs for BSCs of $\epsilon = 10^{-1}$ and $10^{-2}$ obtained this way are listed in Table 3.2. Note that there are at most 3 code pairs for each of the channel. Thus, 2 bits are enough to inform the decoder how to switch between the RCPC code rates. Although no explicit constraints are put on the relationship between $r_{RCPC1}$ and $r_{RCPC2}$ in the simulation, $r_{RCPC1} < r_{RCPC2}$ for optimal protection is eventually satisfied. That corresponds to our intuition that important bits at the beginning part of the bit stream should be protected heavily. In fact, such constraint is implied in the maximization of $\overline{L}_{sef}$ and all the weights of $q_i^{L_i}$'s in (3.31). For BSC of $\epsilon = 10^{-3}$,

the 2-rate UEP scheme degenerates into an EEP one, because the necessary condition for UEP gain is not satisfied anymore.

| BER | $R_T(bpp)$ | .1 | .2 | .3 | .4 | .5 | .6 | .7 | .8 | .9 | 1 |
|---|---|---|---|---|---|---|---|---|---|---|---|
| $\epsilon =$ | $\hat{r}^1_{RCPC1}$ | 24 | 24 | 26 | 26 | 26 | 26 | 27 | 27 | 27 | 27 |
| $10^{-1}$ | $\hat{r}^1_{RCPC2}$ | 22 | 22 | 24 | 24 | 24 | 24 | 24 | 24 | 24 | 24 |
| $\epsilon =$ | $\hat{r}^2_{RCPC1}$ | 11 | 11 | 11 | 11 | 11 | 12 | 12 | 12 | 12 | 12 |
| $10^{-2}$ | $\hat{r}^2_{RCPC2}$ | 10 | 10 | 10 | 10 | 10 | 11 | 11 | 11 | 11 | 11 |

**Table 3.2** Optimal 2-rate UEP code pairs for BSCs $10^{-1}, 10^{-2}$ (denominators only, numerators = 8)

The partition results for 2-rate UEP schemes on BSC of $\epsilon = 10^{-1}$ and $10^{-2}$ are depicted in Figure 3.12. It is apparent that the number of source bits under weaker protections are small, especially for very noisy channel conditions.

The 3-rate UEP scheme is then tested on BSCs $\epsilon = 10^{\{-1,-2\}}$. The optimal RCPC code rate tri-tuples for those two BSCs are listed in Table 3.3. Again, the constraint of $\widehat{r}_{RCPC1} < \widehat{r}_{RCPC2} < \widehat{r}_{RCPC3}$ was not imposed in the simulations. But the results for the optimal protection schemes always satisfy the constraint. Thus, the necessary condition for UEP optimality is justified. It can also be seen that for the BSC with $\epsilon = 10^{-2}$, only two rates are present until $R_T = 0.5$ $(bpp)$. This is due to the fact that there is no UEP gain for the 3-rate scheme over the 2-rate one at low bit rates. Since there are at most 4 code rate tri-tuples for those two BSCs, a total of 17 bits overheads will provide all the necessary side information for the decoder.

For the BSC of $\epsilon = 10^{-1}$, the optimization result at $R_T = 0.6$ $(bpp)$ is illustrated in Figure 3.11(b). Due to the constraint of $L_1 < L_2$, no searching is done in the area of $L_1 \geq L_2$ and the computational burden is reduced by half. For each point on the surface, there is a corresponding RCPC code rate tri-tuple and this tri-tuple has been optimized. By reaching the highest point of the surface and getting its coordinates and the corresponding optimal code rate tri-tuple for that point, optimization is done for the current bit rate constraint.

The optimal partitions for the 3-rate UEP scheme on BSC of BER=0.1 are depicted in Figure 3.13(a). The conclusions can be drawn from this figure are two-fold. First, for the optimal UEP schemes, the strongest protection levels should never exceed what is optimal for EEP schemes. Second, weaker protections should be provided near the end of the source bit streams. Thus, the prevailing *ad hoc* practice of providing heavier protections for the beginning part of the source bit streams will result in performance penalty. It is of interests to note the correspondence between protection level changes and partition fluctuations at $R_T = 0.2$ and $0.7(bpp)$. Protection levels of EEP and UEP schemes are compared in Figure 3.13(b). The relaxation of the protection levels of the optimal dynamic schemes is quite obvious, especially at low bit rates.

The gains of dynamic EEP, 2- and 3-rate UEP schemes over EEP schemes for the two BSCs are depicted in Figure 3.14. One important observation from this comparison is that the gains of the 3-rate schemes over 2-rate ones are marginal for both of those two BSCs. In fact, there is no gain at all in the BSC of $\epsilon = 10^{-2}$ for bit rates below $R_T = 0.5(bpp)$. This corresponds to the results listed in Table 3.3. With such observations, it may be concluded that for BSCs satisfying $\epsilon \leq 10^{-1}$, at most three rates are enough to achieve almost all the gains with a dynamic UEP scheme. Two rate UEP scheme is an appropriate choice for those BSCs .

| BER | $R_T(bpp)$ | .1 | .2 | .3 | .4 | .5 | .6 | .7 | .8 | .9 | 1 |
|---|---|---|---|---|---|---|---|---|---|---|---|
| $\epsilon = 10^{-1}$ | $\widehat{r}^1_{RCPC1}$ | 24 | 25 | 26 | 26 | 26 | 26 | 27 | 27 | 27 | 27 |
| | $\widehat{r}^1_{RCPC2}$ | 23 | 24 | 24 | 24 | 24 | 24 | 26 | 26 | 26 | 26 |
| | $\widehat{r}^1_{RCPC3}$ | 21 | 22 | 22 | 22 | 22 | 22 | 24 | 24 | 24 | 24 |
| $\epsilon = 10^{-2}$ | $\widehat{r}^2_{RCPC1}$ | 11 | 11 | 11 | 11 | 11 | 12 | 12 | 12 | 12 | 12 |
| | $\widehat{r}^2_{RCPC2}$ | 10 | 11 | 11 | 11 | 11 | 11 | 11 | 11 | 11 | 11 |
| | $\widehat{r}^2_{RCPC3}$ | 10 | 10 | 10 | 10 | 10 | 10 | 10 | 10 | 10 | 10 |

**Table 3.3** Optimal 3-rate UEP RCPC code rate tri-tuples for BSCs $\epsilon = 10^{\{-1,-2\}}$ (denominators only, numerators = 8)

Using LENA image, PSNR performances of SPIHT without arithmetic coding are obtained for both EEP and 3-rate dynamic UEP schemes over the two BSCs.

The results and the upper bounds obtained from (3.54) are depicted in Figure 3.14. Performance improvements over EEP schemes under the same channel conditions and bit rate constraint are around 0.3 $dB$.

Based on the simulation results, the answers to the three questions on progressive UEP scheme optimization at the beginning of this section are as following,

1. For a large class of BSCs with BER satisfying $\epsilon \leq 10^{-1}$, the optimal number of UEP levels is 3!

2. For optimal UEP schemes, protection relaxation usually happens late in the bit stream,

3. Optimal code rates can never be lower than those for optimal EEP scheme on that channel.

## 3.5 UEP with Bit Class Demultiplexing

Various strategies have been devised to improve the robustness of EZW-based bit-streams. The demultiplexing of EZW bit-streams belonging to the different spatial regions of an image makes channel errors localize within the corresponding regions of the reconstructed image. It is shown that this introduces resilience [19]. Such spatially oriented sub-streams can be further improved against error propagation and packet losses, once they are elegantly fit into the fixed-size bit packets [52]. Although these methods improve resilience, simulation results show that the quality of reconstructed images when they reach the receiver are better suited to Forward Error Coding (FEC) methods.

The common drawback of all the FEC-based methods described above, with the exception of the method in [37], is the disregard of the functionality of the bits

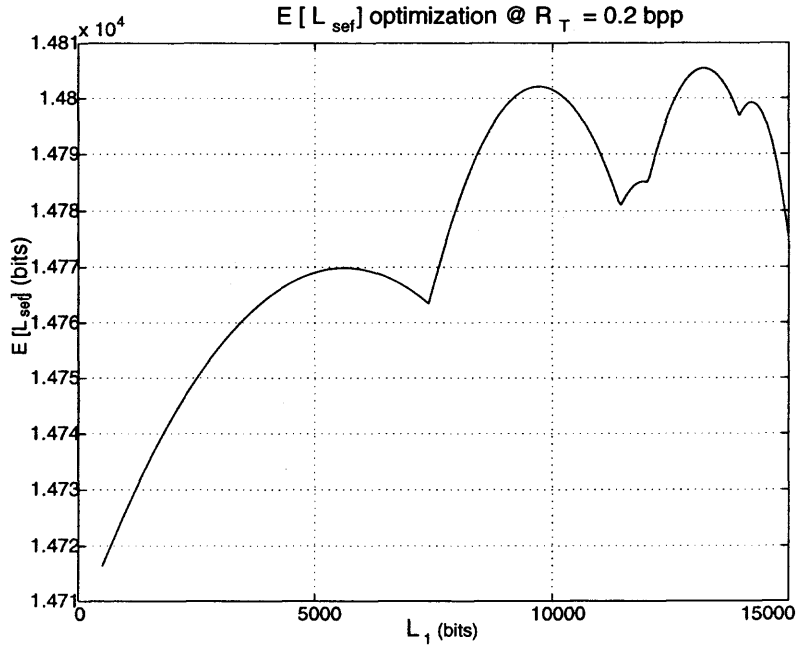


(a) 2-rate

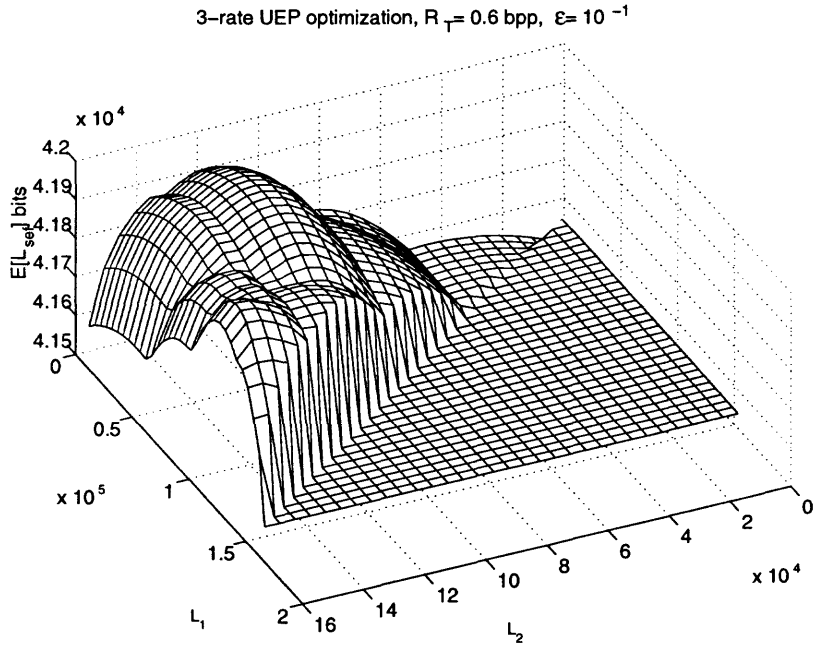


(b) 3-rate

**Figure 3.11** Optimization processes for the BSC of $\epsilon = 10^{-1}$

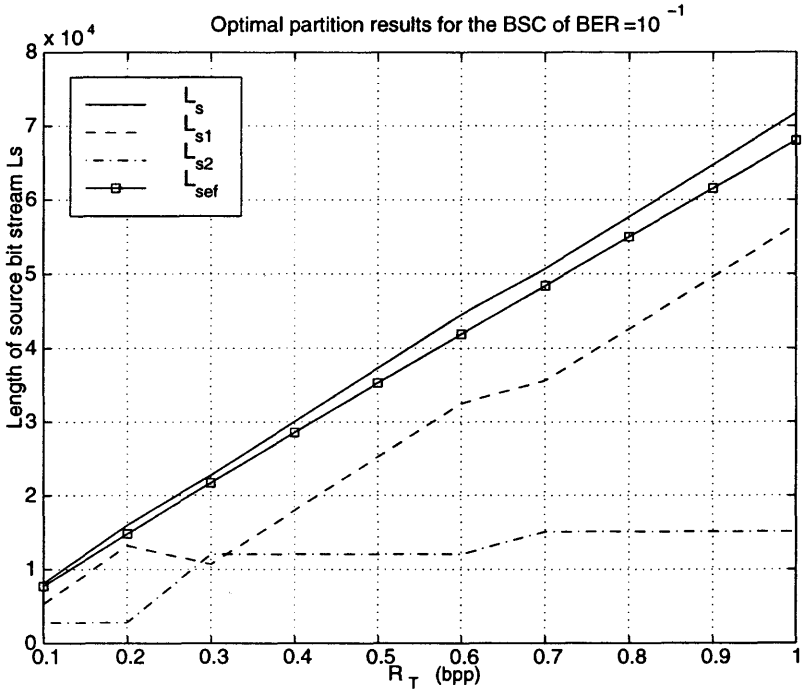


(a) BSC of $\epsilon = 10^{-1}$

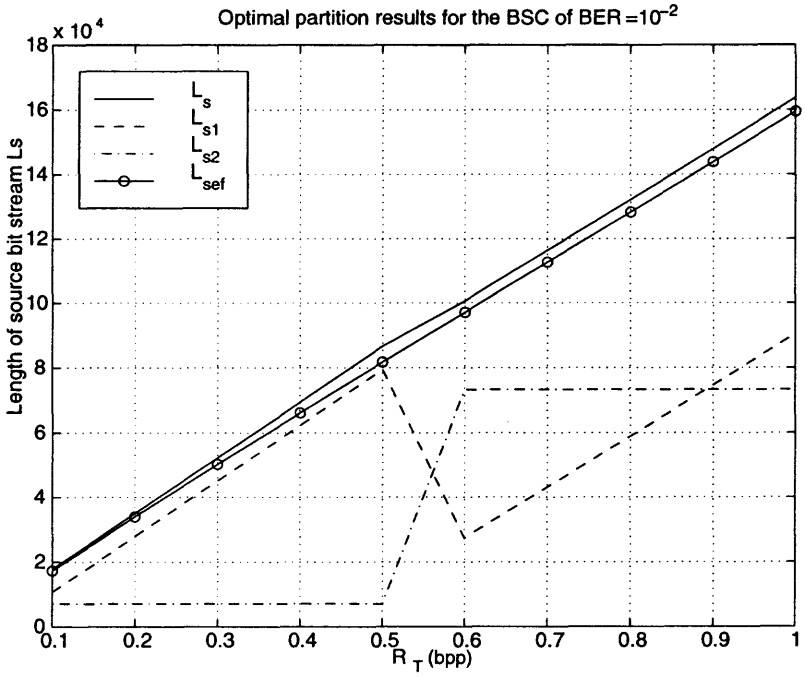


(b) BSC of $\epsilon = 10^{-2}$

**Figure 3.12** 2-rate UEP optimal partition results

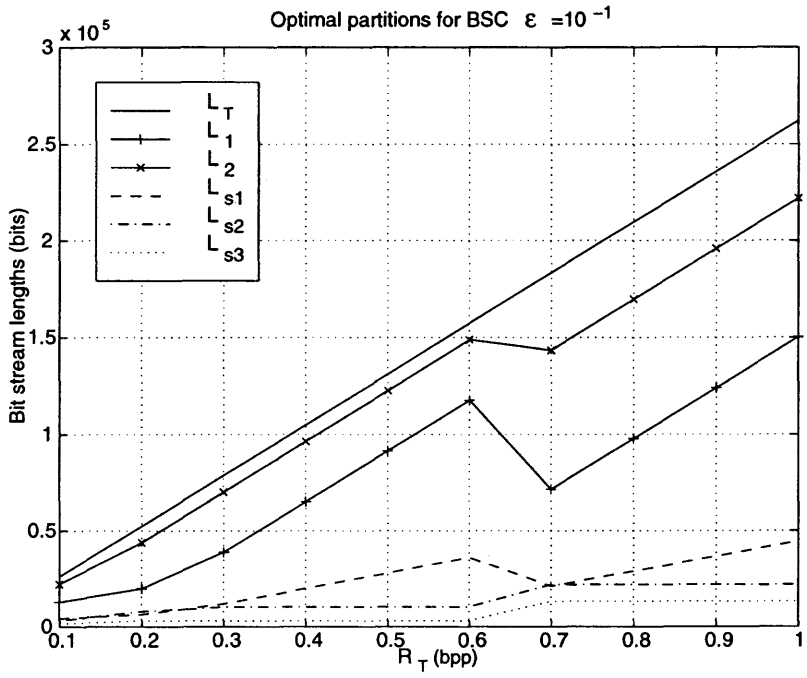


(a) Optimal partitions

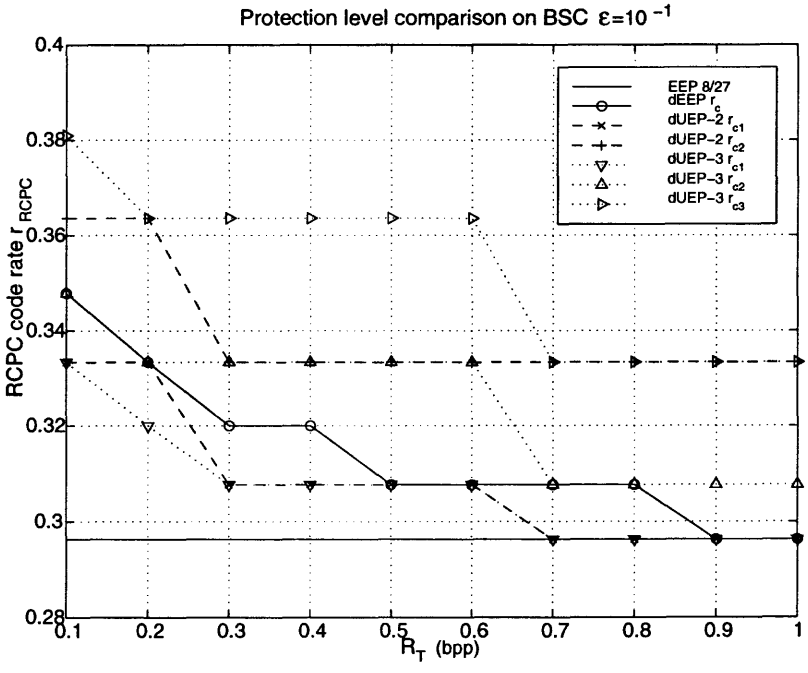


(b) Optimal code rates

**Figure 3.13** 3-rate UEP optimization results, BSC $\epsilon = 10^{-1}$

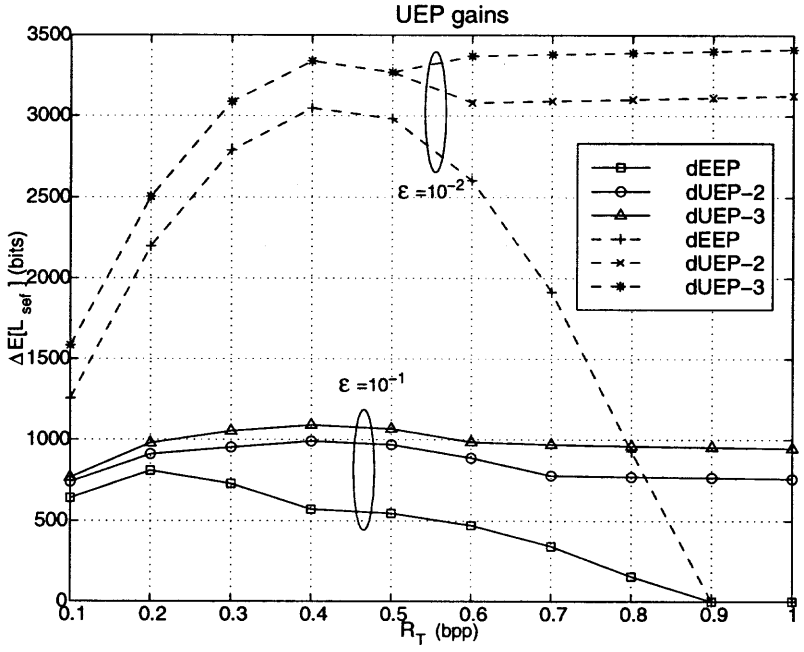


(a) UEP gains $\Delta\widehat{L}_{sef}$ over the optimal EEP schemes

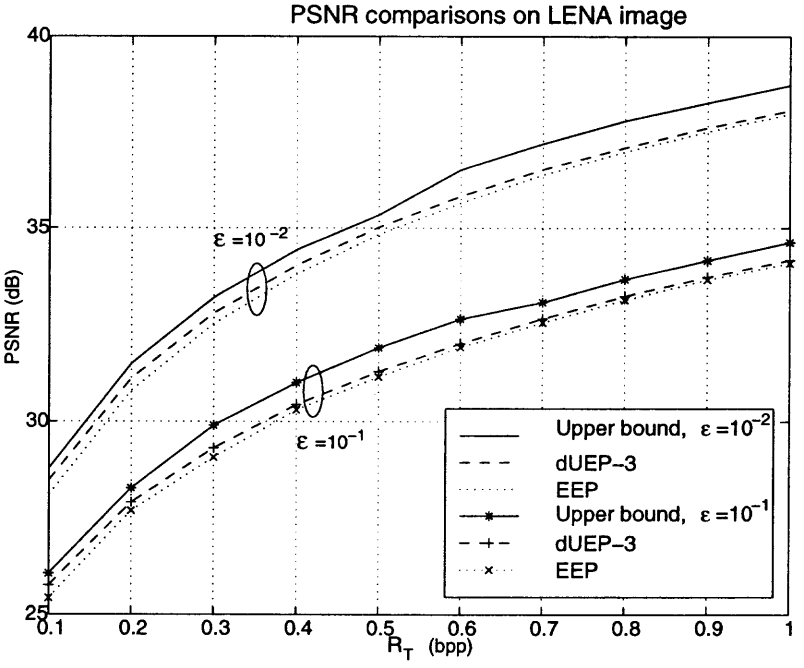


(b) PSNR improvements and upper bounds for LENA

**Figure 3.14** Comparison between EEP and UEP

they protect. In fact, a SPIHT bit-stream can be divided into sub-streams, which have different error immunities and applied appropriate (unequal) protections. The method in [37] uses the sub-streams generated from their own EZW-derivative algorithm which has an inferior error-free performance, compared with other algorithms, such as SPIHT. Hence, the overall performance of this method remains limited, although the approach is intuitively better when compared to other schemes.

The proposed method [5] is a derivative of the SPIHT algorithm [54]. Except for a negligible header and some bit position changes, the resulting bit-stream has almost the same rate-distortion characteristics as the original SPIHT algorithm (without arithmetic coding) for error-free applications. The objective is to modify the SPIHT bit-stream, such that the resulting bit-stream is better protected using FEC.

### 3.5.1 Error Resilience of Bit Classes

It is well known that the SPIHT algorithm encodes images using bit planes and performs two passes for each bit-plane. While one pass determines sign values and the implicit location information of significant wavelet coefficients (i.e. *sorting pass*), the next pass sends the refined bit values of the significant coefficients which are determined up to the current bit-plane (i.e. *refinement pass*) [54]. The bits generated during the sorting pass excluding sign bits are denoted as Location Bit Class (LBC), and bits of the refinement pass and sign bits together are denoted as Value Bit Class (VBC).

It is important to observe the following about these two bit classes: bit errors in LBC lead to a catastrophe, VBC bit errors do not propagate along the bit-stream as long as LBC bits are error-free. In other words, VBC bits behave like a fixed-length codeword sequence, while in LBC, bit errors propagate similar to a fragile variable-length bit-stream. Since dividing a bit-stream into fixed- and variable-length sub-streams and protecting them with unequal FEC is shown to be advantageous in a

noisy channel transmission, a similar approach can also be utilized during protection of SPIHT bit-stream.

The SPIHT bit-stream has different error tolerances of its bits with respect to their positions in the bit-stream. In other words, the importance of each bit (i.e. its effect on the reconstructed image) decreases, as one moves towards the end of the bit-stream. This makes the UEP of different segments of a bit-stream possible. One approach might be dividing the whole bit-stream into different length sub-streams with reduced protection to the end [35]. Note that such an approach does not take into account the implicit bit-plane structure of the SPIHT bit-stream. Since it is necessary to inform the receiver of the location of the point at which FEC rate should change, the UEP of the bits for different bit-planes looks more advantageous. The bit-plane number showing the boundary of the bit-planes at which the protection rate changes, is represented with a lower number of bits in comparison to sending lengths of different sub-streams.

The question remains, how to divide the bit-planes into different classes according to their error resilience? In SPIHT bit-streams, while the image is encoded from the most-significant-bit-plane to the least-significant-bit-plane, the number of the bits encoded at each bit-plane begin to increase rapidly at some critical point. Simulations showed that the last few (1-2) bit-planes usually contain almost half of the total bit-budget. For simplicity, a transition point between the bit-planes of LBC can be determined. The bit-planes before and after this point are protected with two different channel rates. Let us denote the section in LBC before this transition point as LBC- and after that as LBC+. LBC can also be further divided into bit-planes for improved UEP at the cost of increased complexity.

In summary, the original SPIHT stream can be demultiplexed into three sub-streams, as LBC-, LBC+ and VBC. The demultiplexing process is depicted in Figure 3.15.

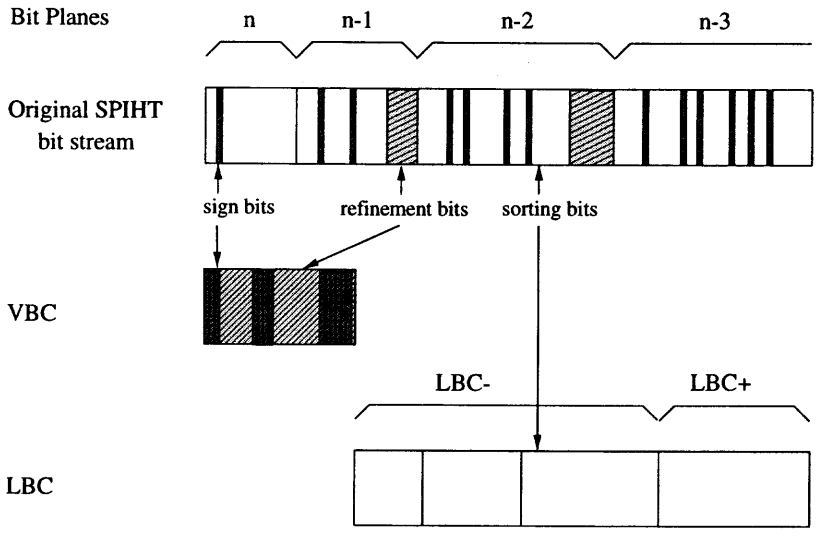


(a) Demultiplexing of SPIHT bit streams

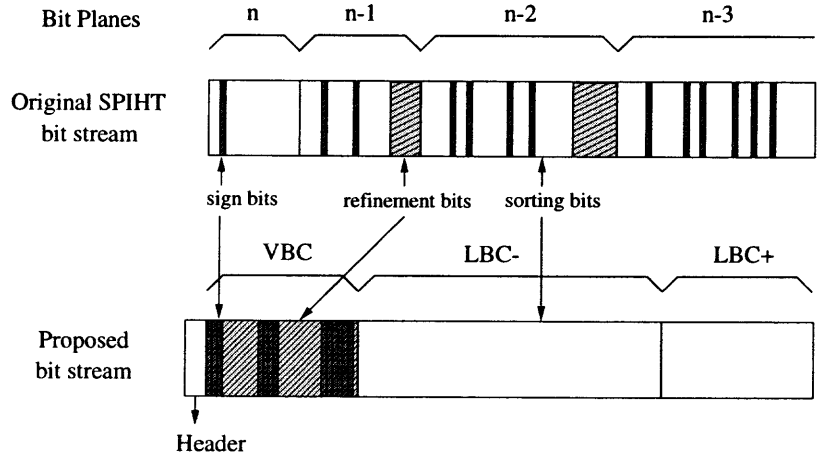


(b) Syntax for re-multiplexing

**Figure 3.15** SPIHT bit stream delmultiplexing and re-multiplexing

### 3.5.2 Bit-stream Syntax and Overheads

After the proposed demultiplexing stage, the sub-streams are ordered for transmission purposes. Since the number of bits in the bit-stream stays almost the same as the original bit-stream for any given budget, the most important remaining measure to be protected is the progression of the bit-stream.

Simulations show that VBC has on the average 25% of the total bit-budget for the compression range of $0.1 - 1$ *bpp* for the standard test images. Thus, if VBC is inserted at the beginning of the bit-stream, as shown in Figure 3.15, the progression at the receiver can still be partially maintained after buffering VBC portion of the bit-stream. The maximum delay incurred by this method is proportional to the size of VBC. Moreover, the overall performance of the proposed method is also proportional to the size of VBC.

Finally, the decoder requires some information header bits to determine when and how to demultiplex the incoming substreams. Signaling the transition between LBC- and LBC+, 3 bits are required to represent the bit-plane number. To detect the end of the VBC, the length of the VBC sub-stream is represented by 10 bits. Thus, a total of 13 overhead bits is sufficient in order to uniquely reconstruct the compressed image at the receiver.

### 3.5.3 Error Protection

With slight modifications in the SPIHT algorithm, three sub-streams with different error resilience properties are obtained. It should be noted that the proposed demultiplexing does not have an immunity against errors without using FEC. Demultiplexing only helps to group the bits which were originally located randomly within the bit-stream into different error resilience classes. Effectively protecting these bit classes is the next goal.

However, there is no analytical way to determine the protection needed to use for LBC+, LBC- and VBC sub-streams, respectively. Although joint source-channel coding methods can analytically judge the optimum rates for some simple sources. With the complex SPIHT algorithm, simulations remain to be the only way to ascertain the best source-channel bit ratios. Intuitively, it is expected to put less protection on VBC compared to LBC; and LBC- should be protected more than LBC+.

LBC- and LBC+ are protected by concatenated rate-compatible punctured convolutional (RCPC) and cyclic redundancy codes (CRC). The inner RCPC code serves to correct bit errors caused by noisy channels. The outer CRC code detects any uncorrected errors after Viterbi decoding for RCPC codes, so that the image will not be corrupted by disastrous error propagation. In the proposed scheme, LBC- and LBC+ are protected by two different RCPC code rates $r_{LBC-}$ and $r_{LBC+}$, respectively.

CRC is mainly utilized for detecting the errors that propagate. Since errors do not propagate in VBC, protecting these bits against errors using only RCPC codes is sufficient. There might be some undetected errors after RCPC decoding, but they stay local within the image. The RCPC code rate $r_{VBC}$ for VBC is expected to be the highest among three sub-streams.

### 3.5.4 Simulation Results and Discussions

The proposed method is tested by using standard images, *Lena* and *Goldhill* ($512 \times 512$), in order to compare its performance with other schemes. The images are encoded for bit-rates ranging from 0.1 to 1 *bpp*. The channel is assumed to be a binary symmetric channel (BSC) with bit error rates of (BER) $\epsilon = 10^{-1}$ and $10^{-2}$. All the experimental results are obtained by averaging 1000 independent simulations over the BSC.

The RCPC codes used are selected from the tables in [24] from a parent code of rate 1/4, puncturing period 8 and memory length 6. A family of $(4-1)\times 8 = 24$ codes are obtained with the rates $\mathcal{R}_{RCPC} = \{\frac{8}{32}, \frac{8}{31}, ..., \frac{8}{9}\}$. Before RCPC encoding, the output sub-streams are packetized separately into length $L$ ($L = 202$) blocks. For LBC- and LBC+, 16 checksum bits (CRC) are then added to the packets. Finally, 6 zero bits are added to the end of each packet to flush the memory of the Viterbi decoder. These packets are then multiplexed appropriately and sent over the channel.

First, the method in [57] was repeated, for each image and channel. The method divides the SPIHT bit-stream into length $L$ packets and protects them equally using RCPC and CRC codes. By 1000 simulations, the optimal RCPC code rates for the channels with BER $\epsilon = 10^{-1}$ and $10^{-2}$ are obtained as $r_1 = 8/28$ and $r_2 = 8/12$, respectively. These rates are equal to those used for the equal error protection scheme (EEP) in [57] and will be further used in the selection of RCPC code rates for the proposed UEP scheme. The resulting rate-distortion (PSNR vs. bit-rate) curves for this method are shown (as solid lines) in Figure 3.16 and 3.17.

Since a closed form solution for the optimal RCPC code rate set based on rate-distortion measure is very difficult to obtain, a careful inspection of the optimization problem reveals the following facts which can be used as guidelines for the rate selection:

1. For the two channels used in simulation, the RCPC code rates for the EEP scheme from [57] are assumed to be appropriate for the LBC- sub-streams,

2. Protection provided by RCPC codes for LBC+ and VBC sub-streams should be weaker than that for LBC-, which means $r_{LBC+} > r_{LBC-}$ and $r_{VBC} > r_{LBC-}$,

3. Protection for VBC should be weaker than that for LBC+ sub-streams, which means $r_{VBC} > r_{LBC+}$.

Based on these guidelines, the available choices of code rates are restricted to those higher than $r_1$ and $r_2$ in the given set for the two selected channels. Thus optimal code sets can be obtained through a few experiments. The optimal RCPC code sets are obtained as $\{r_{LBC-}, r_{LBC+}, r_{VBC}\} = \{8/28, 8/25, 8/20\}$, and $\{8/12, 8/11, 8/10\}$, respectively, for the channels with BER $\epsilon = 10^{-1}$ and $10^{-2}$, under the constraint on the total transmitted bits, which includes source channel coding bits and overheads. These RCPC code rates are selected from the available set such that the overall PSNR performance of the proposed scheme is the best for each channel over the range of tested bit rate.

Figure 3.16 and 3.17 display the simulation results for the proposed method. In Figure 3.16 (a) and (b), the performance curves for the individual approaches are also plotted, namely Case 1 and Case 2. In Case 1, demultiplexing is achieved only as VBC and LBC, whereas in Case 2, only bit-plane segmentation (LBC- and LBC+) is tested. Case 3 is simply the proposed method which divides the bit-stream into three substreams.

From Figure 3.16 (a) and (b), it is clear that most of the improvement over performance comes from Case 1, while Case 2 provides the flexibility of keeping the progression of the original SPIHT. It is expected that the proposed scheme will perform better at higher bit rates, because the percentage of the sign and refinement bits will increase in the resulting bit stream.

It is observed that the proposed scheme outperforms the method of [57] by approximately 0.3 $dB$ for the two tested channels. The method in [37] is outperformed by about 1.0 $dB$ for the channel with $\epsilon = 10^{-2}$. The PSNR improvement over the method in [37] is due to the efficiency of source compression (SPIHT) and sign bit protection. The method based on ARQ achieves better performance than the proposed one with help from a feedback channel. Since feedback cannot increase

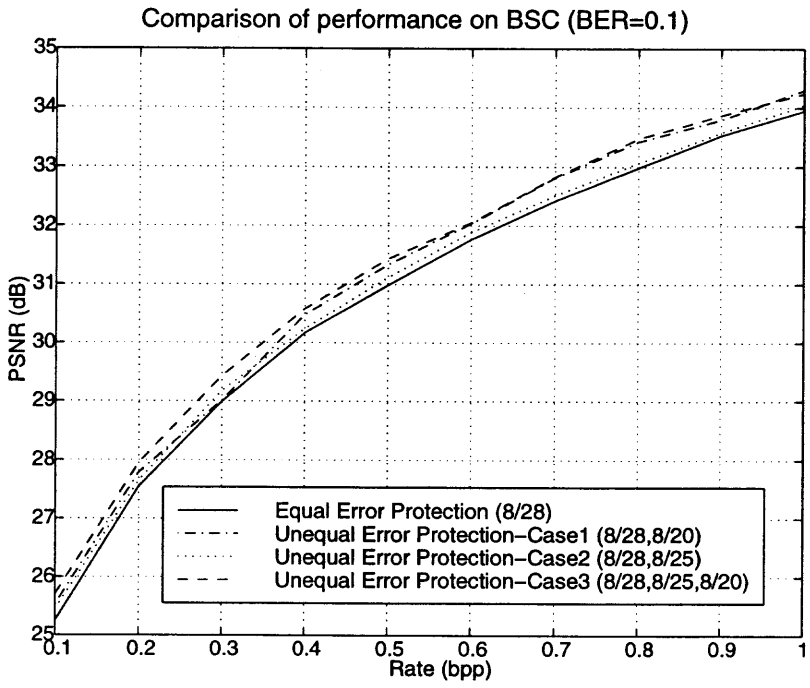


(a) BSC $\epsilon = 10^{-1}$

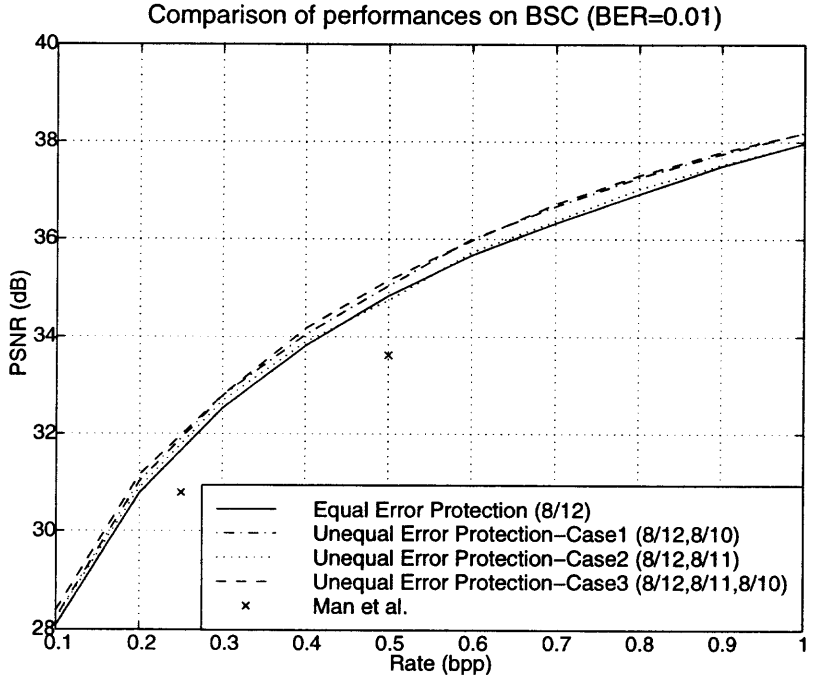


(b) BSC $\epsilon = 10^{-2}$

**Figure 3.16** PSNR comparisons with LENA

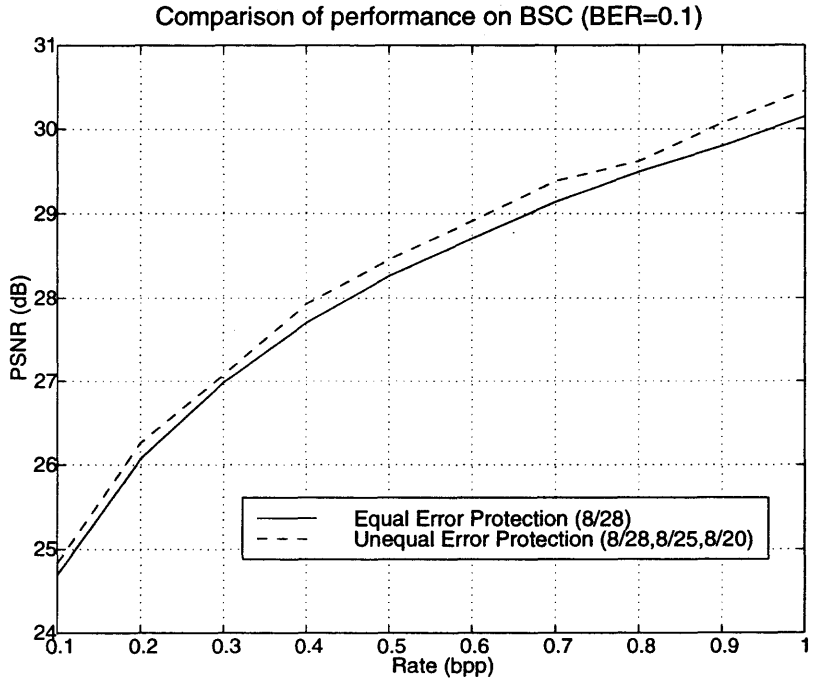


(a) BSC, $\epsilon = 10^{-1}$

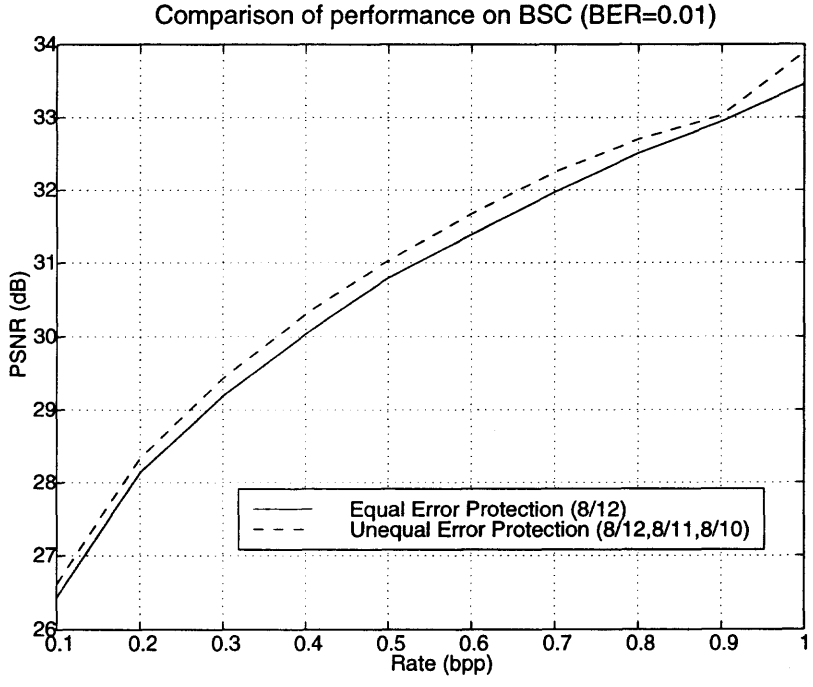


(b) BSC, $\epsilon = 10^{-2}$

**Figure 3.17** PSNR comparisons with GOLDHILL

channel capacity, better performance is achieved at the price of an additional time delay.

## 3.6 Concluding Remarks

In this chapter, a new framework for the JSCC design of progressive image transmission in memoryless channels was presented. Based on the fact that the FEFRL model is general for any channel conditions, mathematical after-channel source models were developed for EEP and UEP schemes, all in closed-form. These models are independent of operational rate-distortion functions of the source codec and training images and provide the possibility of analyzing the performance of embedded image sources in more complicated channel conditions and other interesting issues such as necessary condition of UEP gain and its limit. An equivalent problem for optimal rate allocation between source and channel coding budget is defined and the maximization of $\overline{R}_{sef}$ and PSNR are shown to be equivalent.

Optimization problems for EEP and UEP schemes are proposed and algorithms are presented in this chapter. For EEP schemes, it is discovered that shorter bit streams may require less protection. Performance improvements based on such a fact are obtained by setting up dynamic EEP scheme without any overhead. Simulation results justify the equivalence of the two methods.

For the progressive UEP schemes, the optimization problems definition were clearly defined and complete solutions for BSCs were provided. The necessary conditions were proved and the theoretical upper bounds provided for UEP gains. Optimization algorithms for 2- and 3-rate UEP schemes are also developed. In computer simulations, obtained PSNR improvements are about 0.3 dB over the optimal EEP schemes under the same channel conditions. This gain comes at the price of off-line searching load of the optimization algorithm and negligible rate overhead while the system complexity is unchanged compared to that of [57]. The

progression of the source bit stream is also kept. It is also discovered that for BSCs with $\epsilon \leq 10^{-1}$, at most three rates are enough to achieve almost all the UEP gains. Further increase in the number of protection levels will not be beneficial.

The idea of demultiplexing the SPIHT bit stream by the classifications of VLC and FLC bits and providing UEP accordingly were also investigated. Monte Carlo simulations on the scheme show similar performance to those of progressive UEP. The SPIHT algorithm without arithmetic coding is used for all the simulations in the dissertation.

# CHAPTER 4

# PROGRESSIVE IMAGE TRANSMISSION IN FADING CHANNELS

Reliable delivery of digital multimedia content is an important issue in the next generation of wireless communication systems. Usually the content such as images and video clips needs to be compressed to fit into the band-limited wireless channels. The new generation of wavelet-based image codecs [56, 54] produce efficiently embedded bit streams with decreasing bit significance, which are quite suitable for such purposes. But due to the variable length coded (VLC) bits used in the algorithms, bit errors propagate in the bit stream and all the bits after the first error are unusable in image reconstruction. For the embedded image bit streams transmitted over binary symmetric channels (BSCs), the quality of the reconstructed images can be evaluated by either the conventional peak signal to noise ratio (PSNR) averaging or the error-free source rate averaging technique developed in the research. The idea of obtaining the average of the first error-free run lengths (FEFRL) will also be adopted in this chapter and the result is shown in closed-form.

In wireless communications, the channel is much more complicated than BSCs due to the multipath reflections and receiver movements. By quantizing the received signal to noise ratio (SNR) envelope properly, both the slow fading and Doppler effects can be well approximated by finite state Markov chain (FSMC) channels [70, 67] in which each state corresponds to a BSC. With such a general model, the correlated bit errors can be modeled by hidden Markov models and the existing Markov chain theory can be applied to the bit streams transmitted over them. The most widely used FSMC channel models are the two state class (or Gilbert-Elliott models) [59, 35, 36, 1, 60, 78] which represent the simplest structure of the general FSMC model. However, even for this simple two-state channel model, channel simulation could be a formidable task and some further simplifications are usually

exploited to investigate the performance of information transmission over such a kind of models.

To evaluate the performance of the embedded bit streams transmitted over an FSMC channel with two or more states, existing techniques use either single or multiple BSCs to simplify the memory channel. In [59, 35], the BSC with the worst bit error rate (BER) is selected to approximate the Gilbert-Elliott (G-E) channel. In [58, 78, 10], single BSC with crossover probability equivalent to the overall BER of the fading channel were used. In [78, 61], the transmission of bit streams is assumed to happen in each state of the FSMC model independently. System performances are represented by the statistical averaging of the performances in each state. Assumptions and approximations in those methods are obvious and the question still remains: for the embedded image bit streams transmitted over a G-E or a more general FSMC channel, how to get the system performance *analytically*, *accurately*, and *optimally*?

To solve the problem, a new technique called error sequence analysis (ESA) is developed in this chapter to evaluate the performance of the embedded image bit streams transmitted over general FSMC channels. Based on the fact that the FEFRL model is also valid for the embedded image bit streams transmitted over FSMC channels and the corresponding error sequence can be modeled by an hidden Markov model [67], both the probability density function and the average FEFRL are obtained in closed-form which include the result for the BSCs as a special case. This is not surprising since a single BSC is a special or the simplest form of a general FSMC model. It is further shown that existing techniques are also special cases of the proposed method. Computer simulations on the new approach reveal the shortcomings of the existing techniques and the Doppler effect on system performances.

In [59], the concatenated RCPC-CRC protection scheme is further combined with product channel codes or interleaving technique to reduce the bursty error

effect of fading channels. However, those techniques trade the progression of the embedded source codec to obtain better performances and are not considered in this dissertation.

## 4.1 Fading Channel Modeling

It is well known that wireless communication channels are characterized by fluctuating received signal to noise ratio (SNR) which is Rayleigh distributed due to the multipath effects. User movement results in time variations of the channel responses because of Doppler effect. There are well developed fading envelope models in the literature. But for the joint source-channel coding problem addressed in this dissertation, those models are difficult to use due to the lack of closed-form expression for high dimension error sequence distributions. On the other hand, FSMC models are general enough to model various types of fading phenomena, since ther are capable of approximating the correlations in and between the states. The theory is well developed so that it is easy to calculate the distribution of different error sequences and evaluate the corresponding system performances.

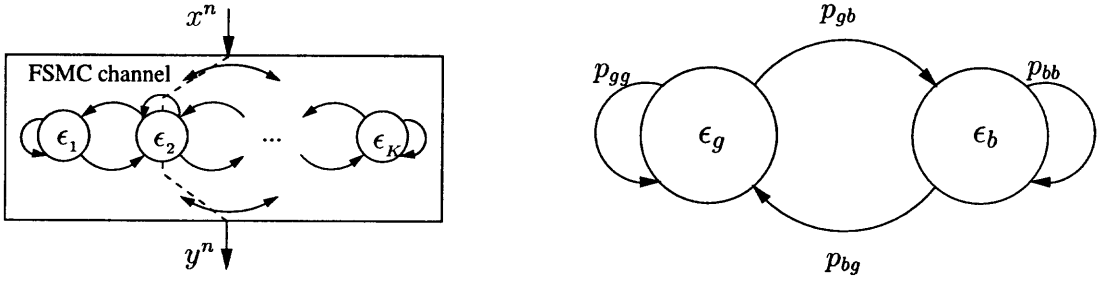


(a) $M$-state FSMC model (b) 2-state (G-E)

**Figure 4.1** Finite state Markov chain channel models

For binary communications, a bit stream $x^n$ is transmitted over an FSMC channel and $y^n$ is received (Figure 4.1(a)). The corresponding error sequence can be

defined as

$$e^n = x^n + y^n \mod 2 \tag{4.1}$$

where $e \in \mathcal{E} = \{0, 1\}$. It is apparent that $e = 0$ means a correctly received bit and 1 means the bit is incorrect. The $K$ state FSMC model in Figure 4.1(a) can be uniquely described by its state space $S$, state transition matrix $\mathbf{P}$, and stationary distribution $\boldsymbol{\pi} = \{\pi_i\}_K$. For stationary FSMC channels, the state equilibrium constraint $\boldsymbol{\pi}\mathbf{P} = \boldsymbol{\pi}$ and $\boldsymbol{\pi}\mathbf{1} = 1$ are satisfied. For such a symmetric channel, $e^n$ is stationary and we have [66]

$$p(e^n) = \boldsymbol{\pi} \prod_1^n \mathbf{P}(e_k)\,\mathbf{1} \tag{4.2}$$

where $\mathbf{1} = \{1, 1, ..., 1\}'_K$, $\mathbf{P}(e_k)$ is the error matrix probability and can be expressed as

$$\mathbf{P}(e) = \mathbf{P}\mathbf{F}(e) \tag{4.3}$$

where $\mathbf{F}(e) = \text{diag}\{p(e|i)\}_K$ is the state error probability matrix, and $p(e|i) = \epsilon_i$ are the crossover probabilities for the BSCs. In summary, an error sequence can also be described by the parameters of the FSMC channel $\{S, \mathbf{P}, \mathbf{F}(e)\}$. From (4.2), the overall or average crossover probability of the FSMC channel can be obtained by letting $n = 1$, i.e.,

$$p(e) = \boldsymbol{\pi}\mathbf{P}(1)\mathbf{1} = \bar{\epsilon} \tag{4.4}$$

By partitioning or quantizing the received SNR level into two levels, parameters of Gilbert-Elliott (G-E) models can be obtained using the procedure described in [70]

$$\mathbf{P} = \begin{pmatrix} 1 - p_{bg} & p_{gb} \\ p_{bg} & 1 - p_{gb} \end{pmatrix}$$

For the 2-state FSMC or G-E channel, the overall bit error rate $\bar{\epsilon}$ corresponds to that of the fading channel [45]

$$\bar{\epsilon} = \frac{1}{2}\left(1 - \sqrt{\frac{\rho}{1+\rho}}\right)$$

where $\rho$ is the average SNR of the fading channel. Note that there is no one to one correspondence between the set of valid FSMC models and the real world fading channels. So it is of interest to investigate the models constructed from physical fading channels. The discussions are limited to slow fading channels in this dissertation because they can be well approximated by birth-and-death processes [67].

## 4.2 Single-BSC-Based Techniques

For the embedded image bit streams transmitted over a memory channel, transitions between the channel state make the analysis and simulations of the channel difficult. The first solution of the problem is to further simplify the channel by using only one BSC in the model. Then the existing optimization techniques can be used to assign an 'optimal' protection level for that single BSC. Usually the worst channel state $\epsilon_w$ is one of the choices since the resulting scheme will be robust for any channel situations.

When the average SNR $\rho$ of the fading channel is known, the corresponding FSMC model can also be represented by an equivalent BSC whose BER can be obtained from (4.4). Protection level can then be optimized by matching the RCPC code rate to $\bar{\epsilon}$. It is of interest to investigate this simple method since all the independent parameters of the FSMC model are involved in (4.4) and it represents a simplified version of the ESA method which is to be developed in later sections of this chapter. The performance of the system might be improved by using the average channel state $\bar{\epsilon}$. The expectation is reasonable since more channel state information is exploited in the $\bar{\epsilon}$-based optimization.

However, both of the solutions are incomplete because the performance of the "optimally" protected bit streams can not be evaluated properly. So there is no way to compare even between the above two schemes.

## 4.3 Statistical Averaging Approach

When an embedded image bit stream is transmitted over a two-state memory channel with statistics $\{\epsilon, \pi, \mathbf{P}\}$, and protected by RCPC code with rate $r_{c_i} \in \mathcal{R}_{RCPC}$, under the assumption that exact channel state information is not available, the expected first error-free run length (FEFRL) of the embedded image bit streams transmitted over G-E channels can be expressed or defined as

$$\begin{aligned} \overline{L}_{sef} &= \pi_g \overline{L}^g_{sef} + \pi_b \overline{L}^b_{sef} \\ &= \pi_g \psi(q_g, L_s) + \pi_b \psi(q_b, L_s) \end{aligned} \tag{4.5}$$

where $\overline{L}^{\{b,g\}}_{sef}$ is the average FEFRL when the channel is in state $b$ and $g$, respectively (Figure 4.1 (b)). It is already shown in Section 3.3.1 that the maximization of $\overline{L}_{sef}$ and average PSNR are equivalent. Thus, by using (4.5) as the target function, both states of the G-E channel are involved and the following constrained joint source-channel optimization problem need to be solved

$$\hat{L}_{sef} = \max_{R_s + R_c \leq R_T} \overline{L}_{sef} \tag{4.6}$$

Note that the performance obtained from (4.5) is rate-based and can easily be generalized to the $K$-state cases. In fact, the statistical averaging approach can also be applied to the distortion-based analysis, as in [61, 10].

The implied assumption for this statistical averaging method is that the state transitions of the memory channels always happen after the whole bit stream of an image is completely transmitted over each of the states. Obviously such an assumption is not true for most wireless communication channels. The system performance obtained from such a method, be it rate- or distortion-based, might have been exaggerated. It will seen in the later sections of this chapter.

## 4.4 Error Sequence Analysis (ESA)

The FEFRL model has been used in BSCs by many researchers [57, 35]. In fact, there is no constraint on the channel type when the model is derived. The only concern is the position where the first bit error happens. Obviously such a model is also applicable to any kinds of noisy channels, e.g. FSMC channels. By applying the FSMC theory on the error sequence of the FEFRL model, both its probability density function and the ensemble average can be obtained in closed-form. With such a closed-form performance metric, the performance optimization of the EEP protection scheme on FSMC channels is quite similar to that in the BSC case, which has been solved in Chapter 3 with ease.

Now consider the scenario in which a binary embedded image bit stream is transmitted over an FSMC channel as depicted in Figure 4.1(a). Again, the FEFRL is denoted as $L_{sef} \triangleq k$. Obviously the first bit error happens at $k+1$. From (4.1) we immediately have the corresponding error sequence for the first $k+1$ bits as

$$e^{k+1} = 0^k 1 \tag{4.7}$$

Combining (4.2) and (4.7), the probability density function of the FEFRL $k$ can be expressed by the following bi-modal matrix-geometric distribution

$$p(k) = \begin{cases} \boldsymbol{\pi}\,\mathbf{P}^k(0)\mathbf{P}(1)\,\mathbf{1} & 0 \leqslant k < L_s \\ \boldsymbol{\pi}\,\mathbf{P}^{L_s}(0)\,\mathbf{1} & k = L_s \end{cases} \tag{4.8}$$

where $L_s$ is the length of the source bit stream. The average of the FEFRL can be obtained from (4.8) as

$$\begin{aligned} \overline{L}_{sef} &= \sum_{k=0}^{L_s} k p(k) \\ &= \boldsymbol{\pi}\left\{\mathbf{P}(0)\left[\mathbf{I}-\mathbf{P}^{L_s}(0)\right]\left[\mathbf{I}-\mathbf{P}(0)\right]^{-1}\right\}\mathbf{1} \\ &\triangleq \Psi(\boldsymbol{\pi}, \mathbf{P}, \mathbf{F}(0), L_s) \end{aligned} \tag{4.9}$$

where $\mathbf{F}(0) = \mathrm{diag}\{p(0|i)\}_K = \mathrm{diag}\{q_i\}_K$, $q_i \triangleq 1-\epsilon_i$, $\epsilon_i$ are the error probabilities of the BSCs. By using spectral decomposition of the matrix $\mathbf{P}(0)$, the calculation

of its exponentials can be greatly simplified especially when the length of the source bit stream $L_s$ is long. Let

$$\mathbf{P}(0) = \boldsymbol{\lambda}^{-1}\boldsymbol{\Lambda}\boldsymbol{\lambda} \tag{4.10}$$

where $\boldsymbol{\Lambda} = \text{diag}\{\lambda_i\}_K$, $\{\lambda_i\}_K$ are the eigenvalues of $\mathbf{P}(0)$, $\boldsymbol{\lambda}$ is a matrix whose rows are the eigenvectors of $\mathbf{P}(0)$. Substitution of (4.10) into (4.9) yields

$$\overline{L}_{sef} = \boldsymbol{\pi}\left\{\mathbf{P}(0)\left[\mathbf{I} - \boldsymbol{\lambda}^{-1}\boldsymbol{\Lambda}^{L_s}(0)\boldsymbol{\lambda}\right]\left[\mathbf{I} - \mathbf{P}(0)\right]^{-1}\right\}\mathbf{1}$$

which greatly reduces the computational load of $\overline{L}_{sef}$ for very long image bit streams.

It is of interest to note that both (4.8) and (4.9) are quite similar in outlook to their counterparts for the BSCs. In fact, let $\boldsymbol{\pi} = \{0, 0, ..., 0, 1\}_K$ and $\mathbf{P} = \text{diag}\{p_{ii}\}_K$ where

$$p_{ii} = \begin{cases} 1 & i = K \\ 0 & \text{otherwise} \end{cases} \tag{4.11}$$

we immediately have

$$p(k) = \begin{cases} (1-\epsilon)^k\epsilon & 0 \leqslant k < L_s \\ (1-\epsilon)^{L_s} & k = L_s \end{cases} \tag{4.12}$$

and

$$\Psi\left(\boldsymbol{\pi}, \mathbf{P}, \mathbf{F}(e), L_s\right) = \psi\left(q, L_s\right) \tag{4.13}$$

where

$$\psi(q, L_s) = \frac{q}{1-q}\left(1 - q^{L_s}\right) \tag{4.14}$$

and $q = 1 - \epsilon$. Compare with (3.17) and (3.18), it is clear that (4.12) and (4.13) are exactly the same as those obtained in the BSCs. It is clear now that the approach used to derive the probability density function and the average FEFRL on BSCs in Chapter 3 is also ESA, but with the error sequence implied in the analysis process.

Note that the matrix products in (4.8) and (4.9) are non-commutative, which reflect the dependencies between the elements in the error sequence.

With (4.9) as the target function, the overall system performance can be optimized by solving the following constrained joint source-channel optimization problem

$$\hat{\overline{L}}_{sef} = \max_{R_s+R_c \leq R_T} \overline{L}_{sef} \tag{4.15}$$

Such a problem can be solved by the numerical method similar to that in Chapter 3

$$\hat{r}_{c_i} = \arg\min_{R_T} \left\{ \max_{R_s+R_c \leq R_T} \overline{L}_{sef} \right\} \tag{4.16}$$

## 4.5 Relationship with Existing Techniques

In order to evaluate and optimize the the performance of the embedded image bit streams transmitted over FSMC channels, various techniques have been developed and can be categorized into either single or multiple BSC based approaches [59, 35, 78]. Single BSC based approaches can be further divided into either worst case BSC ($\epsilon_w$) or average BER ($\bar{\epsilon}$) based one. For the multiple BSC based techniques, they can also be further divided into either the statistical averaging approach or error sequence analysis (ESA) technique. It is apparent that different "optimal" RCPC code rates $\hat{r}'_{RCPC}$s might be obtained from different techniques. In fact, it can be easily seen that $\bar{\epsilon}$ obtained by (4.4) for the single-BSC-based method represents a special case of (4.7) in which the error sequence is simply $\mathbf{e} = 1$. Also when $1 - \epsilon$ in (4.12) and (4.13) are replaced with $1 - \epsilon_w$, it can be recognized immediately that this is also a special case of ESA.

For the embedded image bit streams transmitted over $K$-state FSMC channels, the $\overline{L}_{sef}$ can be obtained by the statistical averaging approach as

$$\overline{L}_{sef} = \sum_{1}^{K} \pi_i \, \psi(q_i, L_s) \tag{4.17}$$

where $\{\pi_i\}$ is the stationary distribution of the FSMC channel. On the other hand, setting $\mathbf{P} = \mathbf{I}$ and substituting it into (4.9), we have

$$\begin{aligned} \overline{L}_{sef} &= \Psi(\boldsymbol{\pi}, \mathbf{I}, \mathbf{F}(0), L_s) \\ &= \boldsymbol{\pi}\, \mathrm{diag}\left\{\psi(q_i, L_s)\right\}_K \mathbf{1} \end{aligned} \tag{4.18}$$

Compare (4.17) with (4.18), it can be recognized immediately that the statistical averaging approach (4.17) is also a special case of ESA. Furthermore, it can also be proved that

$$\Psi(\boldsymbol{\pi}, \mathbf{P}, \mathbf{F}(e), L_s) \leqslant \Psi(\boldsymbol{\pi}, \mathbf{I}, \mathbf{F}(e), L_s) \tag{4.19}$$

which means that the PSNR performance from statistical averaging approach might be exaggerated. This is because by setting $\mathbf{P} = \mathbf{I}$, the general FSMC models are turned into a group of isolated (or independent) BSCs without any state transitions between them. However, those transitions represent the Doppler effects caused by receiver motion [70]. Thus, the Doppler effects represented by the probability transition matrix $\mathbf{P}$ are omitted in the statistical averaging approaches and the bit errors in and between each BSCs are independent. Obviously, this is not true for errors caused either by FSMC or fading channels.

## 4.6 Performance Upper Bound

When the exact channel state information for the FSMC channel is available, the protection level can be easily matched to each state of the model optimally. Thus, the performance may serve as an upper bound for the system

$$\overline{L}^*_{sef}\left(\hat{q}_{\{i\}_K}, \hat{L}_s^{\{i\}}\right) > \hat{L}_{sef}\left(q_{\{i\}_K}, L_s\right) \tag{4.20}$$

where

$$\overline{L}^*_{sef}\left(\hat{q}_{\{i\}_K}, \hat{L}_s^{\{i\}_K}\right) = \boldsymbol{\pi}\, \mathrm{diag}\left\{\psi(\hat{q}_i, \hat{L}_s^i)\right\}_K \mathbf{1}$$

and $\hat{L}_{sef}\left(q_{\{i\}_K}, L_s\right)$ are obtained by (4.14). This is easy to prove. Since $\psi(\hat{q}_i, \hat{L}_s^i) > \psi\left(q_{\{i\}}, L_s\right)$ holds for all the BSCs . Note that such an upper bound is for EEP schemes only and it is channel specific.

## 4.7 Simulation Results and Discussions

In the computer simulations, the two state FSMC or Gilbert-Elliott (G-E) channels were used to approximate physical multipath fading channels. To facilitate the comparison between different techniques, G-E channel 1 is selected from Lu et al. [35]. G-E channel 2 is constructed from the physical fading channel in Sherwood et al. [59] with carrier frequency of 900 MHz, data rate 500 kbps, and mobile speed of 4 mi/h. The G-E channel parameters are listed in Table 1.

| Channels | Lu et al. [35] | Sherwood et al. [59] |
|---|---|---|
| $\{\epsilon_b, \epsilon_g\}$ | {.12, .0680} | {.12, .0018} |
| $\{\pi_b, \pi_g\}$ | {.62, .38} | {.18, .82} |
| $\{p_{gb}, p_{bg}\}$ | {.08, .05} | {5.4e-5, 1.2e-5} |
| $\bar{\epsilon}$ | .1000 | .0233 |

**Table 4.1** G-E Channel parameters

The optimization processes of the RCPC code rate for the two channels by the proposed ESA method are depicted in Figure 4.2. It is apparent that G-E channel 1 represents a typical channel condition in which better performances are obtained in the strong protection region. This is because the channel stays in the "bad" state most of the time. In this case, both $\epsilon_b$ and $\bar{\epsilon}$ based strategies produce protection levels close to the optimal one obtained by ESA. G-E channel 2, on the other hand, represents a totally different situation in which the channel stays in the "good" state most of the time. Thus, better performance occurrs in the weakly protected region. It can be expected that the overall performance of this new bit rate allocation strategy will greatly outperform those from conventional single BSC based strategies since the protection rate difference is almost the largest possible. It should also be noted that

for Channel 2, the optimal protection rate switches to the strong protection region when the bit rate is as high as $R_T = 1.0$ $(bpp)$. This is not totally unexpected. When the length of the bit stream is long enough, eventually the correlations between the errors of the fading or FSMC channel will play a more important role in the system performance and stronger protection is required to reach optimality. Considering the facts that the average FEFRL from the weaker protection is close to that of stronger one and a simple EEP scheme is desirable whenever possible, the protection rate for this channel is selected to be 8/9.

To compare various evaluation and optimization techniques, the respective "optimal" rates from those approaches are used to obtain the corresponding performances with SPIHT on LENA image for the two channels, all by ESA. The PSNR results and the performance upper bounds are depicted in Figure 4.3(a) and 4.3(b), respectively. It can be seen that for G-E channel 2 which represents better channel conditions, the PSNR improvements of ESA over $\epsilon_b$ based strategy can be up to 3 dB. Generally speaking, $\bar{\epsilon}$ based optimization is better than that of $\epsilon_b$ based. This is not a surprise since all the statistics of the FSMC channels are involved in the optimization, although in a simplified manner.

For the two G-E channels selected, the "optimal" protection rates obtained by statistical averaging and ESA are the same. In Figure 4.4, PSNR results from those two methods are compared. As predicted in (4.19), performances exaggeration caused by the statistical averaging approach can be up to 5 dB, especially at high bit rates.

The mobile speed was then increased from 4 to 40 mph to test the Doppler effect on the system performance. It can be seen from Figure 4.5 that after the protection level increases from 8/9 to 8/28, the performance of the received images reduces by about 2 dB for the whole bit rate range tested due to the faster movement of the mobile.

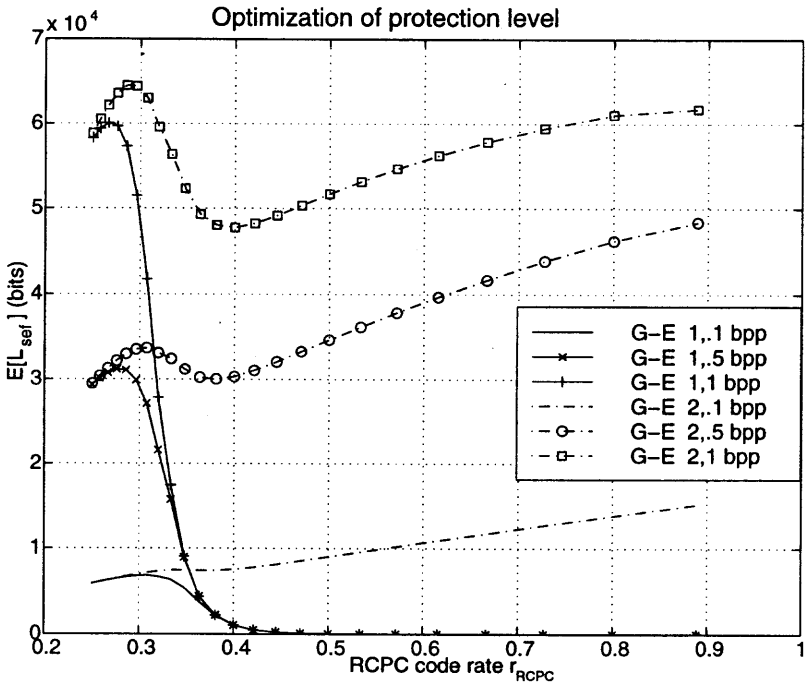


**Figure 4.2** Optimization of protection levels, ESA

## 4.8 Concluding Remarks

The transmissions of embedded image bit streams over FSMC channels were studied in this chapter. With error sequence analysis the probability density function and average FEFRL are obtained in closed-form which are general for any FSMC model structures. Not surprisingly, previous results on BSCs are shown to be a special case of ESA. It should be so because a single BSC is just a special or the simplest FSMC channel. Thus, the performance evaluation and optimization for progressive image transmissions over memory and memoryless channels are unified with the proposed rate-based approach and ESA. Furthermore, other existing performance evaluation techniques for the embedded image bit streams transmitted over FSMC channels are shown to be special cases of the new approach. Computer simulations on EEP optimizations reveal the shortcomings of the other methods and the PSNR improvement is up to 3 dB. Doppler effects on the system performances are also investigated with the new approach by simulations, maybe for the first time on the

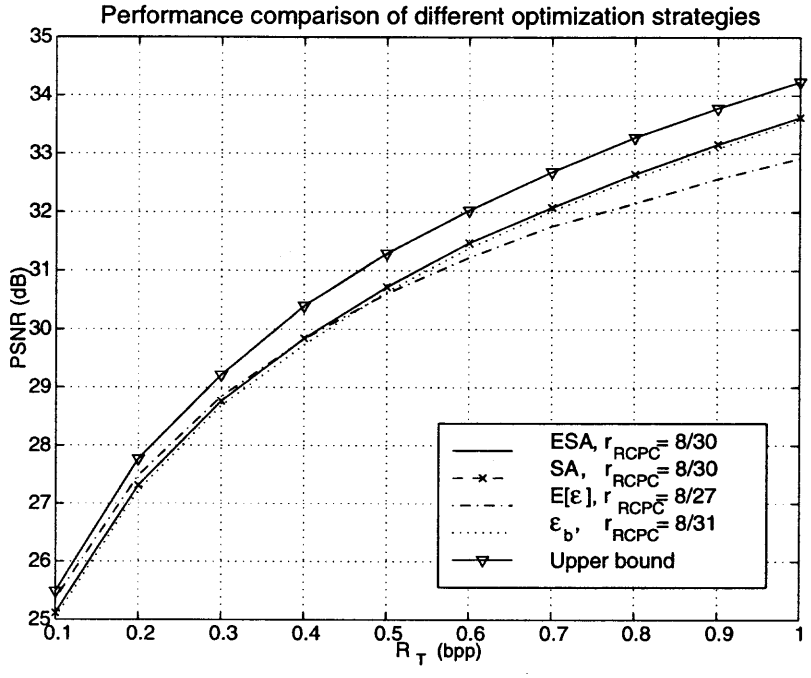


(a) G-E channel 1

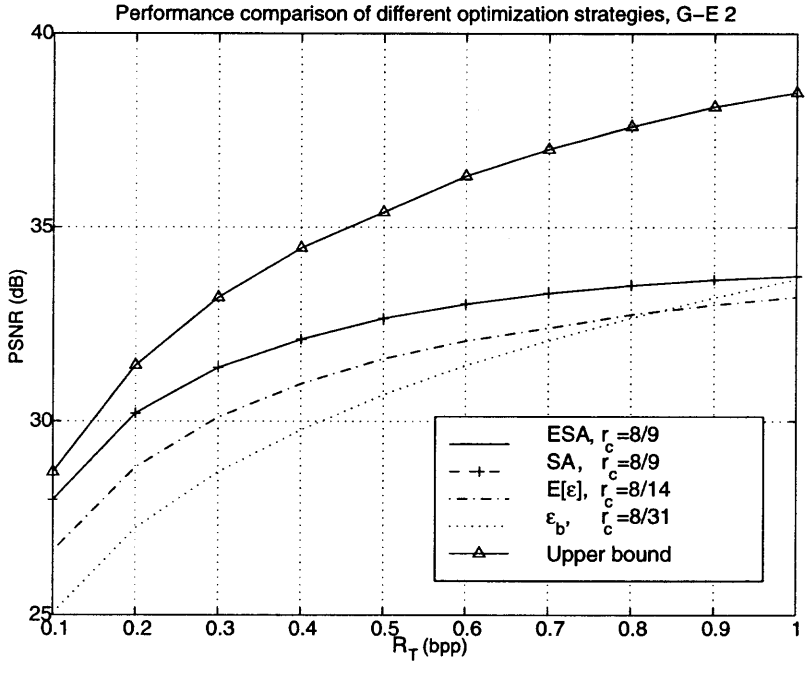


(b) G-E channel 2

**Figure 4.3** PSNR comparisons of the methods with LENA image

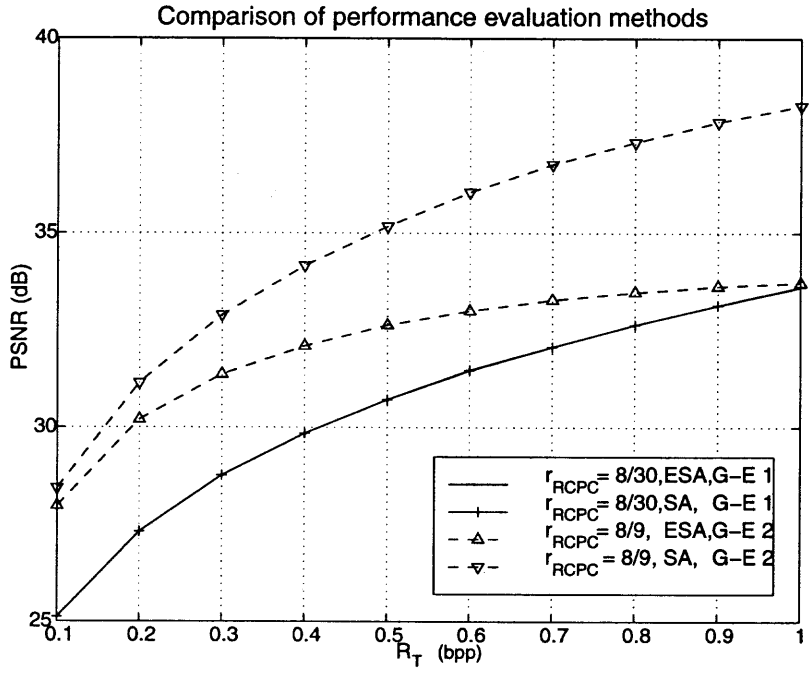


**Figure 4.4** Performance evaluation method comparison with LENA image

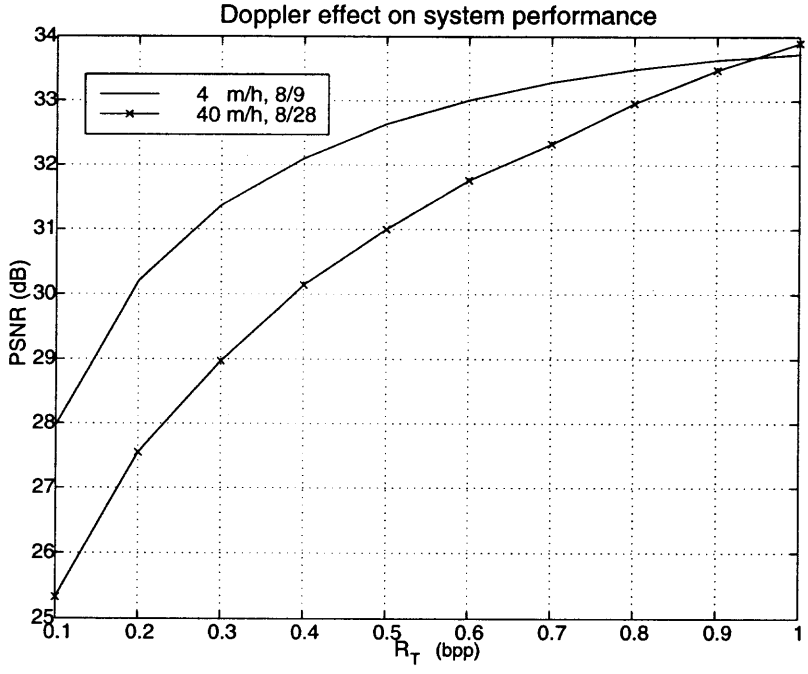


**Figure 4.5** Doppler effect on system performance, G-E channel 2, LENA image

topic. Due to the complexity of fading channels, optimization results for individual memory channel may not be as useful as in the memoryless channel cases. General guidelines for optimal protection strategy on FSMC channels are more practical. Such a general guideline can only be obtained with more experiments on different memory channel conditions. Finally, it is claimed again that with the average FEFRL model derived in the FSMC channel, the performance optimization algorithms for progressive image transmission in BSC and memory channels are unified.

# CHAPTER 5

# PROGRESSIVE IMAGE TRANSMISSION IN CHANNELS WITH FEEDBACK INFORMATION

The new generation of image coders produce embedded image bit streams which can be used for progressive image transmission in multimedia applications. To protect the error-sensitive bit streams in feed-forward channels, forward error correction (FEC) schemes have been proposed and optimized in [57, 84, 76, 36, 12, 14]. In fact the basic concatenated cyclic redundancy check code and rate-compatible convolutional code (CRC-RCPC) scheme used in previous chapters is also well suited for automatic repeat request (ARQ) schemes on channels with feedback information. In wireless communications, such kind of feedback channels usually exist and can be used to obtain better performance through ARQ schemes at the price of delay or throughput reduction. In this chapter, rate-based analysis and optimization algorithms for type-I and -II hybrid ARQ with stop-and-wait (SW) strategy are presented. The algorithms developed are general for both memoryless and memory channel cases. For typical wireless communication scenarios, the additional delay incurred by the stop-and-wait strategy is shown to be close to that of the FEC scheme. With stop-and-wait strategy, no additional system overhead is incurred in the form of packet numbers. The system improvement of the hybrid ARQ schemes can be 1.7 dB better than that of the pure FEC schemes under the same channel condition.

## 5.1 Type-I Hybrid ARQ

For progressive image transmissions in noisy communication channels, FEC schemes must stop decoding and discard all the following packets starting from the one in which the *first* bit error happens. For the optimal FEC schemes, the effective channel is quite "clean". It is highly probable that the first bit errors happen near the end of the bit stream and the number of discarded packets is small. When

a feedback channel is available, the receiver can inform the transmitter with the status of the current packet. By adding an ARQ control protocol, the concatenated CRC-RCPC scheme is transferred into a hybrid FEC/ARQ scheme and the system performance can be improved by using the bits after the first bit error. Furthermore, system performance can also be optimized by adjusting the bit allocation between the source and channel coding rate in the scheme. The discussions on ARQ schemes in this chapter are limited to the stop-and-wait (SW) ARQ schemes only, since they satisfy the requirements imposed by progressive image transmission in multimedia applications. It will also be seen that for typical wireless communications, the stop-and-wait strategy is good enough for the transmission dominant scenario. An added advantage of SW-ARQ is the packet number need not to be piggybacked in the packets so that no additional overhead is incurred compared to that of the FEC schemes. With retransmissions, all the bit rate budget can be used at the receiver side except the discarded packets. This efficiency may save some bit rate for source coding and the system performance might be better than that of the optimal FEC scheme under the same channel conditions.

### 5.1.1 Optimization Algorithm for Hybrid ARQ

In the proposed type-I stop-and-wait hybrid-ARQ system, the concatenated RCPC-CRC channel coding scheme is the same as that of [57] and it is assumed that all the residual errors after RCPC decoding are detectable in such a scheme. After a packet is sent, the transmitter waits for a response from the receiver. It is further assumed that the feedback channel is error-free. Since our source models depend on the accepted packet error rate, this assumption will not affect the analytical results in this dissertation. An illustrated description of the scheme is depicted in Figure 5.1. The transmitter keeps on sending new packets when an *Acknowlegment* ($ACK$) is received. On receiving a *Negative Acknowlegment* ($NAK$), the transmitter simply

retransmits the current packet, thus a new transmission attempt is started. Such a process is repeated until the bit rate constraint is reached. Obviously, the errors in each of the trials under the bit rate constraint are independent of each other, so on the average the FEFRL can also be used to represent the length for each of the sending trials as $\overline{L}_{sef}$. To facilitate further analysis, some necessary definitions of the proposed scheme are listed below.

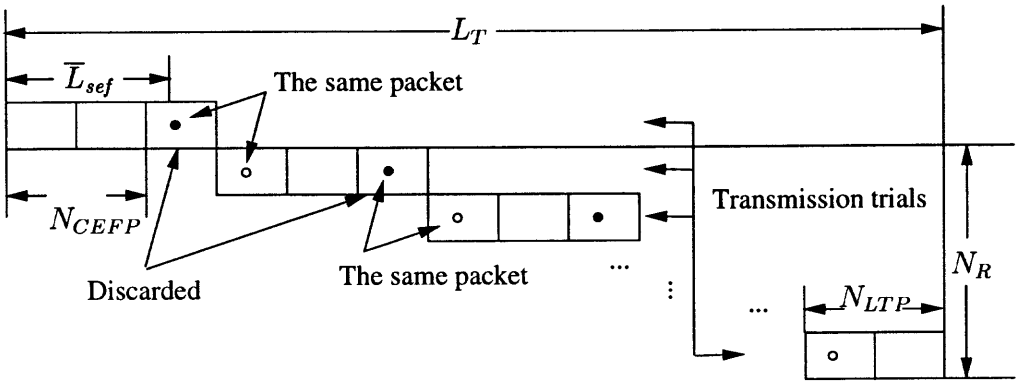


**Figure 5.1** Water-filling for type-I SW-HARQ

**Definition 1** *$N_{TP}$: total number of packets under the total bit rate constraint $R_T$.*

$$N_{TP} = \left\lfloor \frac{N \cdot R_T}{l} \right\rfloor \tag{5.1}$$

where $N$ is the number of pixels in an image and $l$ is the packet size.

**Definition 2** *$\overline{N}_{CEFP}$: number of consecutive error-free packets received in one transmission trial.*

$$\overline{N}_{CEFP} = \left\lfloor \frac{\overline{L}_{sef}}{b} \right\rfloor \tag{5.2}$$

*where $b = 200$ is the source packet size.*

**Definition 3** *$N_R$: total number of retransmissions.*

$$N_R = \left\lceil \frac{N_{TP}}{\overline{N}_{CEFP} + 1} \right\rceil - 1 \tag{5.3}$$

**Definition 4** *$N_{LTP}$: number of packets in the last transmission trial.*

$$N_{LTP} = N_{TP} \mod \left(\overline{N}_{CEFP} + 1\right) \tag{5.4}$$

**Definition 5** *$\overline{N}_{REFP}$: total number of error-free packets received.*

In Figure 5.1, the packets in which the first errors happen are discarded and the image transmission is completed after several independent trials. Thus, the final decoded image quality is determined by the total number of error-free packets received $\overline{N}_{REFP}$. By using a simple water filling on the bit rate constraint $R_T$, we have

$$\overline{N}_{REFP} = N_R \cdot \overline{N}_{CEFP} + \begin{cases} \overline{N}_{CEFP} & N_{LTP} = 0 \\ N_{LTP} & N_{LTP} > 0 \end{cases} \tag{5.5}$$

It is apparent now that the value of $\overline{N}_{REFP}$ can be maximized by adjusting the ratio between source and channel coding budget, i.e.

$$\hat{N}_{REFP} = \max_{R_s + R_c \leq R_T} \overline{N}_{REFP} \tag{5.6}$$

Such an optimization problem can be easily solved by the following numerical method

$$\hat{r}_c = \arg \min_{R_T} \left\{ \max_{R_s + R_c \leq R_T} \overline{N}_{REFP} \right\} \tag{5.7}$$

So the performance of the optimal ARQ scheme on a channel is

$$\hat{L}_{sef}^{ARQ} = \hat{N}_{REFP} \cdot b \tag{5.8}$$

and it is expected to be larger than $\hat{L}_{sef}^{FEC}$ on the same channel.

### 5.1.2 Delay Analysis

The better performance of ARQ over FEC schemes comes at the price of reduced throughput or longer time delay. Comparing a type-I stop-and-wait hybrid ARQ scheme with a pure FEC scheme under the same total bit rate constraint $R_T$, the

following facts can be noticed immediately. First, the total number of bits transmitted in the two schemes are the same, i.e.

$$R_T^{ARQ} = R_T^{FEC}$$

which means the total transmission time of the two schemes are the same

$$T_{FEC} = T_{ARQ}$$

Second, the delay difference between them is simply the additional waiting time of the type-I stop-and-wait hybrid ARQ scheme which is used for the source and channel decoding for all the received packets. Note that the even the discarded packets need to be processed before a feedback message $NAK$ can be generated. In a typical wireless communication scenario with 64 $kpbs$ data rate, users roam in the less than 30 $km$ area around the base stations, the total transmission time for a $512 \times 512$ pixel image will take $4s$. The transmission delay will be less than $10^{-4}s$ and thus is negligible. The total source decoding time $T_s$ of such an image would be in the range of $10^{-2}$ to $10^{-1}$ [54]. It is reasonable to assume that the channel decoding time $T_c$ of the same magnitude as $T_s$. On a specific channel, optimal ARQ and FEC schemes might request different protection levels. Thus, the total decoding times of the two schemes might be different. But notice the fact that transmission time dominates both of the schemes regardless of the optimal protection level difference, it may be concluded that the throughput property of the proposed type-I hybrid SW-ARQ scheme is quite similar to that of the pure FEC scheme. More complicated ARQ schemes such as selective repeat and go-back-N are not necessary for progressive image transmission.

### 5.1.3 Simulation Results

The proposed optimization algorithm for type-I stop-and-wait hybrid ARQ scheme is tested over two BSCs with BER=$10^{-1}$ and $10^{-2}$, and a two state FSMC or G-E channel. The G-E channel parameters are listed in Table 5.1.

| $\{\epsilon_b, \epsilon_g\}$ | $\{\pi_b, \pi_g\}$ | **P** | $\bar{\epsilon}$ |
|---|---|---|---|
| {.12, .0680} | {.62, .38} | {.08, .05} | .1000 |

**Table 5.1** G-E Channel parameters

The optimization results for the BSCs are depicted in Figure 5.2. It is noticeable that at the optimal protection level, the total number of retansmissions $\hat{N}_R$ is small. This is reasonable, because, for this type-I hybrid ARQ scheme, too many retransmissions means many packets should be discarded, thus wasting the bit rate budget. The resulting average FEFRLs for both the FEC and the hybrid ARQ schemes on the three tested channels are illustrated in Figure 5.3. It can be seen that under the same channel conditions, the optimal protection levels of the ARQ scheme are relaxed, which means more source bits are coded and received under the same bit rate constraint, i.e. $\hat{L}_{sef}^{ARQ} > \hat{L}_{sef}^{FEC}$. The optimal protection rates and the corresponding PSNR performances on the three tested channels are depicted in Figure 5.4, together with those of the FEC schemes. The results of [36] and [14] are also put into Figure 5.4(a) for comparison purpose. On the BSC with BER $10^{-1}$, the optimal protection rate of [36] is also 8/19. This is not a surprise since maximization of average PSNR is equivalent to maximization of average FEFRL, as already stated in previous chapters. Of course identical RCPC code rates result in identical system performances. The almost identical PSNR performances in Figure 5.4(a) on BSC of $\epsilon = 10^{-1}$ further justifies the conclusion in Chapter 3 that for optimal protected systems, performances obtained from rate-based evaluation are close to those from distortion-based method. The slightly better performance of [14] on BSC with BER=$10^{-2}$ can be attributed to the 32 byte source packet length and the more efficient type-II hybrid ARQ scheme that uses code combining techniques.

The PSNR performances and the corresponding optimal protection rates for both the pure FEC and type-I hybrid ARQ schemes on the G-E channel are depicted

in Figure 5.4(b). Both curves here are obtained using the proposed performance evaluation approach. The PSNR improvements of ARQ over FEC is slightly better than what are achieved in BSCs. This is because the "separation" principle is violated more severely in the FSMC or fading channels. Thus, more gain is expected and achieved on worse channel conditions. It can be seen that the PSNR improvement of the type-I stop-and-wait hybrid ARQ over the FEC scheme can be up to 1.4 dB. Note that the performance improvements were achieved at weaker protection levels on the same channel conditions. The prices paid for the better performances are the additional time delay and system complexity.

### 5.1.4 Concluding Remarks

With the rate-based performance analysis which is general for both BSCs and FSMC channels, an optimization algorithm of type-I hybrid ARQ schemes was developed for progressive image transmissions. The constraint of progressive transmission is a built-in feature of the scheme and the method is applicable to both memoryless and memory channels. Computer experiments show up to 1.4 dB PSNR improvements over the pure FEC schemes on the same channel conditions. It is also shown that the delay involved in typical wireless communications is dominated by propagation time so that the throughput of the proposed ARQ scheme is close to that of the pure FEC schemes.

## 5.2 Type-II Hybrid ARQ

For progressive image transmissions in noisy communication channels, FEC schemes must stop decoding and discard all the packets starting from the one in which the *first* bit error happens. When a feedback channel is available, the bits

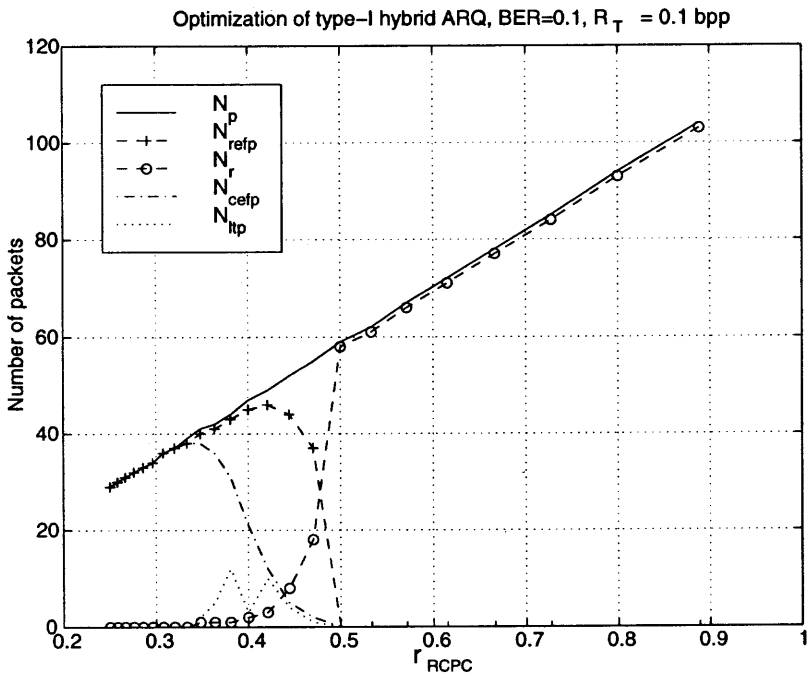


(a) BSC $\epsilon = 10^{-1}$

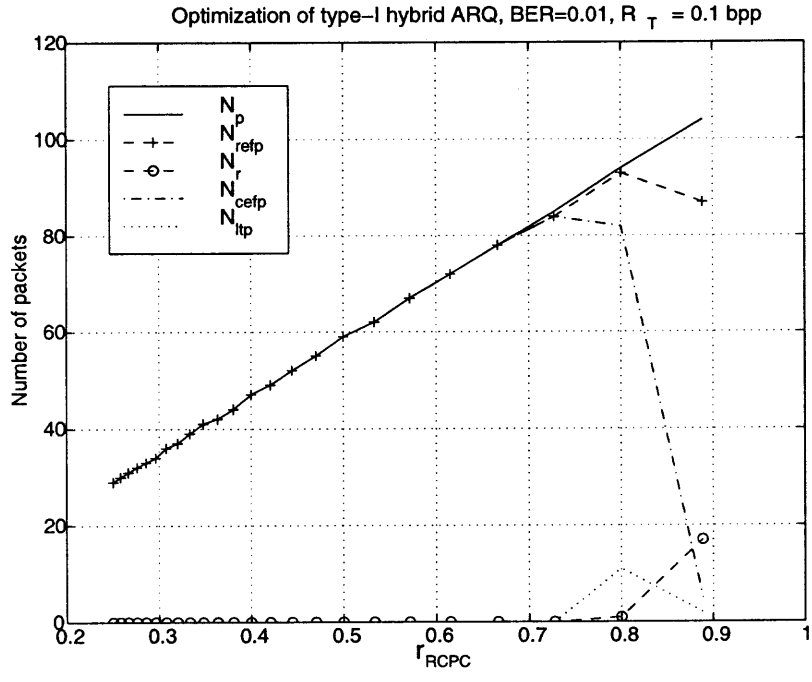


(b) BSC $\epsilon = 10^{-2}$

**Figure 5.2** Protection level optimization for type-I HARQ

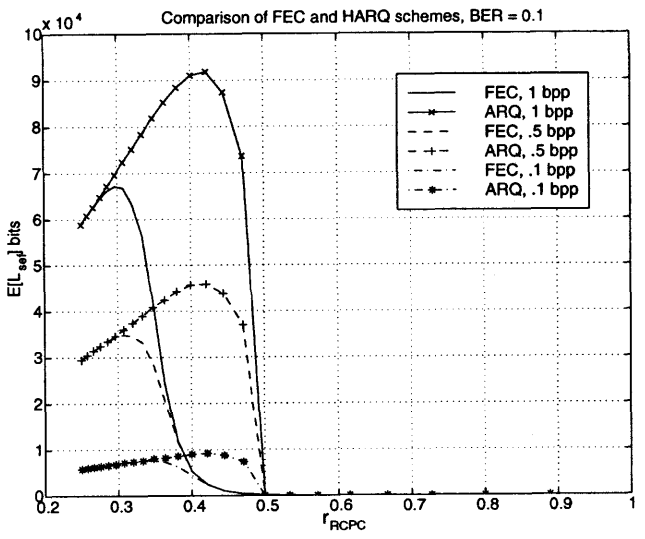


(a) BSC1 $\epsilon = 10^{-1}$

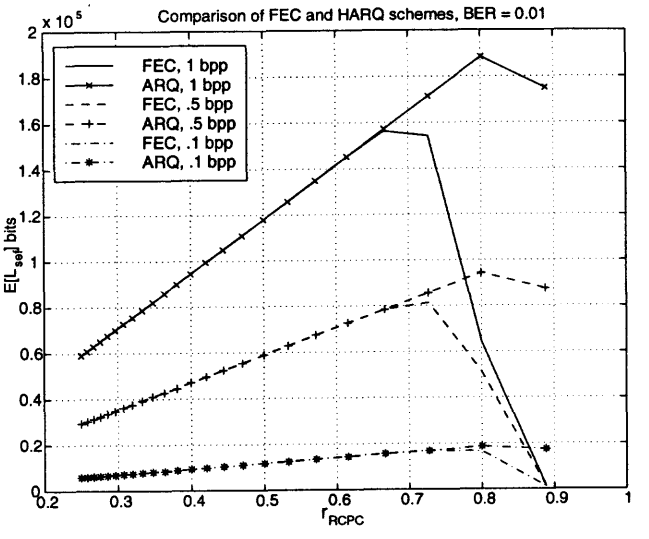


(b) BSC2 $\epsilon = 10^{-2}$

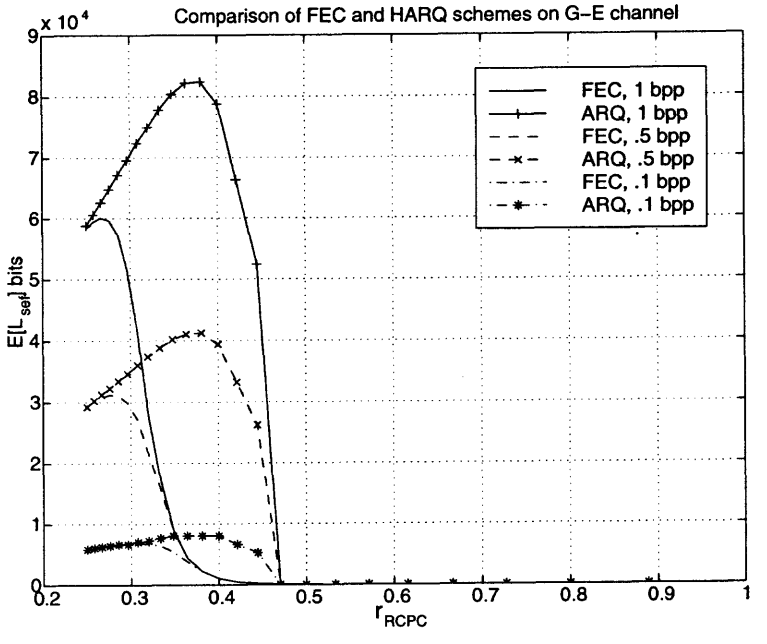


(c) G–E channel

**Figure 5.3** Comparison of FEC and type-I HARQ schemes

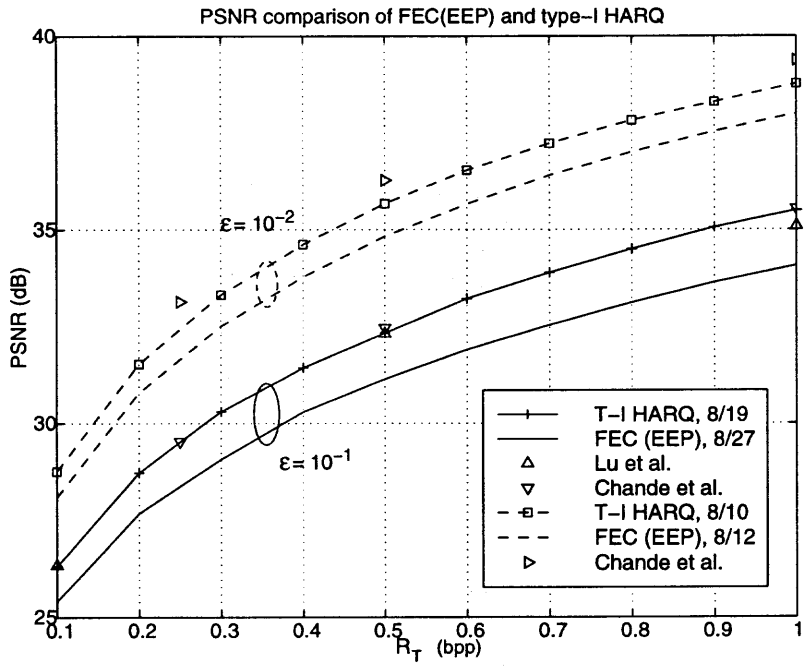


(a) BSCs $\epsilon = 10^{-1}, 10^{-2}$

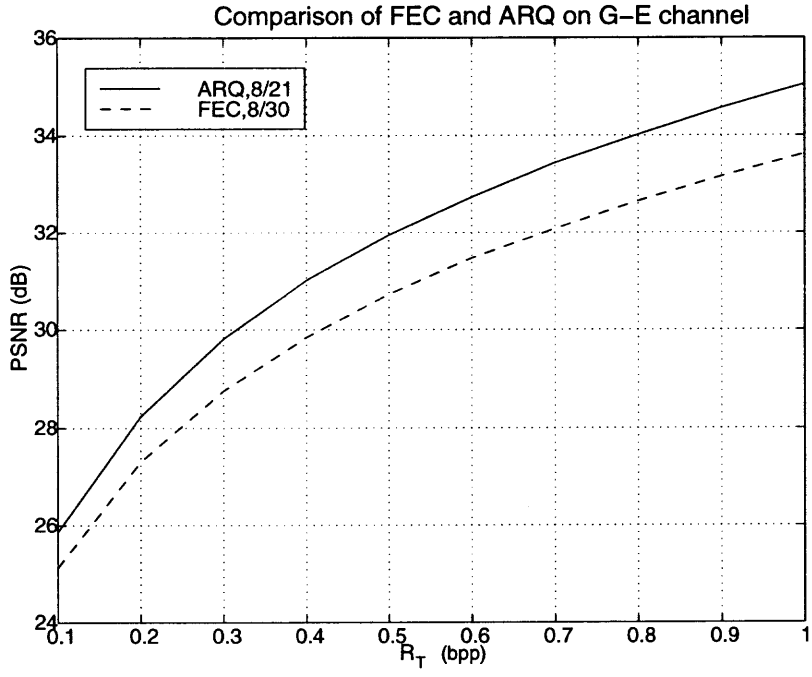


(b) G–E channel

**Figure 5.4** Comparison of FEC and type-I HARQ schemes by PSNR performances with LENA image

after the first bit error are usable with the aid of a hybrid ARQ schemes. In fact, even the discarded packets in the type-I stop-and-wait hybrid ARQ schemes are also usable. By combining with the punctured bits, the current erroneous packet which is discarded by type-I hybrid ARQ might be decoded error-free at a lower RCPC code rate. Thus, the embedded property of both the source and channel coding engines are fully exploited. Its performance can be optimized by adjusting the bit allocation between the source and channel coding and is expected to be better than that of type-I stop-and-wait hybrid ARQ under the same channel conditions.

### 5.2.1 Code Combining of Hybrid ARQ

An illustrated description of the proposed stop-and-wait hybrid ARQ scheme using code combining technique is depicted in Figure 5.5. After a packet is sent, the transmitter waits for a response from the receiver. The transmitter keeps on sending new packets if an $ACK$ is received. On receiving an $NAK$, the transmitter sends a refinement packet containing the punctured bits at the next lower code rate in the RCPC code set which is to be combined with the current packet. The process continues until the current packet is decoded error-free. Here it is assumed that all the erroneous packets are decodable eventually if the lowest (or the optimal rate on a specific channel) is reached. The transmission restarts with an $ACK$ received and the process is continued until the total bit rate constraint is reached. Note that there is no need to retransmit the CRC and the flush bits for the current packet and retansmissions are for individual packet only. Obviously, the errors in each of the trials under the bit rate constraint are independent from each other. Hence, on the average, the length for each of the transmission trials can also be represented by the average FEFRL $\overline{L}_{sef}$. To facilitate further analysis, some necessary definitions of the proposed scheme are listed below.

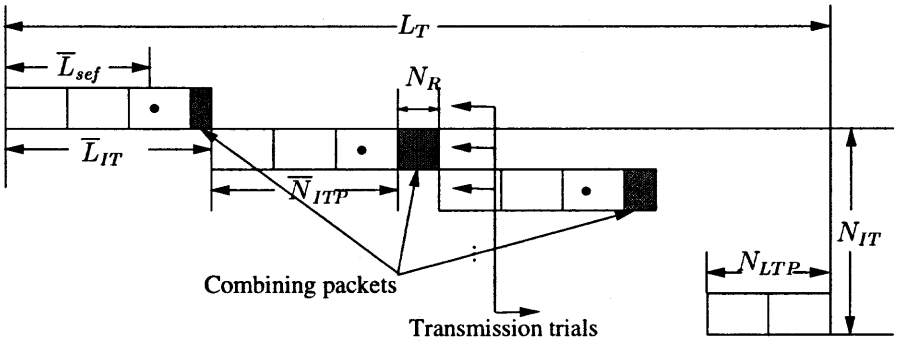


**Figure 5.5** Water-filling for SW-HARQ with code combining

**Definition 6** *$N_{TP}$: total number of packets under the total bit rate constraint $R_T$.*

$$N_{TP} = \left\lfloor \frac{N \cdot R_T}{L_P} \right\rfloor \tag{5.9}$$

where $N$ is the number of pixels in an image and

$$L_P = b \cdot r_{RCPC}^{-1} \cdot r_{CRC}^{'-1}$$

is the packet size, $b$ is the number of source bit in the packet. The RCPC code rate is denoted as $r_{RCPC}(i)$ where $i$ is the index of the RCPC code rate set and

$$r'_{CRC} = \frac{b}{b+c+f}$$

where $c$ and $f$ are the number of CRC and flush bits in each packet, respectively.

**Definition 7** *$\overline{N}_{ITP}$: average number of packets in each independent transmission trials.*

$$\overline{N}_{ITP} = \left\lceil \frac{\overline{L}_{sef}}{b} \right\rceil \tag{5.10}$$

**Definition 8** *$\overline{L}_{cc}$: average length of code combining in each independent transmission trials.*

$$\overline{L}_{cc} = \overline{N}_R \cdot b \cdot \left[ r_{RCPC}(i)^{-1} - r_{RCPC}(i+1)^{-1} \right] \tag{5.11}$$

where $\overline{N}_R$ is the average number of retransmissions needed for an erroneous packet to be decoded error-free.

**Definition 9** $\overline{L}_{IT}$*: average length of each independent transmissions.*

$$\overline{L}_{IT} = L_P \cdot \overline{N}_{ITP} + \overline{L}_{cc} \tag{5.12}$$

**Definition 10** $N_{IT}$*: number of independent transmission trials.*

$$N_{IT} = \left\lfloor \frac{L_T}{\overline{L}_{IT}} \right\rfloor \tag{5.13}$$

**Definition 11** $N_{LTP}$*: number of packets in the last transmission trial.*

$$N_{LTP} = \frac{L_{LT}}{L_P} \tag{5.14}$$

where

$$L_{LT} = L_T \mod \left(\overline{L}_{IT}\right)$$

is the length of bit stream in the last transmission trial.

**Definition 12** $\overline{N}_{REFP}$*: total number of error-free packets received.*

In Figure 5.5, the packets in which the first errors happen are made error-free by code combining and the image transmission is completed after several independent trials. Thus, the final decoded image quality is determined by $\overline{N}_{REFP}$. By using a simple water filling on the bit rate constraint $R_T$, we have

$$\overline{N}_{REFP} = \overline{N}_{ITP} \cdot N_{IT} + N_{LTP} \tag{5.15}$$

It is apparent now that the value of $\overline{N}_{REFP}$ can be maximized by adjusting the ratio between source and channel coding budget, i.e.

$$\widehat{N}_{REFP} = \max_{R_s + R_c \leq R_T} \overline{N}_{REFP} \tag{5.16}$$

Such an optimization problem can be easily solved by the following numerical method

$$\hat{r}_{RCPC} = \arg \min_{R_T} \left\{ \max_{R_s+R_c \leq R_T} \overline{N}_{REFP} \right\} \tag{5.17}$$

So the performance in terms of average FEFRL $\widehat{L}_{sef}$ of the optimal type-II hybrid ARQ scheme on a channel is

$$\widehat{L}_{sef}^{HARQT-II} = b \cdot \widehat{N}_{REFP} \tag{5.18}$$

and it is expected to be larger than $\widehat{L}_{sef}^{HARQT-I}$ and $\widehat{L}_{sef}^{FEC}$ on the same channel.

### 5.2.2 Simulation Results and Discussions

The proposed method is tested over two BSCs with BER of $10^{-1}$ and $10^{-2}$, and a two state FSMC or Gilbert-Elliott (G-E) channel. The G-E channel parameters are selected from [36] and listed in Table 5.2. In the simulation, it is assumed that the average number of codes combining for error-free RCPC decoding is

$$\overline{N}_R = |j - i| \tag{5.19}$$

where

$$j = \left\{ 1 \leq i \leq |\mathcal{R}_{RCPC}| \,\middle|\, r_{RCPC}(i) = \hat{r}_{RCPC}^{FEC} \right\} \tag{5.20}$$

and $\hat{r}_{RCPC}^{FEC}$ is the optimal protection rate for the FEC schemes on that channel. This means that the error-free decoding is achieved when the optimal protection rate of the FEC scheme is reached, on the average.

| $\{\epsilon_b, \epsilon_g\}$ | $\{\pi_b, \pi_g\}$ | **P** | $\overline{\epsilon}$ |
|---|---|---|---|
| {.12, .0680} | {.62, .38} | {.08, .05} | .1000 |

**Table 5.2** G-E Channel parameters

The optimization results for BSC with $\epsilon = 10^{-1}$ are depicted in Figure 5.6. It is noticeable that at the optimal protection level, $\hat{N}_{IT}$ is small. It is also of interests to note the almost flat $\overline{N}_{REFP}$ and $N_{IT}$ curves starting from some RCPC code rate

in Figure 5.6(a). It can be explained as follows. On a very noisy channel like the one here with BER $10^{-1}$, strong protection from RCPC code is usually required for robust transmission in the feed-forward channel. When the protection level is reduced to some very weak level, the first error might happen in the *first* packet! In that case, retransmission is frequent and a new packet can reach the receiver only after the current one is decodable. Not surprisingly, those packets will be decodable when the code rate reach the optimal protection level for the feed-forward channel, on the average, as stated in (5.19) and (5.20). So the final result is that, with very weak channel protection, the code combining technique turns the whole scheme into a 'equivalent' optimal FEC scheme with optimal protection rate expressed in (5.20). Of course this is not economical due to the additional delay involved in the numerous retransmissions.

The resulting average FEFRLs for both the pure FEC and the type-II stop-and-wait hybrid ARQ schemes on the G-E channel are illustrated in Figure 5.7. It is clear that under the same channel conditions, the optimal protection levels of the ARQ scheme are relaxed, which means more source bits are coded and received under the same bit rate constraint, i.e.

$$\hat{L}_{sef}^{ARQ} > \hat{L}_{sef}^{FEC}$$

It can also be seen from Figure 5.7(a) and (c) that on the same the channel, the optimal performance measured in $\hat{L}_{sef}$ of the 'equivalent' FEC scheme is better than that of the 'real' FEC one. In fact, even the optimal 'real' FEC system needs to discard some packets due to the error propagation effects. However, with the 'equivalent' FEC scheme or the type-II stop-and-wait hybrid ARQ schemes at weak protection levels, each packet is assumed to be decodable after the optimal protection rate is reached. This assumed efficiency explains the 'better' performance here. Note that such small performance improvement is achieved at the price of additional time

delay and system complexity since numerous retransmissions are necessary for each packet.

The optimal protection rates and the corresponding PSNR performances on the three tested channels are depicted in Figure 5.8(a) and (b), together with those of the type-I hybrid ARQ and the FEC schemes. It is apparent that the performance for the type-I hybrid ARQ scheme is better than that of the FEC schemes schemes for up to 1.4 dB on the same channel, with less protection. Of course such improvement is obtained with some additional time delay and system complexity such as bufferring. Code combining further improves the system performance for up to 0.3 dB compared to that of the type-I hybrid ARQ. The PSNR improvements of ARQ over FEC can be higher in FSMC or fading channels, as the one selected here, since the "separation" principle is violated more severely therein. Thus, higher performance gain up to 1.7 dB is achieved on worse channel conditions.

The results of [36] and [14] are also put into Figure 5.8 for comparison purposes. On the BSC of $\epsilon = 10^{-1}$, the optimal protection rate of [36] is also 8/19. It means that the rate- and distortion-based optimization criterion are equivalent. This identical optimal protection level also results in identical system performances. The almost overlapped PSNR curves in Figure 5.8 on BSC of $\epsilon = 10^{-1}$ further justifies the conclusion in Chapter 3 that for optimal protected embedded bit streams, performances obtained from the proposed approach and the conventional average PSNR method are very close.

It can be seen from Figure 5.8 that the performance improvement of type-II over type-I hybrid ARQ [85] is about 0.3 dB. This marginal improvement can be explained by the fact that the former is more efficient than the latter only for the packets in which the first bit error happen. However, for optimally protected schemes, the number of such packets is small. The slightly better performance of

[14] on BSC of $\epsilon = 10^{-2}$ can be attributed to the 32 bytes source packets ($b = 256$) and the arithmetic coding of SPIHT.

### 5.2.3 Concluding Remarks

Using rate-based performance analysis, which is general for both BSCs and FSMC channels, an optimization algorithm for type-II stop-and-wait hybrid ARQ schemes was developed for progressive image transmissions in channels with feedback information. The constraint of progressive transmission is a built-in feature of the general source model and the method is applicable to both memoryless and memory channels. The more efficient usage of the erroneous packets of the type-II stop-and-wait hybrid ARQ schemes turns into the best possible system performance, which is about 0.3 dB better than that of the type-I schemes and can be up to 1.7 dB better than the FEC schemes under the same channel conditions. It is also shown that for typical progressive image transmission in wireless communications, the delay incurred is dominanted by transmission time. Thus, the throughput of the proposed ARQ is also close to that of the FEC schemes. Improvement over type-I schemes is marginal since the number of discarded packets in the optimally protected schemes is small. Compared to the type-I stop-and-wait hybrid ARQ scheme, the performance improvement of type-II is achieved without additional increase in system overhead and delay. However, the system complexity of type-II scheme is higher due to the more complicated buffering for the punctured channel bits.

## 5.3 Conclusions

In this chapter, the idea of rate-based performance evaluation and optimization for progressive image transmission in FSMC channels is extended to the communication systems in which feedback channels are available. Within such a practical scenario for current wireless communications, it is of interest to investigate the

performance gain of such systems when processing delay is tolerable. The source model developed for FSMC channels in Chapter 4 is used in the feed-forward channels. The concatenated CRC-RCPC scheme is modified into a hybrid ARQ system by adding a water-filling like rate control algorithm. For type-I hybrid ARQ, the system performance is about 1.4 dB better than what is achievable on feed forward channels with EEP. The performance is then further improved by code combining techniques for about 0.3 dB. Since general FSMC models are used as feedforward channels, the average FEFRL derived by ESA is applicable to the hybrid ARQ schemes for progressive image tranmission in channel with feedback information. The performance optimization algorithms for pure FEC and hybrid ARQ schemes are quite similar.

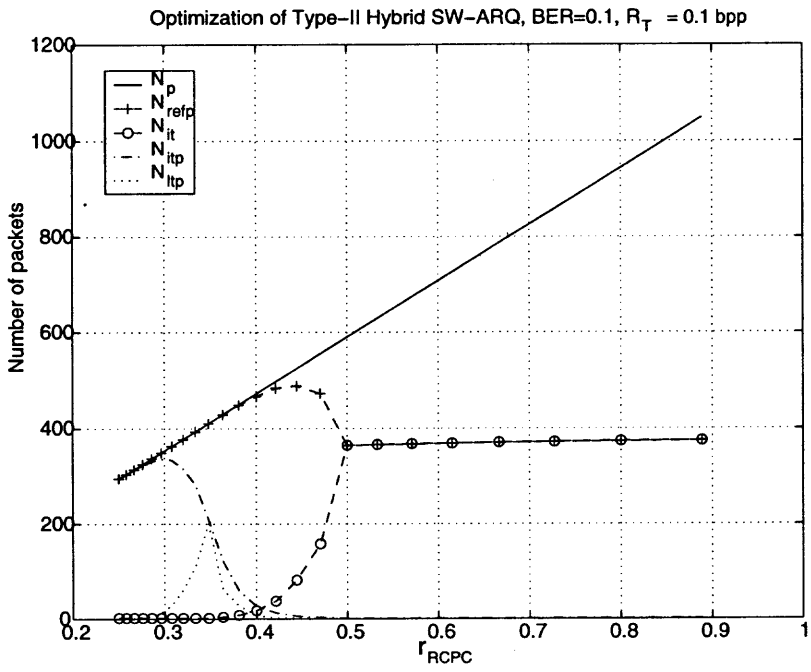


(a) BSC $\epsilon = 10^{-1}$

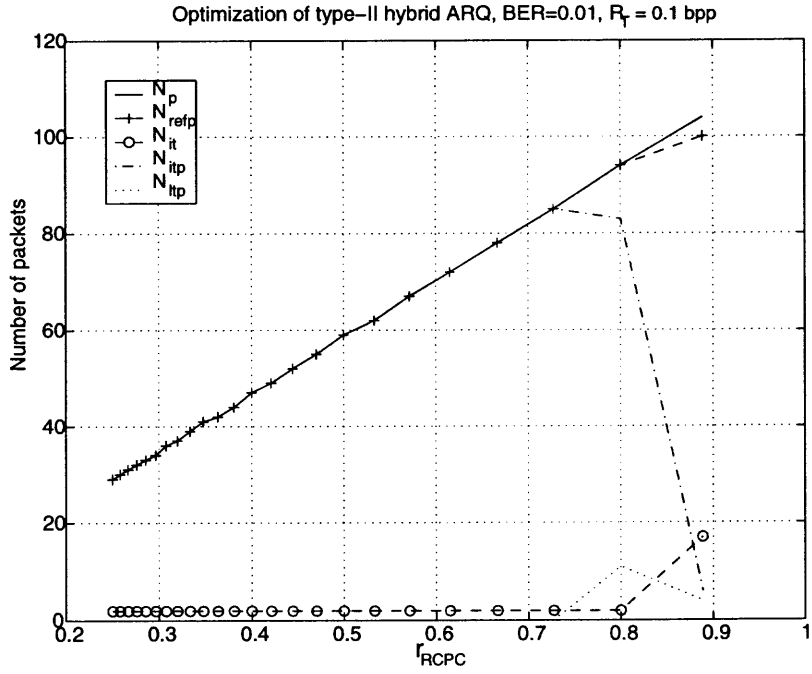


(b) BSC $\epsilon = 10^{-2}$

**Figure 5.6** Protection level optimization for type-II SW-HARQ

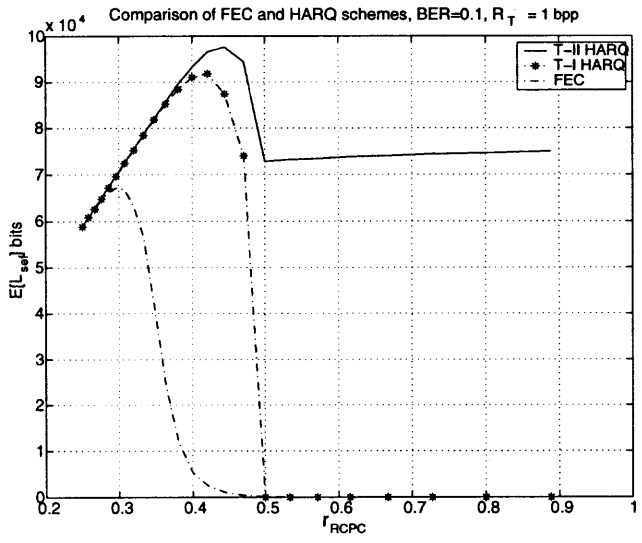


(a) BSC $\epsilon = 10^{-1}$

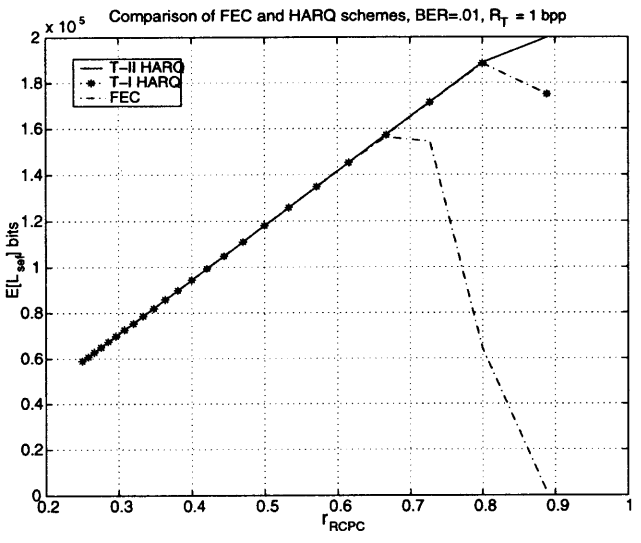


(b) BSC $\epsilon = 10^{-2}$

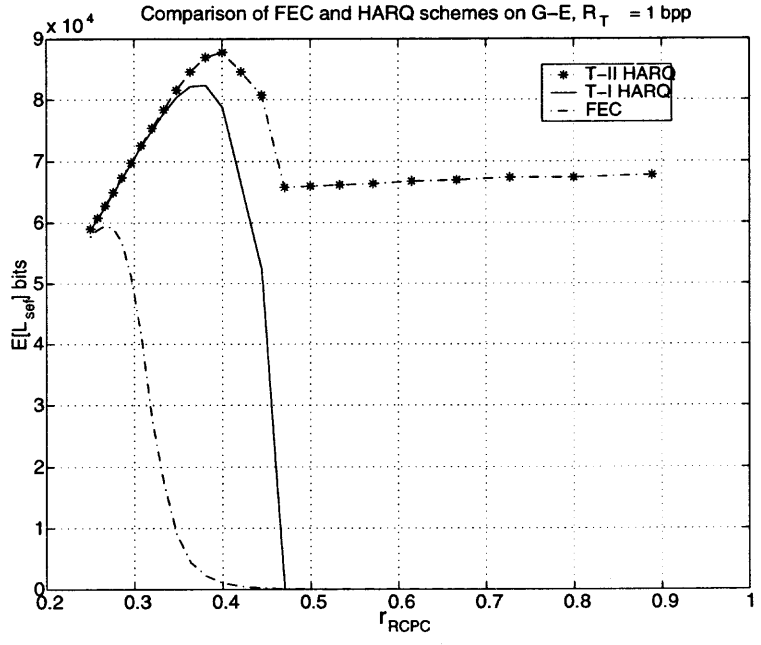


(c) G–E channel

**Figure 5.7** Comparison of FEC, type-I and -II SW-HARQ schemes

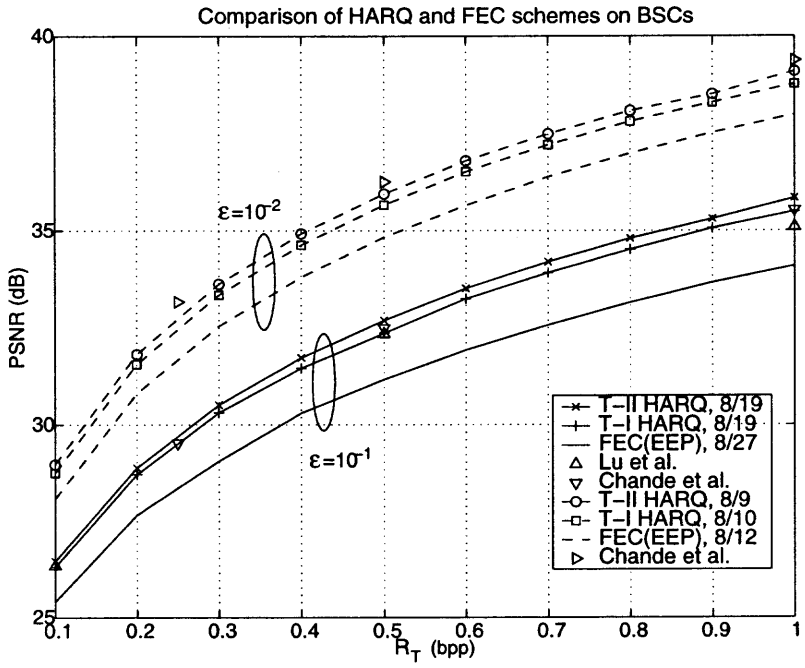


(a) BSCs of $\epsilon = 10^{-1}$, $10^{-2}$

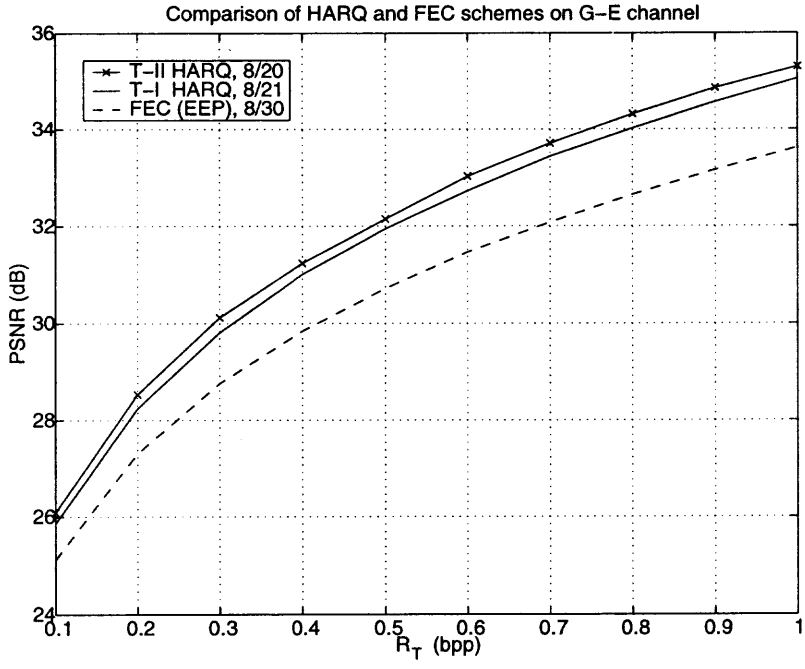


(b) G-E channel

**Figure 5.8** Comparison of FEC, type-I and -II SW-HARQ schemes by PSNR performances with LENA image

# CHAPTER 6
# CONCLUSIONS AND PERSPECTIVES

Just as the image compression algorithms try to provide the best performance with limited bit rate constraint, the target of joint source-channel coding (JSCC) for progressive image transmission is also to achieve the highest performance under the bit rate constraint. The problem tackled in the dissertation is how to obtain the best possible performance for progressive image transmission over finite state Markov chain (FSMC) channels with or without feedback information. The research efforts began from the investigation on the recent successful image compression algorithms such as EZW and SPIHT. A lingering question is why those algorithms can achieve such significant performance improvememnt? And what lesson can be learned so that a similar problem can be solved successfully? One important observation is that even a simple idea can also result in significant performance improvement, such as what is achieved from SPIHT. In fact, the major contribution of the dissertation comes from the slightly different system performance evaluation method, which is also a very simple idea. By moving from point A to B in Figure 1.1, the conventional distortion-based performance evaluation approach is replaced by the proposed rate-based one and the ensuing investigation goes onto a different route. Another lesson learned from the research is to start the investigation from the simplest case whenever possible.

It may seem that the analysis on binary symmetric channel (BSC) cases (Chapter 3) should appear after the discussions on FSMC channel cases (Chapter 4). Such an arrangement might be more concise since both the BSC and related analytical results are special cases of what is obtained for FSMC channels. However, the investigation process can not be reflected with such an order and the current ordering shows the development of error sequence analysis (ESA) from an implicit use of error sequence to an explicit one.

## 6.1 Conclusions and Major Contributions

The major theme of the research is the joint source-channel coding design for progressive image transmission in noisy channels. First, a general first error-free run length (FEFRL) model for the embedded image sources transmitted over general noisy channels was set up and explanations were provided for it. With such a model, a new system performance metric called average error-free source rate $\overline{R}_{sef}$ was then developed. The relationship between the proposed and conventional performance evaluation approach is then explained.

Based on the proposed approach, we move one step further by obtaining the average FEFRLs in BSCs for equal error protection (EEP) and unequal error protection (UEP) schemes, all in closed form. The new models provide an easy way to solve the optimization problem linked with such joint source-channel coding design. In the dissertation, optimization algorithms for EEP and UEP are presented. The UEP optimization problem for progressive image transmission were clearly defined and complete solutions provided on BSCs. In addition, the necessary condition for UEP gains was proved and the theoretical performance limits derived. Simulation results show about 0.3 dB performance improvements over the optimal EEP schemes under the same channel condition.

Memory or FSMC channels are extensively used to approximate the multipath fading channels in wireless communications. The idea of obtaining average FEFRLs is extended to the FSMC channel cases in the research by conducting error sequence analysis (ESA) on the input/output bit streams for the FSMC channels. It was further shown that existing techniques for the joint source-channel coding problem on memory channels such as single BSC based and multiple state based approaches are all special cases of the results from ESA. And it is clear that the method used to obtain source models in BSCs is also ESA with error sequences implied in the derivation process. The performances of the system are then optimized with the

proposed approach and significant PSNR improvements are achieved in some channel conditions.

Since the analytical results for FSMC channels are general enough to include previous ones on BSCs, the model was then used in the feedforward channels in the automatic repeat request (ARQ) schemes . By adding a water-filling like rate control algorithm, the forward error correction (FEC) scheme is turned into a hybrid FEC/ARQ protocol with stop-and-wait strategy. With optimization, optimal type-I hybrid ARQ schemes achieve about 1.4 dB system performance gain over the optimal EEP schemes on the feed forward channel alone. With code combining techniques, the full potentials of the concatenated CRC-RCPC scheme is fully exploited and the optimal performance is about 0.3 dB better than that of type-I hybrid ARQ schemes.

To conclude the research, it is claimed that with the rate-based system performance evaluation approach, the average FEFRL model obtained for the FSMC channels include BSC as a special case. Furthermore, the performance optimization algorithms for progressive image transmissions over memoryless, memory channels and channels with feedback information are quite similar.

## 6.2 Future Work

With such a general approach, the next target is to obtain general guidelines for protecting strategies on fading channels. For simple channel models such as BSCs, such a goal is easy to achieve with a BER-RCPC code rate plot. However, for fading channels and their FSMC model approximations, even a two-state G-E model will need at least four independent parameters and a general guideline on such multi-dimensional space has to be based on more investigations and experiments with the proposed method.

Another interesting topic might be the extension of the idea or even the approach to scalable video transmission problems.

## REFERENCES


1. *IEEE Journal on Selected Areas in Commun.*, vol. 18(6), June 2000.

2. A. N. Akansu and M. J. Medley, *Wavelet, subband, and block transforms in communications and multimedia.* Boston, MA: Kluwer Academic Publishers, 1999.

3. A. N. Akansu and M. J. Smith, *Subband and wavelet transforms: design and applications.* Boston, MA: Kluwer Academic Publishers, 1996.

4. A. N. Akansu, *Multiresolution signal decomposition : transforms, subbands, and wavelets.* Boston, MA: Academic Press, 1992.

5. A. A. Alatan, M. Zhao, and A. N. Akansu, "UEP of SPIHT encoded image bit streams," *IEEE Journals on Selected Areas in Communications*, vol. 18(6), pp. 814–818, June 2000.

6. M. Antonini, M. Barlaud, P. Mathieu, and I. Daubechies, "Image coding using wavelet transform," *IEEE Trans. on Image Proc.*, vol. 1(2), pp. 205–220, April 1992.

7. S. Appadwedula, D. L. Jones, K. Ramchandran, and L. Qian, "Joint source channel Matching for wireless image transmission," in *Proc. of Int. Conf. on Image Processing*, (Chicago, Illinois), pp. 137–141, Oct. 1998.

8. M. Boliek, C. Christopoulos, and E. Majani, *JPEG 2000 Image Coding Systems, FCD ver. 1.0.* ISO/IEC JTC1/SC29 WG1 (ITU-T SG8), Mar. 16, 2000.

9. M. Budagavi, W. R. Heinzelman, J. Webb, and R. Talluri, "Wireless MPEG-4 Video Communication on DSP Chips," *IEEE Signal Processing Magazine*, vol. 17(1), pp. 36–53, Jan. 2000.

10. J. Cai and C. Chen, "Robust joint source-channel coding for image transmission over wireless channels," *IEEE Trans. on Circuits and Systems for Video Technology*, vol. 10(6), pp. 962–966, Sept. 2000.

11. V. Chande and N. Farvardin, "Joint Design of Progressive Fixed-Rate Source-Channel Codes," in *Proc. of Data Compression Conference*, (Snowbird, UT), Mar. 1999.

12. V. Chande and N. Farvardin, "Progressive transmission of images over memoryless noisy channels," *IEEE Journal on Selected Areas in Commun.*, vol. 18(6), pp. 850–860, June 2000.

13. V. Chande, N. Farvardin, and H. Jafarkhani, "Image Communication Over Noisy Channels with Feedback," in *Proc. of Int. Conf. on Image Processing*, (Kobe, Japan), pp. 540–544 (II), Oct. 1999.

14. V. Chande, H. Jafarkhani, and N. Farvardin, "Joint Source-Channel Coding of Images for Channels with Feedback," in *Proc. IEEE Information Theory Workshop*, (San Diego, CA), Sept. 1997.

15. N. T. Cheng and N. G. Kingsbury, "The EREC: An error-resilient technique for encoding position information or sparse data," *IEEE Trans. on Commun.*, vol. 40(1), pp. 140–148, Jan. 1992.

16. B. S. Choi, S. I. Chae, and J. B. Ra, "A feedback channel based error compensation method for mobile video communications using H.263 standard," in *Proc. of Int. Conf. on Image Processing*, (Kobe, Japan), pp. 555–559 (II), Oct. 1999.

17. P. C. Cosman, J. Rogers, P. G. Sherwood, and K. Zeger, "Combined Forward Error Control and Packetized Zerotree Wavelet Encoding for Transmission of Images Over Varying Channels," *IEEE Trans. on Image Proc.*, vol. 9(6), pp. 982–993, June 2000.

18. T. M. Cover and J. A. Thomas, *Elements of Information Theory.* New York: John Wiley & Sons, 1991.

19. C. D. Creusere, "A new method of robust image compression based on the embedded zerotree wavelet algorithm," *IEEE on Image Proc.*, vol. 6(10), pp. 1436–1442, Oct. 1997.

20. I. Daubechies, *Ten lectures on Wavelets.* PA: SIAM, 1992.

21. M. Effros and K. Z. et al., "Workshop report on joint source-channel coding," *NSF*, vol. draft 3, Oct. 1999.

22. E. O. Elliott, "Estimates of error rates for codes on burst-nnoise channels," *Bell Syst. Tech. J.*, vol. 42, pp. 1977–1997, Sept. 1963.

23. M. P. C. Fossorier, Z. Xiong, and K. Zeger, "Joint source-channel image coding for a power constrained noisy channel," in *Proc. of Int. Conf. on Image Processing*, (Chicago, IL), pp. 122–126, Oct. 1998.

24. P. Frenger, P. Orten, T. Ottosson, and A. Svensson, "Multi-rate Convolutional Codes," *Technical Report*, Apr. 1998.

25. R. G. Gallager, *Discrete Stochastic Process.* Boston, MA: Kluwer Academic Publishers, 1995.

26. E. N. Gilbert, "Capacity of a burst-noise channel," *Bell Syst. Tech. J.*, vol. 39, pp. 1253–1266, Sept. 1960.

27. A. J. Goldsmith and M. Effros, "Joint design of fixed-rate source codes and multiresolution channel codes," *IEEE Trans. on Comm.*, vol. 46(10), pp. 1301–1312, Oct. 1998.

28. J. Hagenauer, "Rate-compatible punctured convolutional codes (RCPC codes) and their applications," *IEEE Trans. Commun*, vol. 36, pp. 389–400, Apr. 1988.

29. E. S. Hong and R. E. Ladner, "Group Testing for image compression," in *Proc. of Data Compression Conf.*, (Snowbird, UT), pp. 3–12, Mar. 2000.

30. http://www.cipr.rpi.edu/research/SPIHT.

31. http://www.jpeg.org/JPEG2000.htm.

32. R. L. Joshi, H. Jafarkhani, J. H. Kasner, T. R. Fisher, N. Farvardin, and M. W. Marcellin, "Comparison of different methods of classification in subband coding of images," *IEEE Trans. on Image Proc.*, vol. 6(11), pp. 1473–1486, Nov. 1997.

33. A. S. Lewis and G. Knowles, "Image compression using the 2-D wavelet transforms," *IEEE Trans. on Image Proc.*, vol. 1, pp. 244–250, April 1992.

34. J. Li and S. Lei, "An embedded still image coder with rate-distortion optimization," *IEEE Trans. on Image Proc.*, vol. 8(7), pp. 913–924, July 1999.

35. J. Lu, A. Nosratinia, and B. Aazhang, "Progressive source-channel coding of images over bursty error channels," in *Proc. of Int. Conf. on Image Processing*, (Chicago, IL), pp. 127–131, Oct. 1998.

36. J. Lu, A. Nosratinia, and B. Aazhang, "Progressive joint source-channel coding in feedback channels," in *Proc. of Data Compression Conference*, (Snowbird, UT), pp. 140–148, Mar. 1999.

37. H. Man, F. Kossentini, and M. J. T. Smith, "Robust EZW image coding for noisy channels," *IEEE Signal Processing Letters*, vol. 4, pp. 227–229, Aug. 1997.

38. H. Man, F. Kossentini, and M. J. T. Smith, "A family of efficient and channel error resilient wavelet/subband image coders," *IEEE Trans. on Circuits and Systems for Video Technology*, vol. 9(1), pp. 95–108, Feb. 1999.

39. M. W. Marcellin, M. Gormish, A. Bilgin, and M. Boliek, "An overview of JPEG 2000," in *Proc. of Data Compression Conf.*, (Snowbird, UT), pp. 523–541, Mar. 2000.

40. I. Moccagatta, S. Soudagar, J. Liang, and H. Chen, "Error-resilient coding in JPEG-2000 and MPEG-4," *IEEE Journal on Selected Areas in Commun.*, vol. 18(6), pp. 899–914, June 2000.

41. A. E. Mohr, E. A. Riskin, and R. E. Ladner, "Graceful degradation over Packet erasure channels through forward error correction," in *Proc. of Data Compression Conference*, (Snowbird, UT), pp. 92–101, Mar. 1999.

42. A. E. Mohr, E. A. Riskin, and R. E. Ladner, "Unequal loss protection: graceful degradation of image quality over packet erasure channels through forward error correction," *IEEE Journal on Selected Areas in Commun.*, vol. 18(6), pp. 819–828, June 2000.

43. D. Mukherjee and S. K. Mitra, "A vector set partitioning noisy channel image coder with unequal error protection," *IEEE Journal on Selected Areas in Commun.*, vol. 18(6), pp. 829–840, June 2000.

44. T. Ottosson, "Coding, Modulation and Multiuser Decoding for DS-CDMA systems," *Ph.D. thesis*, Nov. 1997.

45. J. G. Proakis, *Digital Communications 3/e.* New York: McGraw Hill, 1995.

46. J. G. Proakis and M. Salehi, *Communication systems engineering.* New York: McGraw Hill, 1995.

47. R. Puri, K. Ramchandran, and A. Otega, "Joint Source Channel Coding with Hybrid FEC/ARQ for Buffer Constrained Video Transmission," in *Proc. of 1998 IEEE Second Workshop on Multimedia Signal Processing*, (Redondo Beach, Ca), pp. 567–572, Dec. 1998.

48. L. C. Ramac and P. K. Varshney, "A wavelet domain diversity method for transmission of images over wireless channels," *IEEE Journal on Selected Areas in Commun.*, vol. 18(6), pp. 899–914, June 2000.

49. T. S. Rappaport, *Wireless Communications, principles & practice.* Upper Saddle River, NJ: Prentice-Hall, 1996.

50. P. Rault and F. Kossentini, "Robust subband image coding for wireless transmissions," in *Proc. of Int. Conf. on Image Processing*, (Kobe, Japan), pp. 374–378 (III), Oct. 1999.

51. D. W. Redmill and N. G. Kingsbury, "The EREC: An error-resilient technique for coding variable-length blocks of data," *IEEE Trans. on Image Proc.*, vol. 5(4), pp. 565–574, Apr. 1996.

52. J. Rogers and P. C. Cosman, "Wavelet Zerotree Image Compression with Packetization," *IEEE Signal Processing Letters*, vol. 5(5), pp. 105–107, May 1998.

53. M. J. Ruf and J. W. Modestino, "Operational rate-distortion performances for joint source and channel coding for images," *IEEE on Image Proc.*, vol. 8(3), pp. 305–320, Mar. 1999.

54. A. Said and W. Pearlman, "A new, fast and efficient image codec based on set partitioning into hierarchical trees," *IEEE Trans. on Circuits and Systems for Video Technology*, vol. 6, pp. 243–250, June 1996.

55. C. E. Shannon, "A mathematical theory of communications," *Bell Syst. Tech. J.*, vol. 27, pp. 379–423, July 1948.

56. J. M. Shapiro, "Embedded image coding using zerotree of wavelet coefficients," *IEEE Trans. Signal Processing*, vol. 41, pp. 3445–3462, Dec. 1993.

57. P. G. Sherwood and K. Zeger, "Progressive image coding on noisy channels," *IEEE Signal Processing Letters*, vol. 4, pp. 189–191, Jul. 1997.

58. P. G. Sherwood and K. Zeger, "Error protection for Progressive image transmission over memoryless and fading channels," *IEEE Trans. Comm.*, vol. 46(12), pp. 1555–1559, Dec. 1998.

59. P. G. Sherwood and K. Zeger, "Error Protection for Progressive Image Transmission over Memoryless and Fading Channels," in *Proc. of Int. Conf. on Image Processing*, (Chicago, IL), pp. 324–328, Oct. 1998.

60. B. S. Srinivas, R. E. Ladner, M. Azizoglu, and E. A. Riskin, "Progressive transmission of images using MAP detection over channels with memory," *IEEE Trans. on Image Proc.*, vol. 8(4), pp. 462–475, April 1999.

61. M. Srinivasan and R. Chellappa, "Adaptive source-channel subband video coding for wireless channels," *IEEE Journal on Selected Areas in Commun.*, vol. 16, pp. 1830–1839, Dec. 1998.

62. G. Strang and T. Q. Nguyen, *Wavelets and filter banks.* Wellesley, MA: Wellesley-Cambridge Press, 1996.

63. N. Tanabe and N. Farvardin, "Subband image coding using entropy-coded quantization over noisy channels," *IEEE Journal on Selected Areas in Comm.*, vol. 10(5), pp. 926–943, June 1992.

64. D. Taubman, "High performance scalable image compression with EBCOT," *IEEE Trans. on Image Proc.*, June 2000.

65. D. Taubman and A. Zakhor, "Multirate 3-D subband coding of video," *IEEE Trans. on Image Proc.*, vol. 3(5), pp. 572–588, Sept. 1994.

66. W. Turin, *Digital Transmission Systems: Performance Analysis and Modeling.* New York: McGraw Hill, 1999.

67. W. Turin and R. Nobelen, "Hidden Markov modeling of flat fading channels," *IEEE Journals on Selected Areas in Communications*, vol. 16, pp. 1809–1817, Dec. 1998.

68. W. Turin and M. M. Sondhi, "Modeling errors in digital channels," *IEEE Journals on Selected Areas in Communications*, vol. 11(3), pp. 340–347, April 1993.

69. H. S. Wang and N. Moayeri, "Modeling, capacity and joint source/channel coding for Rayleigh fading channels," *Proc. 43rd IEEE Trans. Vehicular Technol. Conf.*, pp. 473–479, May 1993.

70. H. S. Wang and N. Moayeri, "FMSC-a useful model for radio communication channels," *IEEE Trans. Vehicular Technology*, vol. 44, pp. 163–171, Feb. 1995.

71. S. B. Wicker, *Error control systems for digital communication and storage.* Englewood Cliffs, NJ: Prentice-Hall, 1995.

72. Z. Xiong, B. Kim, and W. A. Pearlman, "Progressive video coding for noisy channels," in *Proc. of Int. Conf. on Image Processing*, (Chicago, IL), pp. 334–337, Oct. 1998.

73. Z. Xiong, K. Ramchandran, and M. T. Orchard, "Space-frequency quantization for wavelet image coding," *IEEE Trans. on Image Proc.*, vol. 6, pp. 677–693, May 1997.

74. M. Zhao and A. N. Akansu, "Optimal protection of progressive images in BSCs," to be submitted to *IEEE Trans. on Multimedia*, in preparation.

75. M. Zhao and A. N. Akansu, "Robust transmission of progressive images in wireless channels," to be submitted to *IEEE Trans Circuits Sys. Video Tech.*, in preparation.

76. M. Zhao and A. N. Akansu, "Adaptive protection of progressive images in fading channels," in *Proc. of 34th Asilomar Conf. on Signals, Systems & Computers*, (Asilomar, CA), Oct. 2000.

77. M. Zhao and A. N. Akansu, "Optimization of dynamic UEP schemes for embedded image sources in BSCs," in *Proc. of Int. Conf. on Image Processing*, (Vancouver, Canada), Dec. 2000.

78. M. Zhao and A. N. Akansu, "Robust transmission of progressive images over Gilbert-Elliott channels," in *Proc. of Conf. Info. Sciences and Systems*, (Princeton, NJ), pp. TA5–25–30, Mar. 2000.

79. M. Zhao and A. N. Akansu, "UEP of embedded images in wireless communications," in *Proc. of VTC*, (Boston, MA), Oct. 2000.

80. M. Zhao and A. N. Akansu, "Optimal protection of embedded image sources: a general approach," in *Data Compression Conf.*, (acceptted. Snowbird, Utah), Mar. 2001.

81. M. Zhao and A. N. Akansu, "Performance evaluation and optimization of embedded image bit streams in BSCs," to appear in *IEEE Signal Processing Letters* 2001.

82. M. Zhao and A. N. Akansu, "Progressive image transmission by ARQ with code combining," in *Int. Conf. on Acoustic, Speech, Signal Proc.*, (submitted. Salt Lake City, UT), Jun. 2001.

83. M. Zhao, A. A. Alatan, and A. N. Akansu, "Dynamic UEP of progressive image bit streams over noisy channels," in *Proc. of Int. Conf. on Acoustic, Speech, Signal Proc., vol. IV*, (Turkey), pp. 2095–2098, Jun. 2000.

84. M. Zhao, A. A. Alatan, and A. N. Akansu, "A new method for optimal rate allocation for progressive image transmission over noisy channels," in *Proc. of Data Compression Conf.*, (Snowbird, Utah), pp. 213–222, Mar. 2000.

85. M. Zhao, W. A. Pearlman, and A. N. Akansu, "JSCC of Hybrid ARQ schemes for progressive image transmissions," in *Conf. Info. Sciences and Systems*, (submitted, Baltimore, MD), Mar. 2001.

86. H. Zheng and K. J. Liu, "Robust image and video transmission over spectrally shaped channels using multicarrier modulation," *IEEE Trans. on Multimedia*, pp. 1–39, Mar. 1999.